Testing of Fast Transfer Relay by an EMTP-based Approach

Wenbin Wu

Project Report

TU Delft Delft University of Technology

Testing of Fast Transfer Relay by an EMTP-based Approach

By

Wenbin Wu

In partial fulfilment of the requirements for the degree of

Master of Science
in Electrical Sustainable Energy

at the Delft University of Technology,
To be defended publicly on Monday, 16 July 2018 at 10:00 AM

Supervisor:	Dr. Dipl-Ing Marjan Popov,	TU Delft- IEPG
Thesis Committee:	Prof. Ir. Mart van der Meijden,	TU Delft- IEPG
	Dr.Ir. Mohamad Ghaffarian Niasar	TU Delft-DCSECS
	Ir. Steven.A.de Clippelaar	DOW Energy System Technology Center (ESTC)

Abstract

Industries such as chemical companies need a continuous power supply and the fast transfer relay Siemens 7uv68 is designed to transfer from present feeder which encounters a fault to an auxiliary feeder and minimizes the transient torque of the induction motors during transfer. The relay will be installed in a DOW power plant in South Tarragona, and it should be validated that the relay can operate well in all kinds of fault scenarios and no mal-operation would occur in such power plant.

To perform the relay testing, first, the fault signals which reflect the dynamic performance of DOW Tarragona are generated by ATP-EMTP. The EMTP model of the DOW power plant has two main parts: the Tarragona power plant with auxiliary relays (overcurrent 50/50N, differential 87T) which send tripping and blocking command to 7UV68. Besides, in order to track the frequency and phase deviation between auxiliary feeder bus and the motor bus during transfer and configure a proper setting of the relay, the frequency measurement is accomplished by a zero-crossing method and the phase angle is measured by Clarke transformation. The test setup is made by 2 Omicron Amplifiers and a PLC which is used to simulate breakers' behavior for main-tie configuration.

Based on the testing requirements, the relay settings are tuned to ensure the motor bus transfer can be initiated by all kinds of faults in feeder bus, and the relay is blocked when faults occur in motor bus. .Besides, the motor bus can also be transferred to the auxiliary bus when a fault occurs in transmission grid with the help of relay self-start function. Furthermore, the trip delay of differential relay 87T and the communication delay affects the transfer time and the transfer inrush behaviors.

Keywords: ATP-EMTP, Mot Bus Transfer, Frequency Tracking, Induction Motors, Transient torques, Fast transfer relay, Industrial Plant Protection

Table of Contents

List of Figures

List of Tables

Acknowledgements

First of all, I would like to give the greatest gratitude to my supervisor Dr. Dipl-Ing. Marjan Popov who helped me during the whole period I worked on my master thesis. Besides, I would like to express my sincere thanks to Steven A. de Clippelaar from DOW for providing countless academic guide.

Besides, great thanks are going to my family. Without your support, it was impossible for me to go so far. Finally, I thank all my friends in Delft. I will never forget the colourful days in Delft.

Delft, University of Technology Wenbin Wu
July *5, 2018*

"*Whatever is reasonable is true, and whatever is true is reasonable.*"

— *Georg Wilhelm Friedrich Hegel*

Nomenclature

U_{res} : Motor bus residual voltage after an open-circuit

U_{ref} : Feeder voltage of the auxiliary bus which acts as a reference for motor transfer

U_{diff} : Voltage difference between motor bus residual voltage and the reference voltage

df : Frequency difference between motor bus residual voltage and the reference voltage

$d\theta$: Phase angle difference between motor bus residual voltage and reference feeder voltage

T_l : Torque of mechanical loads

ω_r : Rotor speed of motors

$\mathbf{I}_{\text{diff}}$: Differential current of differential relay 87T

$\mathbf{I}_{\mathbf{Res}}$: Restraint Current of differential relay 87T

$\boldsymbol{U_s}$ $\boldsymbol{U_s^*}$ $\boldsymbol{U_0^*}$: The representation of three phase voltage in space vector domain

U_a U_b U_c : Instantaneous voltages in abc frame

U_α U_β : Two perpendicular signals transferred by Clarke Transformation

I_a I_b I_c : Instantaneous currents in abc frame

I_0 : Zero Sequence Current

I_{rdc} : DC current induced in rotor winding when motor loses power supply

δ : Load Angle of Synchronous motor

Glossary

ATP-EMTP Alternative Transient Programs- ElectroMagnetics Transient Programs

MBT Motor Bus Transfer

ABT Automatic Bus Transfer

CB Circuit Breaker

OCC Omicron Control Centre

DFT Discrete Fourier Transformation

IO Input and Output

ANSI American National Standards Institute

MMF Magnetic Motive Force

PLC Programmable Logic Controller

RDFT Recursive Discrete Fourier Transformation

HSBT High Speed Bus Transfer

RTDS Real-time Digital Power System Simulator

GTAO Gigabit Transceiver Analogue Output

GTFPI Gigabit Transceiver Front Panel Interface

Chapter 1

Introduction

1-1 Background and Introduction

A typical chemical plant relies heavily on electricity to supply mechanical equipment, drive electrochemical processes, and implement process controls. The majority of electrical loads in the chemical industries for instance DOW are induction motors which serve for the pumps, fans as well as compressors.

In the absence of protection and control equipment, a power blackout would lead to an uncontrolled shutdown of the process operations. If the process operation involves large quantities of hazardous chemicals, an uncontrolled shutdown can release hazardous chemicals with catastrophic consequences and even contributes to severe explosions. Statistics indicate that electrical faults account for 7%-11% of accidents for chemical industries [1]. A severe blackout may contribute to the losing speed of all motors and the failure of all control units such as PLC and SCADAs. Consequently, it is crucial that a chemical company should maintain the continuity and increase the reliability of power supply.

In order to ensure the reliability of such electrical power plant, a network with an auxiliary power supply is designed (main-tie configuration). During the fault, motor buses require a transfer from a present feeder to an auxiliary feeder. A simplified diagram of the motor bus transfer (MBT) system is shown in figure 1-1.

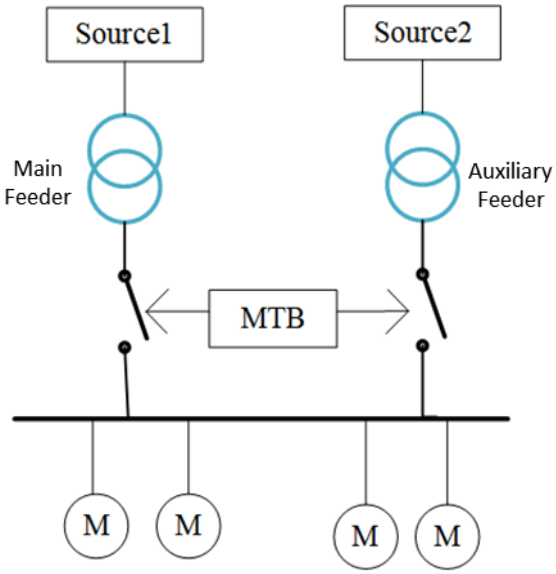

Figure 1-1: A Motor Bus Transfer System with Main-Tie Configuration

The motor bus transfer (MBT) schemes are employed to maintain the continuity in processes served by aggregates of motors. Following an event such as the generator trip, all the motors which connect with the feeder bus are disconnected from their main power source and shift to the auxiliary bus (healthy feeder). However, if there is no intelligent electronic device to control such transfer, the re-closing of the breaker in the auxiliary bus would contribute a large inrush current and torque which reduces the lifetime of all motors. Based on that, the fast transfer (high speed bus transfer) relay has been designed. Such relay has some significant benefits: the disruption (transfer time) is quite short to ensure the continuous operation of the critical loads, and more importantly, the fast transfer relay can decrease the large transient current and torque of induction motors when a motor transfer happens. The secure transfer is realized by monitoring the difference of voltage magnitude U_{diff}, phase angle $d\theta$ and frequency df between motor bus and feeder bus. If those three parameters fulfill particular thresholds, the breaker of the healthy feeder (auxiliary feeder) will close and motors are transferred successfully.

1-2 Literature Review

The bus transfer system has been analyzed and employed for a long period of time and the first research paper on motor bus transfer was published in 1950 by Lewis and Marsh [2]. They gave a basic understanding and modelling of a bus transfer based on statistically analyzing the behavior of motors. Walter [3] indicated that the first 0.5s are the most critical time period for bus transfer by determining the auxiliary bus voltage and angle from the dynamic equivalent circuit of a single motor. Yeager [4] presented the result of multi-motor transfer behaviors in several conditions by transient stability analysis method. Beckwith and Hartmann [5] in 2005 used an experimental way to analyze the voltage behavior of motor bus during transfer and suggested that the decaying rates of the residual voltage magnitude and frequency depend on various factors including the type and size of the motors, combined

inertia and open-circuit time constant of the motors, and motor loads.

After the 2000s, more research was focused on the automatic bus transfer (ABT) system design. Murty [6] from Beckwith electric company addressed the design of both hardware and transfer algorithm of a high-speed motor bus transfer relay. That paper elaborated the motor bus transfer scheme which includes fast, in phase and residual transfer mode and proposed an adaptive time window Discrete Fourier Transform (DFT) algorithm for both frequency and phase angle measurement. This was realized by changing the sampling rate and decreasing the error of conventional DFT method when frequency deviates from the nominal value.

As illustrated in chapter 1-1, the frequency should be measured continuously after the breaker in fault bus trips to ensure a successful motor transfer and therefore, many researchers developed different frequency measurement method. The most intuitive method for frequency tracking is zero-crossing where the frequency is measured based on the time interval of two zero crossing point [7]. However, such method will lose frequency information during one measurement circle, and Begovic [8] designed a modified method to enhance the accuracy. E. Aboutanios [9] adopted Clarke transformation which represented the three-phase single by one phasor and decomposed such vector into 2 orthogonal planes to track the frequency. V.Eckhardt [10] proposed a method which use PLL (Phase Lock loop) to track the frequency, which can achieve high accuracy in quasi-steady state. However, the time delay of the PI controller introduces measurement error in dynamic measurement with steep frequency changes. Furthermore, Pony method and Smart DFT method were elaborated by J.Z.Yang [11] and T. Lobos [12] for more accurate frequency tracking with existing of high order harmonics, but such method requires a high computational complexity and RAM storage.

Except for the scientific study, industries have also developed some standards for motor transfer. The ANSI (American National Standards Institute) published standards in 1978 for fast transfer criterion C50.41-2000 [13] which suggests that the resultant voltage vector per frequency $\frac{U_{diff}}{freq}$ (the voltage phasor difference between motor bus and incoming bus divided by instantaneous frequency) should not exceed 1.33 PU. The testing of the MBT relay was shown by Thomas R. [14]. The Beckwith relay has been tested, and the relay setting has been proposed for general power plants. Case studies of a number of live MBTs were presented and analyzed, and finally, a transfer metric has been shown based on the transfer mode and transfer time.

1-3 Objectives

Although a lot of research has been done for the motor bus transfer, most of those studies were mainly focused on the transient simulation of the system. Only a few papers are referred to the fast Transfer relay testing. However, the fast relay testing only gave the general result based on simple testing cases instead of the fault recording from power system simulations. Besides, the previous testing designed by other engineers only focused on the transfer mode and transfer time of the fast transfer relay and gave no testing results about transient torque behavior of motors controlled by the relay. Hence, this thesis combines both relay testing of Siemens fast transfer relay and transient torque behavior analysis of induction motors by

building EMTP models of the DOW Tarragona.

The research objectives of the thesis are listed as follow:

1. Studying and understand the basic theory of fast transfer relay;
2. Building an EMTP model for the testing signals generation and system dynamics study;
3. Designing the testing setup for fast transfer relay testing;
4. Selecting a proper setting of the fast relay 7UV68 and test the relay based on the testing requirements.

1-4 Research Methodology

The whole project is performed in 4 steps. First, the basic transfer scheme and theory should be analyzed to make preparation for the system modelling and testing setup design. Then, in order to have the analog signals (voltage and current signal) and binary signals (breaker position and auxiliary input) which act as the relay input, the power system of DOW South Tarragona with protection relays (over-current and differential relays) need to be modelled and configured in ATP-EMTP to get different dynamic fault signals. Third, the testing setup should be developed with a combination of software (Omicron Control Center) and hardware (Omicron CMC356, CMS156, Siemens Logo PLC) configuration. Finally, the testing results (transfer time and transfer modes) recorded by Omicrons will be re-applied to the EMTP simulation to analyze the transient inrush torque of all induction motors a when the breaker in reference feeder closes.

1-5 Thesis Layout

There are six chapters in this thesis:

Chapter.1: Introduction:

This chapter addresses the importance of fast transfer relay for industries and highlights the previous studies about the fast transfer system. Then the objectives of the thesis are introduced, followed by the thesis layout.

Chapter.2: Basic theory of fast transfer:
This chapter gives a brief illustration of fast transfer relay. First, the motor behavior when losing power supply is analyzed by the space vector method, followed by the introduction of typical transfer scheme of motor transfer relays. Finally, the Siemens fast transfer relay 7UV68 is introduced.

Chapter.3: DOW Tarragona power plant modelling:
This chapter mainly illustrates the power plant modelling in DOW Tarragona. First, the power network including electrical loads, transmission and distribution grids is modelled. Then, to acquire suitable analog and binary signals for the fast transfer relay testing, the measurement instruments and auxiliary relays are modelled. Finally, to analyze the testing results, the real-time amplitude, phase angle and frequency of voltages in both motor bus and reference feeder bus are measured.

Chapter.4: Testing Setup Design:
This chapter focuses on the testing setup design for fast transfer relay testing. The hardware setup and software configuration of the testing are illustrated in detail.

Chapter.5: Fast transfer relay testing:
This chapter elaborates detailed testing results of fast transfer relay based on the EMTP model of DOW Tarragona. In this chapter, the test requirements are shown at the beginning. Next, the relay settings based on the testing requirements are configured. The testing results including the transfer mode, the transfer time and the inrush torque of each fault scenarios are shown in this chapters. Finally, sensitivity testing on both tripping delay of 87T and communication delay are proposed, and the most severe cases for motor bus transfer can be examined.

Chapter.6: Conclusion and Future Work
This chapter makes an overall conclusion based on previous chapters and gives recommendations for future research.

Chapter 2

Basic Theory of Fast Transfer 7UV68

2-1 Introduction

When talking about a fast transfer relay, two things should be clear: what is the motor bus transfer and why the fast transfer relay is needed. As the brief introduction in chapter 1 shows, motor bus transfer relays transfer all motors from fault feeder to the healthy bus, but why it is not possible to transfer the motors by manually open the fault feeder and close the auxiliary feeder. This chapter elaborates the significance of fast transfer relay by showing the motor behaviours during transfer. Besides, an introduction about the testing object, Siemens fast transfer relay 7UV68 in this thesis will be introduced.

2-2 Motor Behaviors during Motor Bus Transfer

In industry companies such as DOW, a majority of mechanical loads are pumps driven by induction motors. As figure 1-1 shows, when feeder 1 encounters contingencies such as a single phase fault, the breaker CB1 should trip to cut the fault from the source. Therefore, all induction motors will lose power supply. It is essential to understand the motor behavior in such open circuit period.

To simplify the problem, we only consider the condition where a single induction connects to an infinite bus. As the schematic of induction motor shows (figure 2-1), typical induction motors have two winding groups stator windings and rotor windings. The three windings phase have a 120° shift in space. When a symmetrical 3 phase AC voltage applies to such three phase windings, a rotating magnetic field will be generated. The relative movement between rotating magnetic motive force F_1 and rotor windings induces a current in rotor winding. With the help of the rotating field and induced current, the induction motors can generate torques.

If the power source of a single induction motor trips, the stator current of the motors disappears immediately, and the MMF (magnetic motive force) F_S generated by stator current disappears simultaneously. However, based on the magnetic theory, the magnetic flux density B generated by three-phase current cannot change immediately. Therefore, to maintain the magnetic flux density, the rotor winding should induce a DC current which compensates the vanishing of stator current.

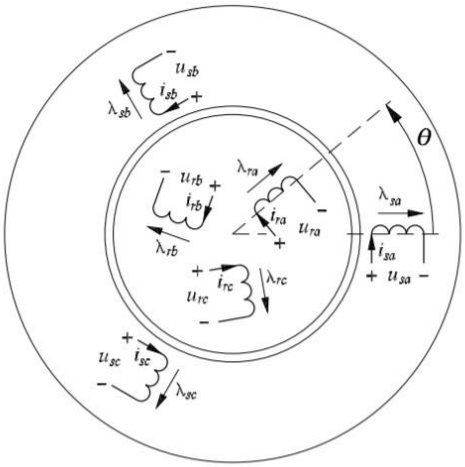

Figure 2-1: The schematic diagram of the induction motor [15]

Some books and studies [5] [15] indicate that the DC rotor current decays by the rotor winding time constant $T_r = L_r / R_r$. The MMF generated by the decaying DC rotor current F_r has a relative rotation speed ω_r (mechanical speed of rotor) with the stator. Therefore, the stator winding can induce a voltage called motor residual voltage U_{res}. When the motors lose power supply, the air gap torque of the motor becomes to zero as there is no electrical power input. Therefore, the rotation speed will decrease because of the drag force of the mechanical load. With the decaying amplitude of the dc rotor current I_{rdc} and rotor rotation speed ω_r, the amplitude and frequency of motor residual voltage will decay. However, until now, there are no anayltical solutions for the motor behavior after an open circuit of a running motor. Therefore, this thesis derives the anayltical solutions for an open-circuit of a single motor.

Some assumptions should be made before solving those equations: the magnetic saturation and eddy current are neglected. In order to represent the three phase voltages by one parameter, a space vector method has been developed in the book [15]. The three-phase voltages in abc domain are converted into the space vector coordinate by equation 2-1.

$$\begin{bmatrix} \mathbf{u}_s \\ \mathbf{u}_s^* \\ \mathbf{u}_{s0} \end{bmatrix} = \frac{2}{3} \begin{bmatrix} 1 & a & a^2 \\ 1 & a^2 & a \\ \frac{1}{2} & \frac{1}{2} & \frac{1}{2} \end{bmatrix} \begin{bmatrix} u_a \\ u_b \\ u_c \end{bmatrix} \tag{2-1}$$

In equation 2-1, $a = e^{j120^\circ}$, $a^2 = e^{j240^\circ}$ are the constants of space vector transformation. The instantaneous voltage u_a, u_b and u_c are converted to voltage space vector $\mathbf{u_s}$. $\mathbf{u_s}^*$ is the conjugate of the voltage vector $\mathbf{u_s}$ and can be ignored. $\mathbf{u_{s0}^*}$ is the zero sequence voltage which can be neglected in symmetrical conditions.

Based on the same transformation, we can convert the current and flux linkage in the space vector domain. Based on Faraday's law, we can have both the rotor and stator voltage equation in space vector domain:

$$\begin{aligned} \mathbf{u_s} &= R_s \mathbf{i_s} + \frac{d\boldsymbol{\Psi}_\mathbf{s}}{dt} \\ \mathbf{u_r} &= R_r \mathbf{i_r} + \frac{d\boldsymbol{\Psi}_\mathbf{r}}{dt} \end{aligned} \tag{2-2}$$

Where $\boldsymbol{\Psi}_\mathbf{s}$ and $\boldsymbol{\Psi}_\mathbf{r}$ are flux linkages in stator and rotor winding.

Such flux linkages are calculated by self-inductance and mutual inductance.

$$\begin{aligned} \boldsymbol{\Psi}_\mathbf{s} &= L_s \mathbf{i_s} + M_m \mathbf{i_r} e^{j\theta} \\ \boldsymbol{\Psi}_\mathbf{r} &= L_r \mathbf{i_r} + M_m \mathbf{i_s} e^{-j\theta} \end{aligned} \tag{2-3}$$

Where M_m is the mutual inductance between rotor and stator; L_s and L_r are the self-inductance of stator and rotor respectively; θ is the angle difference between the rotating rotor frame and stator frame which is equal to $\theta = \omega_r t$; ω_r is the mechanical speed of the motor.

If we convert the rotor side parameters into the stator frame then we have:

$$\begin{aligned} \boldsymbol{u}_r^{'} &= \boldsymbol{u}_r e^{j\theta} \\ \boldsymbol{i}_r^{'} &= \boldsymbol{i}_r e^{j\theta} \\ \boldsymbol{\Psi}_r^{'} &= \boldsymbol{\Psi}_e e^{j\theta} \end{aligned} \tag{2-4}$$

Where the $\boldsymbol{u}_r^{'}, \boldsymbol{i}_r^{'}, \boldsymbol{\Psi}_r^{'}$ represent the rotor quantities in the stator frame.

Applying equation 2-4 to 2-2 and 2-3 respectively, we can have the voltage and flux linkage equation respectively:

$$\begin{aligned} \mathbf{u_s} &= R_s \mathbf{i_s} + \frac{d\boldsymbol{\Psi}_\mathbf{s}}{dt} \\ \mathbf{u}_r^{'} &= R_r \mathbf{i}_r + \frac{d\boldsymbol{\Psi}_r^{'}}{dt} - j\omega \boldsymbol{\Psi}_r^{'} \\ \boldsymbol{\Psi}_\mathbf{s} &= L_s \mathbf{i_s} + M_m \mathbf{i}_r^{'} \\ \boldsymbol{\Psi}_r^{'} &= L_s \mathbf{i}_r^{'} + M_m \mathbf{i_s} \end{aligned} \tag{2-5}$$

If the power supply is tripped, the three-phase current becomes 0, which means $\mathbf{i}_s = 0$, and since the rotor winding is short-circuited (rotor voltage is zero), $\mathbf{u}_r' = 0$ and equation 2-5 changes to:

$$\mathbf{u}_{im} = \frac{d\boldsymbol{\Psi}_s}{dt}$$
$$0 = R_r \mathbf{i}_r + \frac{d\boldsymbol{\Psi}_r'}{dt} - j\omega_r \tag{2-6}$$

Suppose the motor was tripped at t_0, and the rotor current at that moment is I_{rt0}. Based on the first order response of LR circuit, current flows the rotor can be derived as:

$$\mathbf{i}_r' = I_{rt0} e^{\frac{t-t_0}{Tr}} e^{j\theta} \tag{2-7}$$

Where $Tr = \frac{L_r}{R_r}$ is the time constant of rotor winding (a RL circuit).

Combining equation 2-6 and 2-7, we can have the analytical solution of residual voltage for a single induction motor:

$$\mathbf{u}_{im} = M_m I_{dc0} e^{\frac{t-t_0}{T_r}} (jw_r - \frac{1}{Tr}) e^{j\omega_r t} \tag{2-8}$$

Based on the equation 2-8, the amplitude of motor residual voltage for single induction motors is proportional to the mutual inductance of rotor and stator M_m, the time constant of the rotor winding T_r as well as the rotor speed ω_r. The complex notation $e^{j\omega_r t}$ indicates that the voltage vector is rotating is in the space vector coordinate with a rotating speed ω_r. Therefore, the frequency of the residual voltage in abc coordinate depends on the rotating speed.

At the mechanical side, if we assume that the inertia of the induction motor is J, the friction constant is D, and the load torque T_L,we can have:

$$J\frac{d\omega_r}{dt} + T_L + D\omega_r = 0 \tag{2-9}$$

From equation 2-10 we can see that the inertia and mechanical load impacts the rotating speed. High motor inertia and low mechanical load contributes to a slow rotor speed decaying and consequently leads to a slow decaying of voltage frequency.

However, for synchronous motors which have a constant excitation loop, we will have a different expression of motor bus residual voltage. For a synchronous motor with a constant excitation, during the open circuit period, we have equation 2-10, where I_f is the constant excitation current:

$$\mathbf{i}_r' = I_f e^{j\theta} \tag{2-10}$$

Applying 2-11 into 2-7, we have:

$$\mathbf{u}_{sm} = M_m I_f (j\omega_r) e^{j\omega_r t} \tag{2-11}$$

From equation 2-11 we can conclude that the magnitude of the motor residual voltage of synchronous motors will also decrease with the respective of decaying rotating speed. However since the excitation current I_f is constant for a synchronous motor, the attenuation $e^{\frac{t-t_0}{Tr}}$ disappears.

Therefore, we can conclude that the residual voltage of a single synchronous motor will decrease slowly than the induction motor. Based on that, the magnitude of residual voltage in a motor bus with both synchronous motors and induction motors delays slower than purely induction motors.

For some power plants such as DOW Tarragona, the induction motors and static loads are connected to the same bus. When losing power supply, the inductions motors generate a residual voltage, and therefore, the static load is supplied by the motor bus residual voltage U_{res}, and the current will flow from the motor groups to the loads. In such cases, the induction motors act as generators and supply electrical power to the static loads. Based on the law of conservation of energy, the electrical power flows through such loads must be converted from the remaining flux, which leads to further decay of flux. Therefore, the residual voltage will decay fast when connecting a static load.

The analytic way is only suitable for a single motor and numerical ways are used to simulate the motor residual voltage with more motors. In this thesis, we use ATP-EMTP to simulate the motor bus residual voltage for mutli-motors with loads (chapter 3).

2-3 Basic Transfer Scheme

For motor bus transfer, both the motor bus residual voltage U_{res} and the feeder bus voltage U_{ref} which acts as the reference for transfer should be measured. Equation 2-8 and 2-11 indicate that both the magnitude and frequency of the residual voltage in motor bus decays. The decaying of frequency contributes to a fast changing of phase angle. Figure 2-2 indicates the phasor diagram of motor bus residual voltage and the reference voltage.

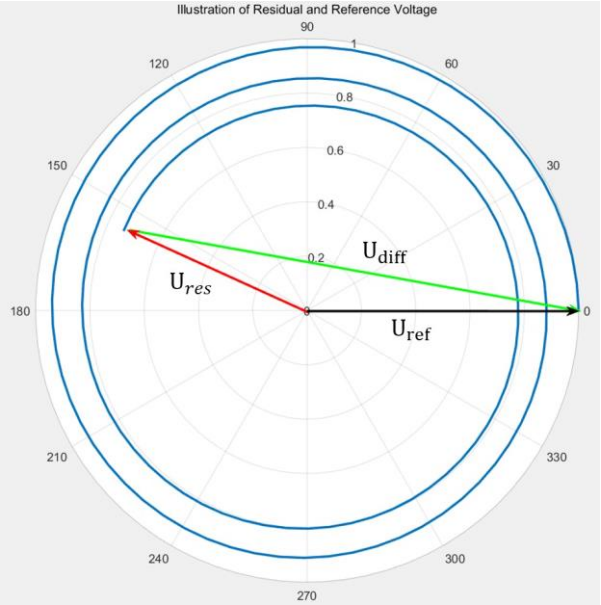

Figure 2-2: Illustration of Residual and Reference Voltage

Suppose at the instant t_0 , the breaker opens (no fault occurs before breaker opens), then the root of residual voltage phasor follows the blue line, with a changing magnitude and initial phase angle. Consequently, the rotating residual voltage phasor U_{res} and stationary reference voltage phasor in auxiliary feeder U_{ref} may lead to a voltage difference U_{diff} which is also called resultant voltage. When motors transfer from fault feeder to auxiliary feeder, the voltage difference contributes to a large inrush current which is usually 8-12 times higher than nominal motor current. [5] The large current may lead to overheating of the stator winding and a large inrush torque which damages the motors' mechanical structure and eventually curtails the lifetime.

To decrease the inrush current and current and limit the damage to the motors, the American National Standards Institute (ANSI) standard C50.41-2000 claims that the resultant voltage should follow the criterion below: $\frac{U_{diff}}{freq} < 1.33(PU / Hz)$.

Here 1 PU represents the nominal line to line voltage of the motor.

Based on the ANSI regulations, an intelligent device called fast transfer relay is designed.

Before talking about the motor bus transfer modes, the breaker switching sequence which plays a significant role in the motor bus transfer should be analyzed. Breaker switching sequence means the operating sequence of running source breaker and an alternative feeder breaker during the whole transfer

Typically, there are three kinds of transfer sequences: parallel sequence, simultaneous sequence and sequential sequence.

1. Parallel Sequence

In parallel sequence transfer, the auxiliary source is already connected to the motor bus before the fault bus is tripped. The aim of the parallel sequence is to initiate a transfer of

all motors without any interruption, so there would be an over-leaping period when both the

two feeder sources connect to the motor bus. However, there would be a small voltage angle difference between two sources. Therefore, a parallel connection of two power source leads to a circulation of power flow in steady state. Besides, the parallel sequence transfer has another significant shortcoming. Once there is a fault, the fault would be fed by both two sources during the over-leaping period which results in an increase of short-circuit current and instability of power system. In practice, such mode is only used for synchro-check of two feeders.

2. Simultaneous Sequence

As the name indicates, in a simultaneous transfer scheme, the trip command is sent to the breaker in faulty feeder, and at the same time, the close command is sent to the breaker in the auxiliary bus. Theoretically, this breaker sequence is the best since there is no blank time that all motors lose power supply for such scheme. In addition, there is no fault feeding from the auxiliary bus. However in practice, if the breaker at the faulty bus takes more time to open (usually occurs due to the arc) or refuse to open, the simultaneous closing of the breaker in auxiliary bus contributes to a fault feeding from two sources and leads to a severe problem. Appendix F shows the parallel operation of two sources when the fault time is longer than the breaker closing time during the simultaneous seqeunce. Besides, appendix F also supplies some basic testing result based on DOW's request.

3. Sequential Sequence

In sequential transfer, the auxiliary source only connects to the motor bus after the tripping of the faulty bus. Sequential sequence deliberately avoids the parallel operation of the two source and will have a blank time that motors lose power supply. In order to avoid the parallel operation of two power sources, the sequential sequence with a more conservative breaker transfer scheme is chosen in this thesis.

Based on the sequential sequence transfer sequence, the fast transfer relay supplies the following transfer modes:

1. Fast Mode

From figure 2-2, we can see that after the breaker trips, the phase difference and voltage amplitude difference $|U_{diff}|$ are quite small at the first 10-100ms. Therefore, the fast transfer scheme attempts to decrease the delta phase angle between feeder bus and motor bus $d\theta$ by minimizing the motor tripping time before transferring to an auxiliary bus. The fast transfer mode requires high speed and accurate phase angle measurement algorithm. Based on the factory testing [16], Siemens proves that when the boundary of the delta phase angle is about 60°, $\frac{U_{diff}}{freq}$ is less than 1PU/Hz. Considering the breaking time of the breaker (usually 50ms), Siemens suggests that the threshold of delta phase angle should be about 20° to 40° and the real-time delta frequency df should be set as 1.0 to 2.0 Hz. As the relay needs time to analyze the faulty signals, the shortest action time is one electrical cycle (20ms). The fast mode is only valid for the first 120ms. A time expiration leads to other transfer modes.

2. Real-time Fast Mode

If fast mode fails (usually most fault cases cannot fulfill the fast mode threshold), then the

relay automatically goes to a real-time fast mode. This mode extends the threshold of the

delta phase angle $d\theta$ to 90° meanwhile the resultant voltage per frequency $\frac{U_{diff}}{freq}$ should be less than 1.33PU/Hz. Besides, the typical setting value of frequency difference d_f ranges from 3Hz to 6Hz.

3. In Phase Mode

If fast transfer and real-time fast mode fail, the device can turn into in-phase transfer mode. As the name indicates, the motor bus residual voltage is almost in phase with the reference voltage, which is pretty good to decrease the inrush current. The typical value of the phase angle difference $d\theta$ is set from 5° to 10° and the typical setting of the delta frequency df is range from 5Hz-10Hz.

4. Residual Voltage Mode

If in-phase mode fails, then the relay would change to the residual voltage mode. In this mode of transfer, the motors are transferred if the amplitude of the motor bus voltage A_u reaches a low value to prevent motor damage. However, it takes a very long time for the motor bus residual voltage to decay to a low value. In this case, we do not care about the phase angle difference since the magnitude of the motor bus voltage is relatively low. The typical setting of A_u is from 0.2 PU to 0.3 PU. However, it is crucial for motors transferring in this mode, as in such transfer mode, the motor speed would be quite low and stalling would occur for system with a very low inertia. Besides, the long transfer time (typically 300-600ms) would interrupt the continuous chemical process.

5 Long-Time Mode

If all previous modes fail due the to the software or hardware problem of the relay itself (usually not possible), the long-time mode which acts as the final backup would be initiated and the system will transfer to the auxiliary bus after 2s. The figure 2-3 summarize all transfer modes:

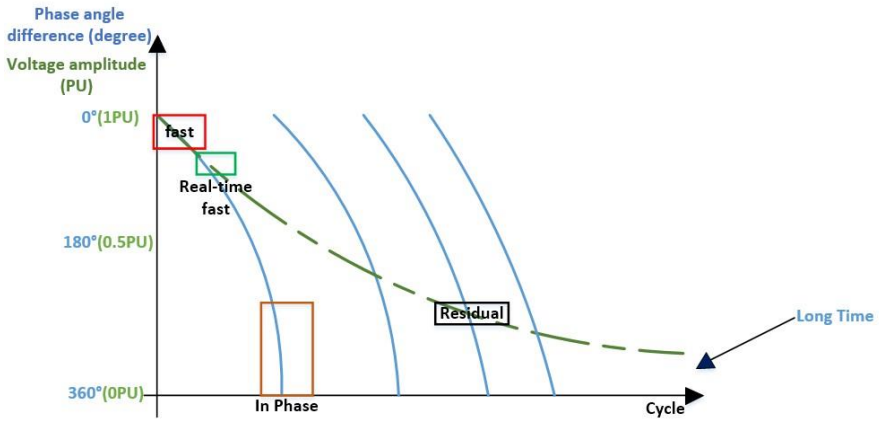

Figure 2-3: Illustration of Different Transfer Modes

2-4 Introduction of Fast Transfer 7UV68

The relay 7UV68 (testing object) is a Siemens fast transfer device, which is designed for a very fast motor bus transfer with rotating motors. The relay can be used for main-tie and main-tie-main configuration with 2 or 3 CBs respectively. The integrated programmable logic (CFC) allows the users to design and implement new functions. The communication interfaces follow the IEC 61850 standard with Ethernet and Profibus-DP [16]. The Siemens relay contains all transfer modes which are illustrated in chapter 2-3 and the users can activate only one mode or make a combination of different modes in the relay setting. Except of the basic motor transfer function, the relay also has an overcurrent protection for the tie-breaker in the main-tie-main configuration (not in this thesis).
To initiate a successful transfer, the fast transfer relay requires three types of signals: analog signals, breaker states and auxiliary binary signals. To analyze the fault signals, both the feeder bus and motor bus voltage should be measured by such relay. The current signal in feeder bus should be sent to 7UV68 by current transformers. Besides, the relay also needs to know the exact state of breakers in two feeder buses. In addition, the relay requires two essential binary signals (initiation signal and blocking signal). The initiation signal is sent to the fast transfer relay to initiate a transfer for feeder bus faults. When a fault occurs in the motor bus, it is meaningless to initiate a transfer and a blocking signal should be sent to fast transfer relay and block the transfer.

The rate values of the relay inputs are shown in figure 2-4.

Auxiliary voltage:	24-48 VDC, 60-250 VDC, 115/230 VAC
Tolerance	+20 %, -20 %
Rated voltage	80 ~ 125 VAC (U_n)
Rated current	1/5 A (I_n)
Rated frequency	50/60 Hz
Overload capability:	
Current overload capability	4*I_n continuous
	30*I_n for 10 s
	100*I_n for 1 s
Voltage path overload capacity	230 V continuous
Power consumption:	
Current	Approx. 0.3 VA (I_n=5 A)
	Approx. 0.05 VA (I_n=1 A)
Voltage	Approx. 0.10 VA/Phase
Power Consumption:	Quiescent, Approx. 8 W
	Energized, Approx. 15 W

Figure 2-4: Rate Input of the relay 7UV68 [16]

Chapter 3

Network modelling in DOW Tarragona South

3-1 Introduction

In order to perform the testing of 7VU68, the chemical plant in DOW Tarragona should be modelled properly to ensure that the testing signal generated from the simulation (analog and binary signals) can reflect the dynamic behavior of the DOW power plant during all kinds fault. The modelling consists of three parts. The first is the power network modelling of transmission and distribution grids. Then, to acquire accurate binary signals for relay testing, the auxiliary relays are modelled. Finally, to configure the relay setting and to analyze the testing result, the real-time amplitude, phase angle and frequency of voltages in both motor bus and reference feeder bus are measured by Clarke Transform and Zero-Crossing method respectively.

3-2 Network Description

As figure 3-1 indicates, the Tarragona South site has a single feeder with a transfer capability to a second feed. The DOW process plant is connected to the 25kV bus with a fast transfer relay which controls the switches of the two 25kV feeders. Such two 25kV feeder bus is connected to the 230kV transmission grid via 2 transformers 'TP' and 'TR'. In 2015, a large generator connected directly to the tertiary winding of the transformer TP. However, such a generator has been already removed. Consequently, the tertiary winding of TP can be regarded as an open circuit. Besides, the dynamic behavior of motor bus voltage will not be affected by the generator after breaker opens.

Figure 3-2 is a brief indication of the distribution network of DOW plant. The 6kV buses all connect to the 25kV motor bus by 25/6kV transformers. Normally, the tie-switches of the 6kV bus are open. Except for aggregation of small power induction motors, four large synchronous compressors are running on the 6kV.

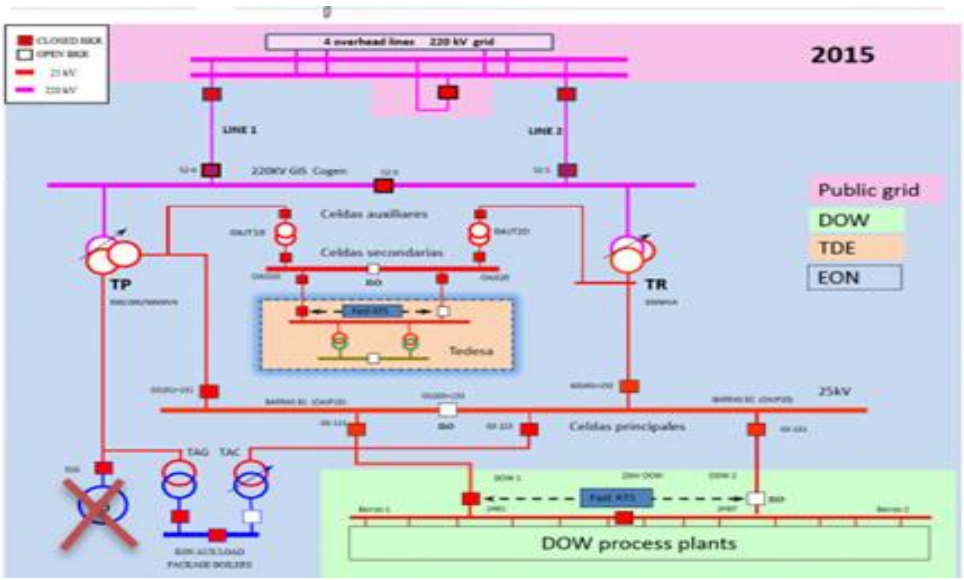

Figure 3-1: The Transmission Network in DOW South Tarragona

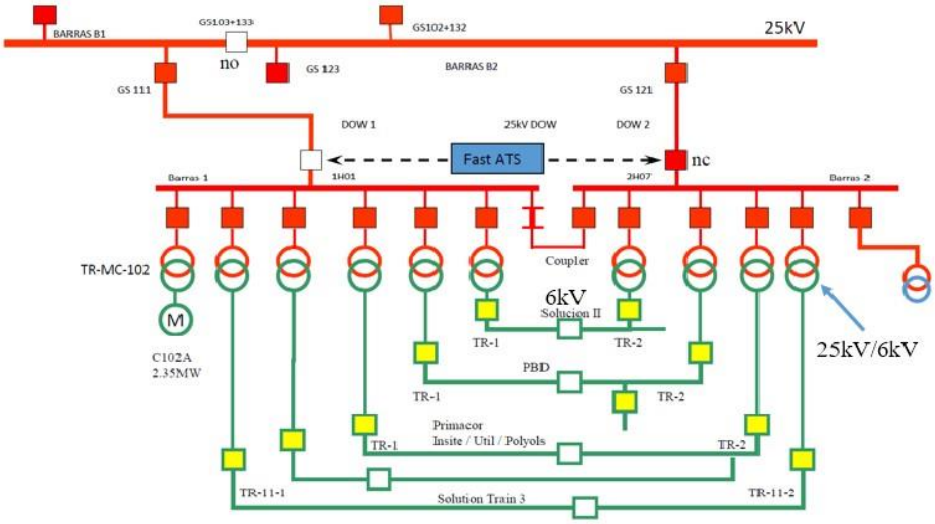

Figure 3-2: The Distribution Network in DOW South Tarragona

3-3 Transmission and Distribution Network Modelling

3-3-1 The 230kV Transmission System Modelling

Since in this thesis the voltage behavior in the 25kV bus are emphasized, the transient and dynamic process of the 230kV transmission system is not taken into consideration. In order to decrease the computational complexity and simplify the modelling system, such a transmission system can be regarded as a swing bus. More specifically, the swing bus can be modelled by an infinite power source with RL coupled lines. In ATP - EMTP such a line model requires the positive and zero sequence resistance and inductance R_0, L_0 R_1 and L_1 as the input parameter.

The equivalent impendence seeing from DOW plant side to transmission grid is given by DOW (figure 3-3):

Equivalent Impedance of Transmission Grid Nominal Voltage : 230kV Voltage Correction Factor : 1.1				
3 Phase Fault level (kA)	Positive Seqeunce impedance(%)		Zero Seqeunce impedance(%)	
9.109	R1	X1	R0	X0
	0.0162	3.03	0.0792	1.78

Figure 3-3: The Short Circuit Level of 230kV Transmission Grid

The value of the sequence impedance can be calculated as follow:

$$Z_{base} = \frac{U_n^2}{S_{base}} = 529\Omega \tag{3-1}$$

And based on the base value we can have that: $R_1 = 0.162\% * 529 = 0.85\Omega$ and then we have $L_0 = 9.42\Omega$ $R_0 = 0.42\Omega$ and $L_1 = 15.87\Omega$ can be calculated. In order to increase the convergence of the modelling, a large resistor ($10^7\,\Omega$) is added, and the model of the 230kV bus is shown in figure 3-4:

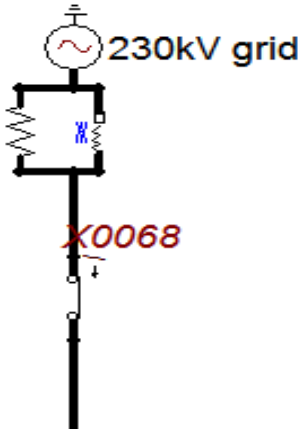

Figure 3-4: The 230kV Transmission Grid Model

Then a validation of the short circuit level can be made. Based on IEC 60909 and considering the voltage correction factor, the theoretical short-circuit current can be calculated by: $I_{short} = \frac{9.1}{1.1} = 8.3KA$. From figure 3-5, it can be seen that the RMS value of short circuit current in simulation (three-phase fault) is the same as the calculated value.

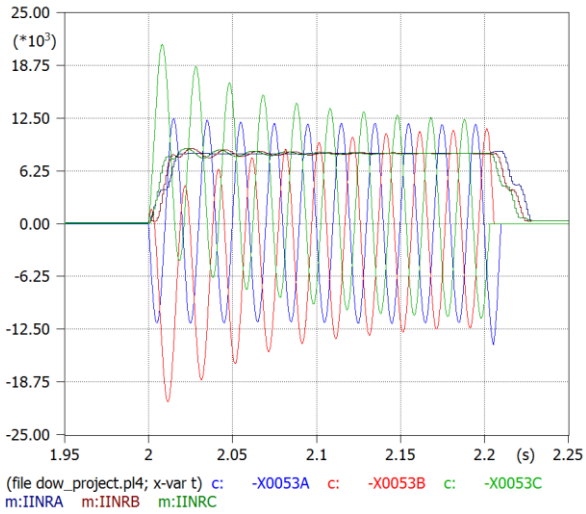

Figure 3-5: Simulated Short Circuit Level in 230kV Bus for Three Phase Fault

3-3-2 Cable Modelling

In this thesis, cables are modelled by a combination of uncoupled RLC components, where resistors represent the 50Hz ac resistance, and the inductors represent the impendence of the cable under power frequency. The cable data are shown in Appendix B.

3-3-3 Transformer Modelling

The transformers in DOW plant are shown in table 3-1:

As the table indicates, there are nine two-winding transformers and 2 three-winding transformers. In ATP-EMTP software, there are a variety of transformer models which can be chosen such as the ideal model and BCTRAN model. Considering the accuracy and the transformer data given by DOW, BCTRAN models can be used.

Table 3-1: The Transformer Data

Bus name	Transformer Type	Grounding resistors (Ω)
PDB-3 (A and B side)	25/6kV 14MVA uk 7.2% DYn5	11 (low voltage side)
Train-1 (A and B side)	25/6kV 10MVA uk 9% DYn11	11 (low voltage side)
Train-2 (A and B side)	25/6kV 10MVA uk 8.8% DYn11	11 (low voltage side)
Train-3 (A and B side)	25/6.3kV 20MVA uk 10% DYn11	11 (low voltage side)
Train-MC102	25/6.3kV 2.6MVA uk 11.5% DYn11	11.5 (low voltage side)
TP	230±12%/26/19kV 500/200/500MVA YNyn0d1	24 (low voltage side)
TR	230±15%/26.5/6.8kV 230/230/25MVA YNyn0d1	24 (low voltage side)

The representation of transformers in the BRTRAN models can be described by a combination of branch resistance and inductance matrices [R] and [L]. In this modelling the power transformer is under 50Hz power frequency. The transformer equation of BCTRAN model can be written as: [V]=[R][i]+L[di/dt].

Figure 3-6 shows the input data of a BCTRAN transformer model.

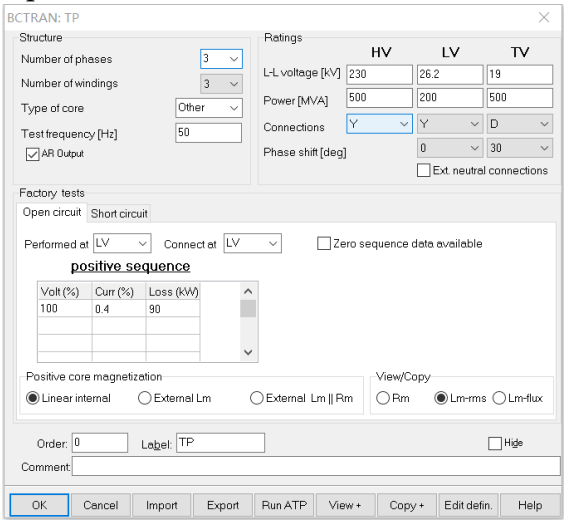

Figure 3-6: Input Data of BCTRAN Transformer Model

Except for the nominal voltage and rate power, the short circuit and open circuit parameters which determine the performance of a transformer are also required in ATP-EMTP. Usually, those data are given by the factory test. Beside in BRTRAN models, the non-linear B-H curve can also be added to the simulation in order to analyze the saturation effect. However, in this thesis, the non-linear character is not considered in the EMTP simulation, as the non-linearity of iron core of transformers cannot affect the short-circuit behavior of the power system.

Besides, the ground resistors of the transformers plays a significant role when ground fault occurs. The grounded resistors of TP and TR in the transformer low voltage winding limits the single phase fault current at 600A RMS value (as figure 3-7 indicates), which impacts the transient performance during and the protection design.

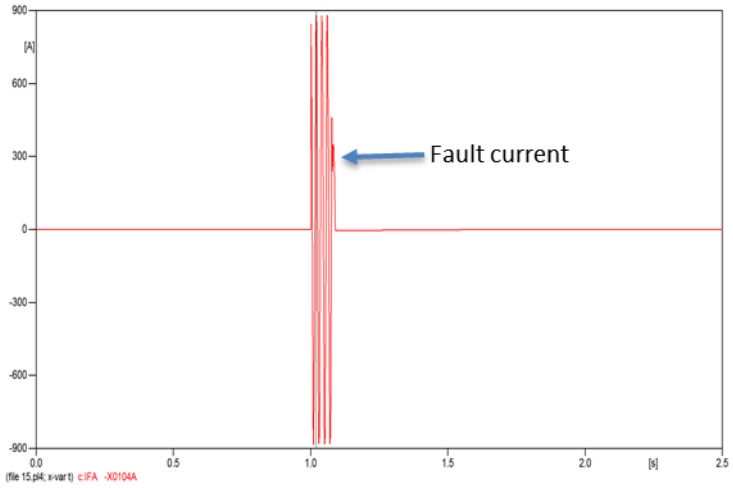

Figure 3-7: A single-Phase Fault in Transformer Low Voltage Winding

3-4 Electrical Load Modelling

There are four kinds of electrical loads in DOW Tarragona: static loads, reactive loads, induction motors and four large synchronous motors. The load data can be found in Appendix B.

3-4-1 Static Load and Capacitor Modelling

Based on the load files given by DOW, the static load can be modelled. The static load can be modelled by a combination of resistors and inductors which represent the active power consumption and reactive consumption of the static loads respectively. Taking static load A in bus 'PDB-3' as an example, the value of the resistors and the inductors can be calculated by two simple equations:

$$R = \frac{U^2}{P} \tag{3-2}$$

$$L = \frac{U^2}{100\pi Q} \tag{3-3}$$

The static load can be modelled as shown in figure 3-8 and the power consumption can be validated by the load data in appendix.

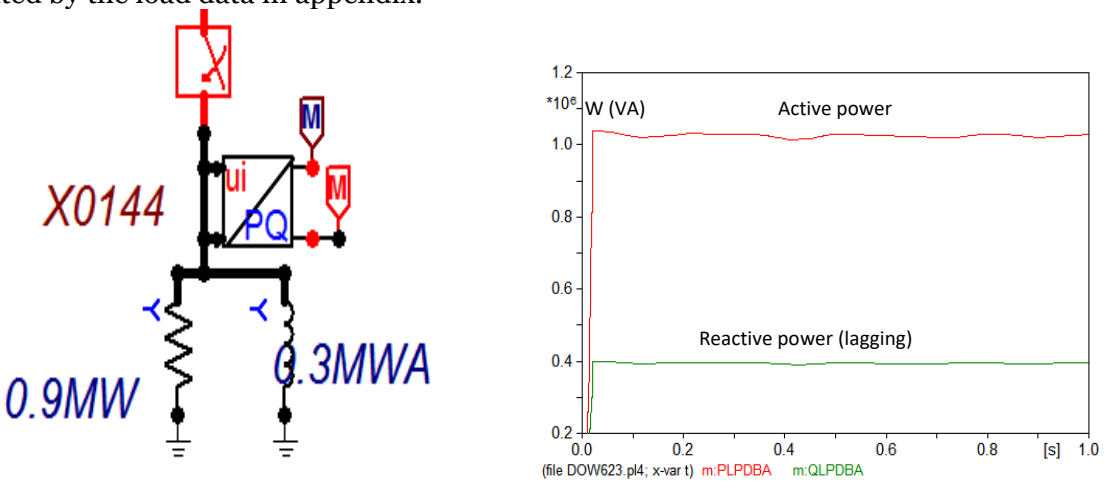

a.The Static Load Model b. The Active and Reactive Power of Static Load

Figure 3-8: The Static Load Model and Result Validation

Besides the static load, there are some capacitors in the DOW power plant. Those capacitors which act as reactive power sources are used to improve the power factor of the system. Usually, those capacitors are disconnected from the system and should be connected if the power system faces a lack of reactive power.

3-4-2 Induction Motor Modelling

Induction motors account for the majority of electrical loads in chemical industries. Typically, the motors used in DOW industries are single cage induction motors. However, in EMTP, there are no single cage induction models. Therefore, in this thesis, the universal motor model with double rotor cages is used. Although the motor structures are different, the universal motor models can have the same dynamic performance as single cage induction motors by choosing suitable motor parameters.

The following industrial motor data (figure 3-9) can be used to simulate the dynamic behavior of single cage motors by using universal motor model.

Inrush Current	6I/In
Pf	85%
LR(lock rotor) pf	20%
LR torque	100%
Max Torque	230-250%
Efficiency	96%
Slip rate	0.6%
H(s)	1s or 2s

Figure 3-9: The Typical Data of Industrial Induction Motors

Since those electrical parameters of induction motors are unknown, a Matlab toolbox "asynchronous motor parameters estimation" can be used to obtain all the electrical parameters. The electrical parameters vector x= (R_s , L_m , R_{r1} , L_{lr1} , R_{r2} , L_{lr2})' can be obtained by a Newton method, which solves six non-linear equation by an approaching way. The estimation function and result are shown in figure 3-10 and 3-11 respectively.

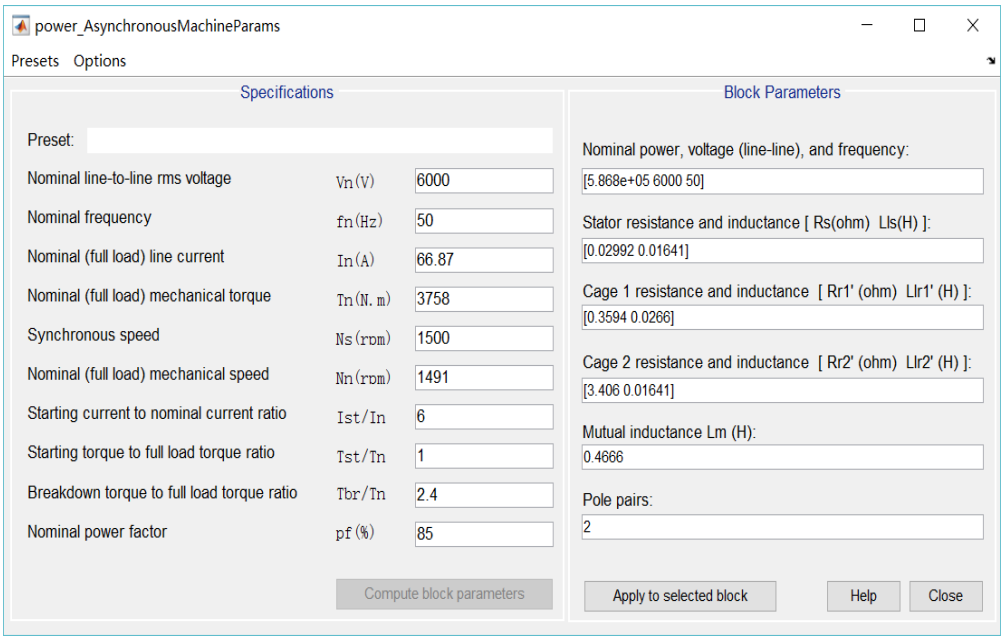

Figure 3-10: The Induction Motor Parameter Estimation

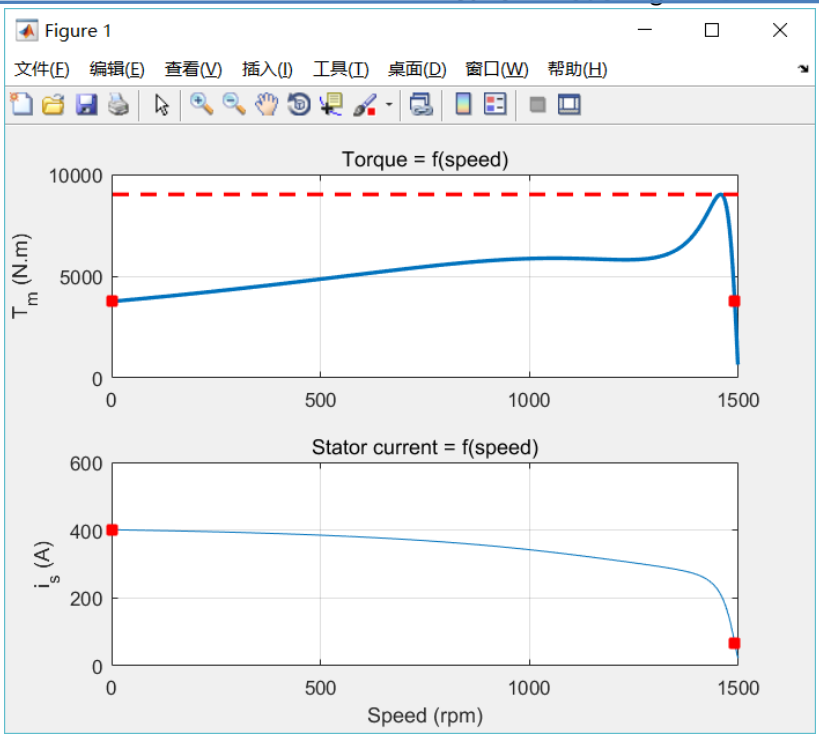

Figure 3-11: The Torque and Current Graph with Speed

From figure 3-11, it is clear that the start torque is the same as the nominal torque and the maximum torque is about 2.5 of nominal torque.

The dynamic model of the induction motor are depicted by the differential equation in 'dq' frame (a rotating frame with rotor speed ω_r).

$$\begin{bmatrix} U_d \\ U_q \\ 0 \\ 0 \end{bmatrix} = \begin{bmatrix} R_s & & & \\ & R_s & & \\ & & R_r & \\ & & & R_r \end{bmatrix} + \frac{d}{dt} \begin{bmatrix} \lambda_d \\ \lambda_q \\ \lambda_r \\ \lambda_r \end{bmatrix} - p\omega_r \begin{bmatrix} \lambda_q \\ \lambda_d \\ 0 \\ 0 \end{bmatrix} \tag{3-4}$$

Where R_a represent the resistor in armature winding, ω_r is the rotor speed, λ_d and λ_q are the flux linkage in dq axis.

The electrical input data of the universal motors in EMTP are shown in figure 3-12 and all input parameters are obtained by a Matlab toolbox.

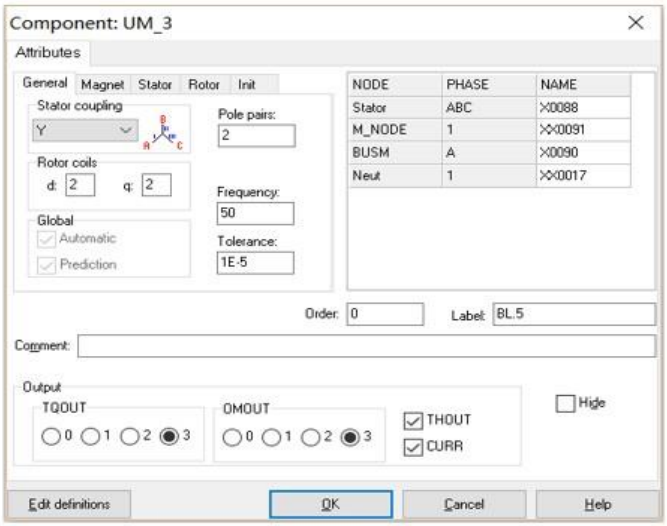

Figure 3-12: Input Data of Induction Motor in EMTP

The mechanical part of the induction motor is modelled in a different way. In the universal motor model, mechanical components must be converted into an equivalent electric network with lumped electric elements R L and C. Those parameters are also treated as the parts of the electric network. The torque is simulated by a current which is injected into the electric network. The table 3-2 indicates the relationship between the mechanical and electrical parameters in the simulation of the mechanical structure.

Table 3-2: The Relationship between mechanical and electrical parameters

Mechanical	Electrical
Torque on Mass (T) [Nm]	Current inject to nodes (I) [A]
Mechanical Angular speed (ω_r) [rad/s]	Node voltage (U) [V]
Angular position of Rotor (θ) [rad]	Capacitor charge (q) [C]
Inertia (J) [kgm^2]	Capacitance (C) [F]
Spring constant (K) [Nm/rad]	reciprocal of inductance (1/L) [1/H]
Mechanical Damping (D) [nms/rad]	Conductance (1/R) [S]

A whole motor both with electrical and mechanical is modelled as figure 3-13:

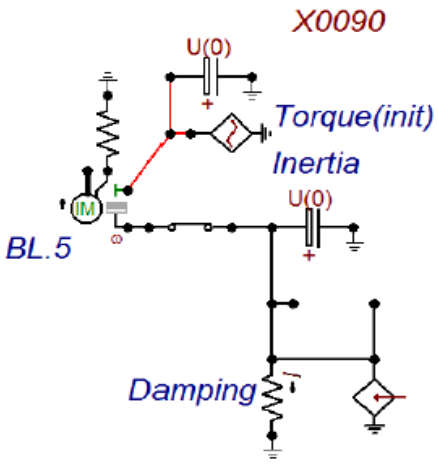

Figure 3-13: The Induction Motor Model

The initial speed of the induction motor is set as the asynchronous speed to decrease transient fluctuation of the motor when the simulation begins. The inertia which plays a significant role in motor bus transfer can be calculated by the inertia H:

$$J = \frac{2HS}{\omega_0^2} \tag{3-5}$$

As the derivation in chapter 2 shows, high overall motor inertia in the system will lead to low decaying of motor bus residual voltage U_{res}.

The mechanical loads of the induction motor are industrial pumps. In practice, for different utilization conditions, the torque curve for pumps are different. There are usually two ways to depict the torque and speed relationship of a mechanical pump: analytically ways which use a look up table and polynomial function fitting [17].

In this thesis, the typical industrial rotary pump curve given by DOW are described by the 3rd order polynomial function with the form like:

$$T_l = A_0 + A_1\omega + A_2\omega^2 + A_3\omega^3 \tag{3-6}$$

The result of the polynomial fitting is shown in figure 3-14:

Figure 3-14: The Load Curve Fitting of Typical Industrial Rotary Pump

After finishing the motor modelling, a validation of the induction motor behavior can be made. The motor speed and torque in steady state are shown in figure 3-15.

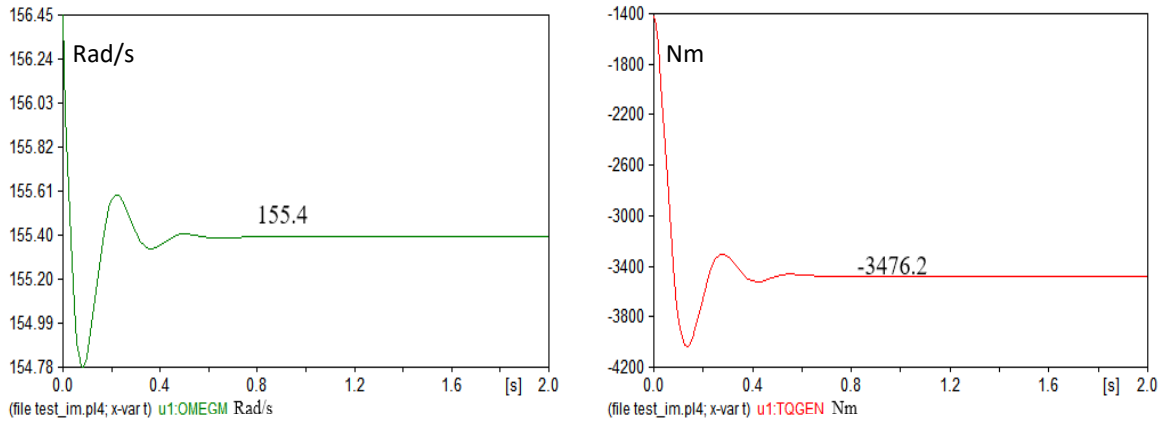

a. Motor Speed b. Motor Torque

Figure 3-15: The Speed and Torque Curve of the Induction Motor

Compared with the nominal torque of motor 'PDB-a' (3758Nm), the steady state torque is lower than the nominal torque. Based on the torque curve (figure 3-14), when the motor runs in asynchronous speed, the mechanical torque is 92.1% of the motor nominal torque and therefore leads to a lower steady state air-gap torque compared with the nominal value.

The start-up of the induction motor can also be simulated to examine the dynamic behavior of induction motors, the simulation results are shown in figure 3-16:

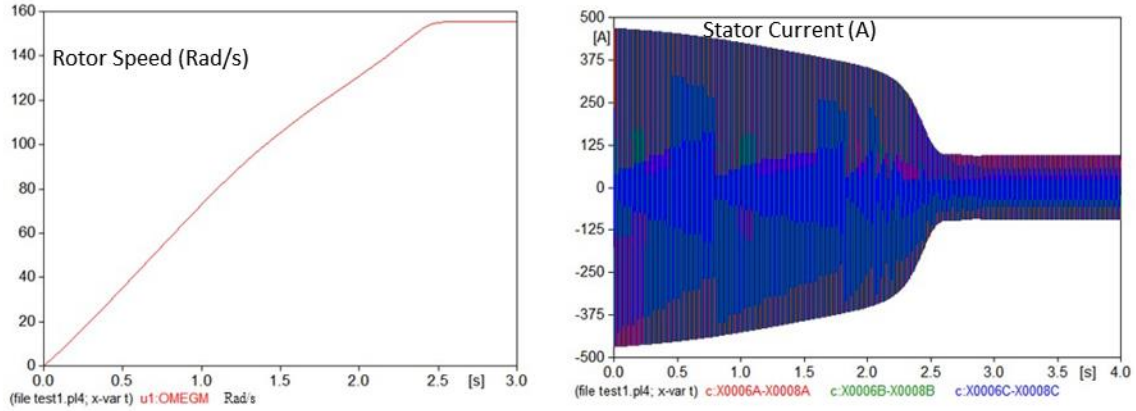

a.Rotor Speed b.Stator Current

Figure 3-16: Speed and Stator Current during Motor Start-up

It can been seen that the startup current is 5.5 times the steady state current and the motor takes 2.2s to reach the steady state which corresponds to the given motor dynamic behavior (figure 3-9).

3-4-3 Synchronous motor modelling

Except for the induction motors, there are four large synchronous motors which drive the compressors in DOW south Tarragona.

The nominal parameters of all synchronous motors are given by DOW, and the nominal power of different motors are listed as follow:

Table 3-3: Load Data of Four Synchronous Motor

Motor name	Nominal Voltage (kV)	Nominal Power (Mw)	Power Factor
MC-102A	6	2.35	0.85
MC-103	6	0.37	0.9
MC-331/341	6	1.6	0.9
MC-331/341	6	7.46	0.95

The main difference between the induction motor and the synchronous motor is as the name indicates, the rotor of synchronous motor operates in synchronous speed (the same speed as the rotating magnetic field). The simple representation (p=1) of salient pole synchronous motor can be schematically depicted in figure 3-17.

The synchronous motor does not rely on the induction effect to produce the rotor's magnetic field and generate the torque. Instead, with the help of rotor field winding which is typically supplied by DC power source, electromagnetic torque can be generated. By changing the excitation, the synchronous motor can both operate in a lagging or leading power factor. By carefully choosing the excitation current, the synchronous motor can have a very high power factor in normal operation.

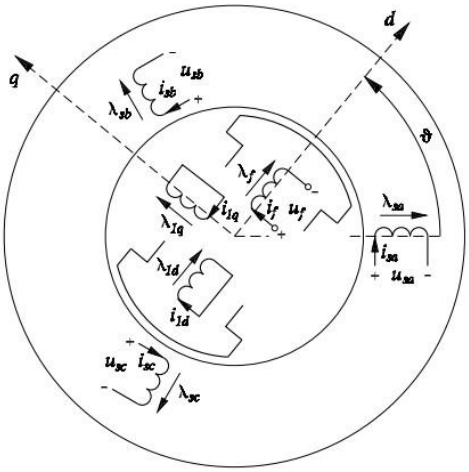

Figure 3-17: Stretch of Synchronous motor [15]

Winding '1d' and '1q' are called damping winding which are used to damp the oscillation during the transient process and with the help of such winding, synchronous motors can start

as an induction motor (short circuit the field winding).

Compared with the induction motors, the synchronous motor has an excitation winding and therefore, the dynamic model of the synchronous motor can be described as follow (d-q frame):

$$\begin{bmatrix} U_d \\ U_q \\ U_f \\ 0 \\ 0 \end{bmatrix} = \begin{bmatrix} R_s & & & & \\ & R_s & & & \\ & & R_f & & \\ & & & R_{1d} & \\ & & & & R_{1q} \end{bmatrix} + \frac{d}{dt} \begin{bmatrix} \lambda_d \\ \lambda_q \\ \lambda_f \\ \lambda_{1d} \\ \lambda_{1q} \end{bmatrix} - p\omega_r \begin{bmatrix} \lambda_q \\ \lambda_d \\ 0 \\ 0 \\ 0 \end{bmatrix} \tag{3-7}$$

In this thesis, we define the open circuit voltage and the motor terminal voltage as E_f and V_t respectively. The angle difference δ between E_f and V_t is called the power angle which determines the active power and reactive power consumption of the motor. Based on the phasor diagram, the active and reacitve power consumption for salient pole motor in steady state has been derived in the book[15]:

$$P = \frac{|V_t E_t|}{X_d} \sin\delta + \frac{|V_t|^2 |X_d - X_q|}{2X_d X_q} \sin 2\delta \tag{3-8}$$

$$Q = \frac{|V_t||E_f|}{X_d} \cos\delta - |V_t|^2 \left| \frac{\sin^2\delta}{X_q} + \frac{\cos^2\delta}{X_d} \right| \tag{3-9}$$

Typically, the load angle δ is quite small for large synchronous motors. By adjusting the load angle δ, different active power consumption P can be obtained. The reactive power Q can be adjusted by changing the excitation field which impacts amplitude of the open circuit voltage E_f.

Compared with the cylinder pole motors, the maximum power point angle for salient pole (small signal stability point) is a bit lower and less than 90 degree due to the salienty. The motor model used in this thesis is S.M 59. The input data of the synchronous motor in EMTP is shown in figure 3-18:

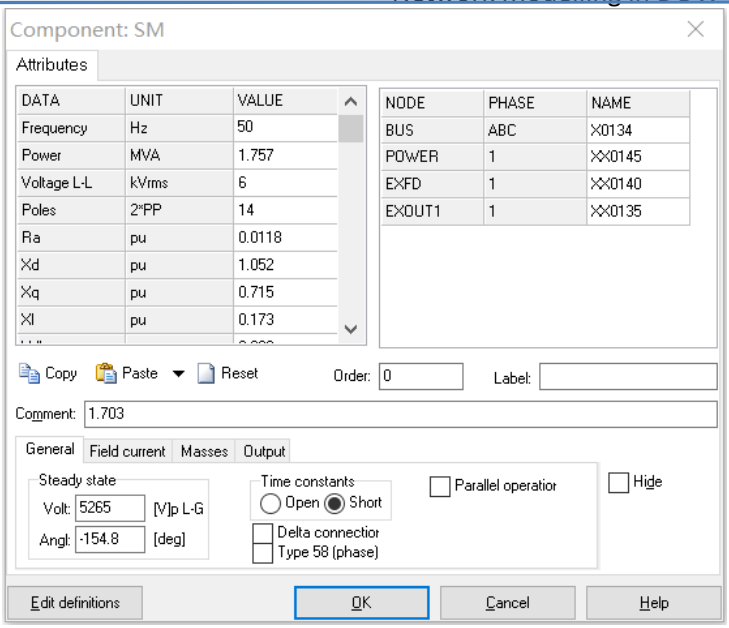

Figure 3-18: Input Data in ATP-EMTP

The excitation of this synchronous motor is a simple DC excitation with under and overexcitation regulator controlled by GTO. The DC voltage input is produced by a three-phase full bridge diode rectifier, which is connected to the 6 kV distribution grid with a 6kV/0.38kV transformer. As the DC excitation is connected to the 6kV bus by transformers, the voltage variation of the motor bus will impact the output of excitation. To simplify the modelling, it can be regarded that the diode in rectifiers are ideal diodes without parasitic capacity and the forward voltages are 0. As the excitation winding is also fed by the 25kV feeder, both the short-circuit and open-circuit of the feeder bus affect the output of motor excitation.

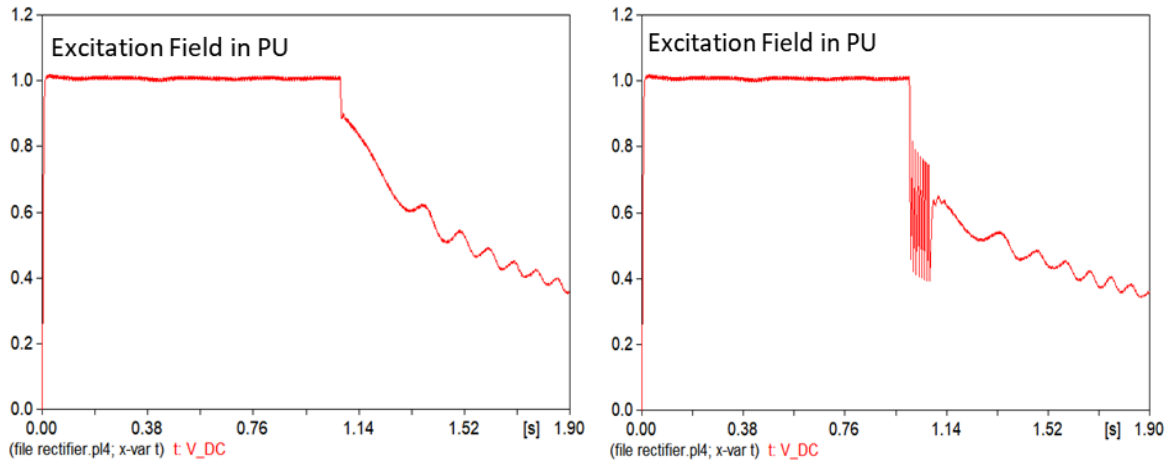

a. Opening Circuit without any Fault b.Open circuit caused by Unsymmetrical Fault

Figure 3-19: Excitation Behavior for Different Fault

As we can see in figure 3-19, a disconnecting with the power source at 1.08s contributes to a voltage dip in the motor bus. Since the field voltage is rectified from the motor bus, the excitation field voltage also decreases. Besides, we can see a very small voltage oscillation

which is the voltage ripple caused by the commutation of the rectifier. However, during the unbalanced fault, the three phase input voltages are not symmetrical anymore and the mutation of diodes lead to steep oscillations of the output DC voltage which detriments the motor stability.

Mechanical load modelling of the synchronous motors is completely different from the induction motor. As equation 3-7 shows, the torque curve of small rotary pumps is time independent and the torque is only dependent with the rotation speed. However, loads of the 4 synchronous motors are large compressors driven by a reciprocated piston.

The sketch of the mechanical structure of a simple compressor is show as follow:

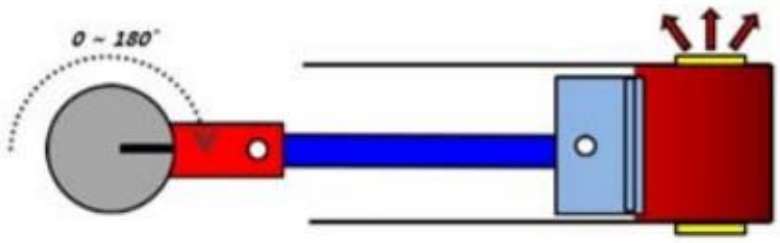

Figure 3-20: The Illustration of a Compressor [17]

In order to compress the gases, the compressors have two working conditions: high load condition and low load conditions. When the piston moves until the maximum point, the pressure will increase gradually. If the gas pressure reaches a certain value, the discharge valve will open to release pressure. Then the compressor goes to the low load stage which is the opposite of the high load condition. In such a process, the pressure of the gas decreases with an increase in gas volume. Therefore, the load curve of the compressors is an oscillating one with maximum and minimum value, and the mechanical load of reciprocated compressors is not only speed dependent but also time dependent. Consequently, the mechanical load of synchronous motor cannot reach to a steady state. It is quite hard to give an analytical solution of the reciprocated compressors since both the time and speed varies. A widely used method is to use FEM (finite element method) to find a numerical solution. [17]

Since DOW did not supply the torque-speed character for compressor load, this thesis cannot model the compressor load precisely (a precise modelling requires a CFD simulation [17] which is not the subject of this thesis). J. Wang [18] supplies a method for the qualitative study of the compressor load based on Fourier Expansion. In this thesis, the following 4th order Fourier series are used for rough modelling of the compressor load:

$$T_l = A_0 + A_1 sin(\omega_r t) + A_2 sin(3\omega_r t) + A_3 sin(5\omega_r t) + A_4 sin(7\omega_r t) \qquad (3\text{-}8)$$

The coefficients of Fourier fitting are tuned based on the stator current behavior given by DOW, as the stator current is directly related to the motor torque. Although such load modelling is not quite accurate when rotor speed decreases dramatically, it at least depicts the fact that the torque would decrease with decreasing rotor speed and the reciprocated behavior of mechanical loads in steady state.

The torque curve and current of motor MC331 are shown in figure 3-21:

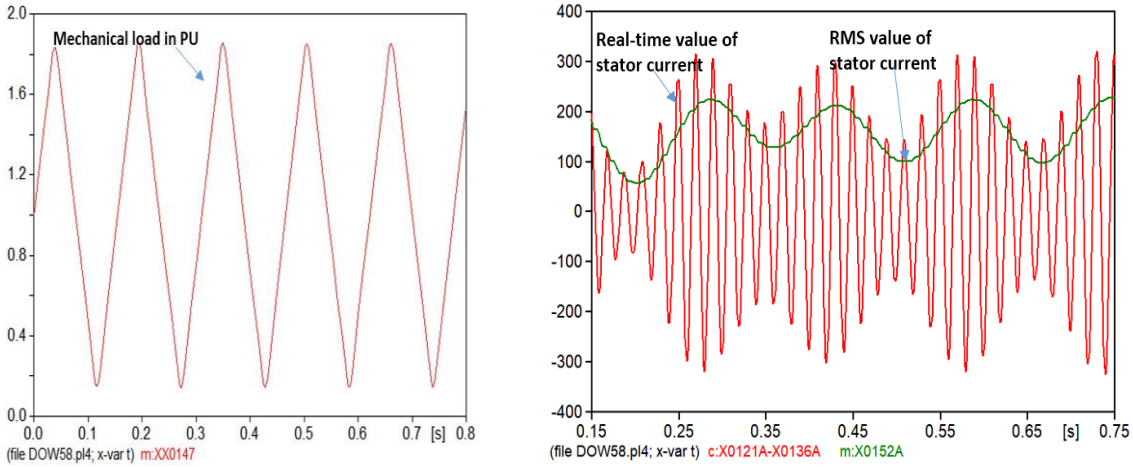

a. Mechanical Load Curve b. Real-time and RMS Current

Figure 3-21: The Mechanical Load and Stator Current of Synchronous Motor MC331

As figure 3-21 indicates, the current of the motor oscillates, and no steady states can be reached. Compared with the current recording, the coefficient of Fourier expansion can reflect the behavior of the motor properly for normal operation. The maximum RMS current is almost 3 times the minimum one, and therefore the input electrical power is oscillating.

The dynamic start of the synchronous motor can be realized by a variable frequency start with power electronic converter, but in industrial companies, the motors can start as induction motors with the help of damper winding. There is a separate section for synchronous startup which can be found in Appendix E.

3-6 Measurement Instruments Modelling

In order to convert the relatively high voltage and current in the power system into a safe value for the relay operation, current and voltage transformers are applied. Typically, the output value is range from 1-5A and 100-120V of the current transformer (CT) and voltage transformer (VT) respectively.

3-6-1 Voltage Transformer Modelling

There are four voltage transformers used for relay testing (seen from the appendix). Two VTs are for the feeder bus voltage measurement and two for the motor bus measurement. All VTs are 25kV/110V with the same parameters. The equivalent circuit of VTs is shown in figure 3-22, and all parameters are referred to the primary side.

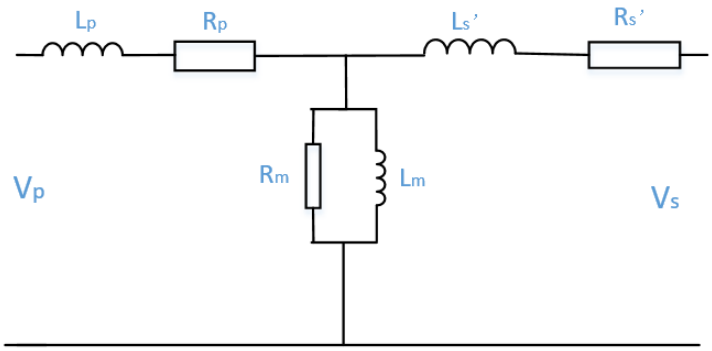

Figure 3-22: The Equivalent Circuit of VT

In this thesis, the core saturation of the VT is ignored since the voltage during fault would not increase too much during the fault, and the iron core is still in the linear region. All the parameters supplied by the DOW power plant are listed in table 3-5:

Table 3-5: The Parameters of Voltage Transformer

I_0	$0.01620(\mathrm{A})$	F_0	$0.0632(\mathrm{Wb})$
R_{mag}	10000	R_p	$0.01(\Omega)$
L_p	$0.00314(\Omega)$	R_s	$0.001(\Omega)$
L_s	$0.000314(\Omega)$		

The VT model in the EMTP is shown in figure 3-23. The VT model is composed by three single-phase TRAFOS saturable transformers.

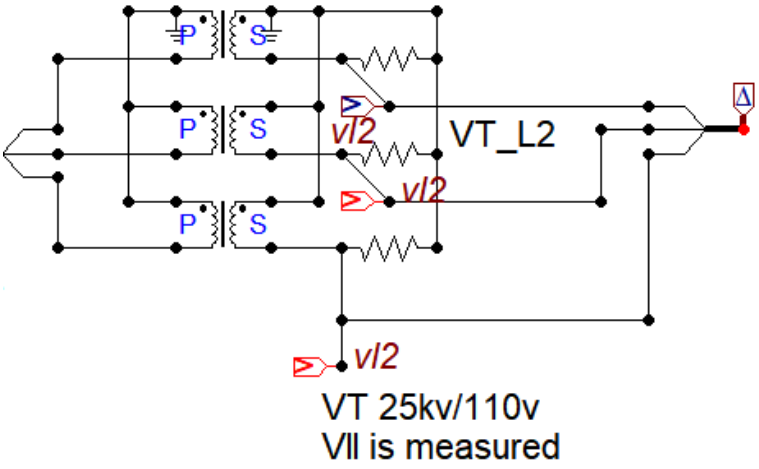

Figure 3-23: The EMTP Model of Voltage Transformer

3-6-2 Current Transformer Modelling

Two current transformers are used to measure the feeder bus current. All the current transformers is 1600/5A with a 5P10 accuracy class. However, compared with the VT, the

saturation of the current transformer must be taken into consideration since the current magnitude during short circuit almost 10-20 times than the nominal current, and the magnetizing current increases, which leads to a non-linear flux behavior. It should be aware that the secondary winding of current transformer should not be open circuit otherwise the primary current would flow through the magnetizing loop and contributes to an extremely high secondary voltage. The schematic diagram of CT is the same as follow:

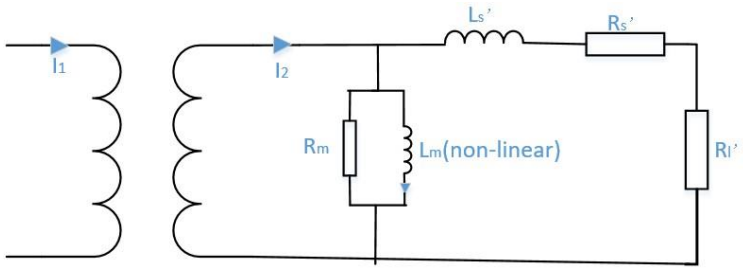

Figure 3-24: The Equivalent Circuit of Current Transformer

The CTs in EMTP are modelled by ideal transformers with non-linear inductance NLIND96. Based on the data given by DOW, the magnetization curve of the nonlinear inductance is illustrated in figure 3-25.

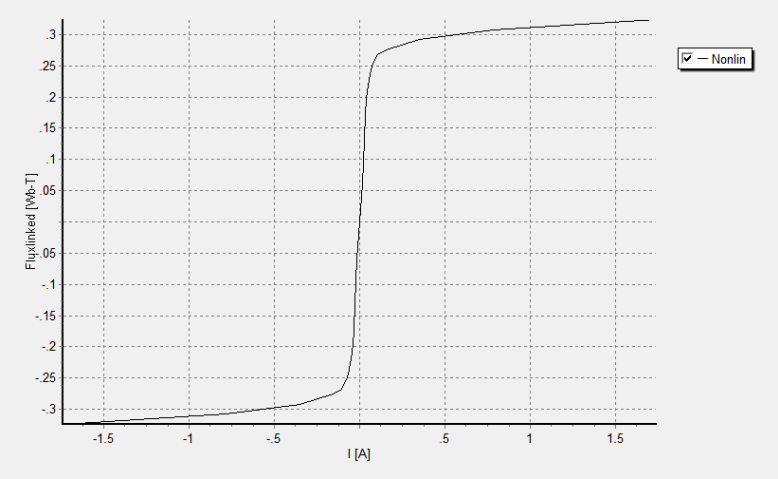

Figure 3-25: The Non-linear Magnetizing Curve

The three-phase current transformers in EMTP are modelled based on figure 3-26. The burden resistor R_l is calculated by the rate power. $R_l = \frac{P}{I_{rate}^2} = 0.4\Omega$.

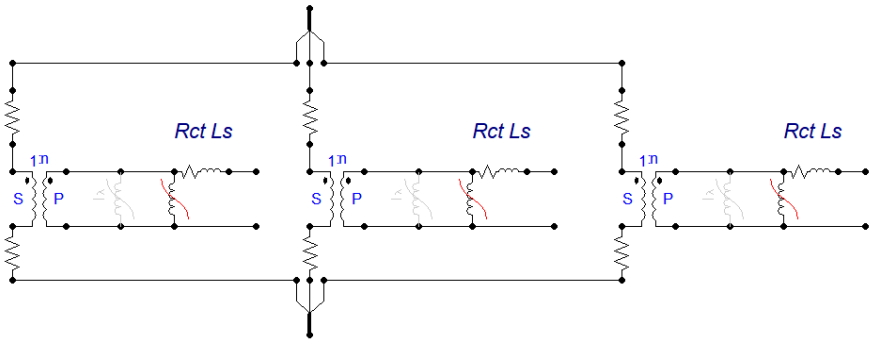

Figure 3-26: The CT Model in EMTP

3-7 Auxiliary Relay Modelling and Configuration

For the relay testing, auxiliary trip and block signals are needed. When a fault occurs in the feeder bus, the transformer differential relay 87T and line differential relay 87 will trip the relevant breakers in feeder bus which leads to a voltage dip. The trip signals from differential relay should also be sent to the relay 7UV68 as an initial signal to initiate the transfer. When a fault occurs in the motor bus, the CB in feeder bus is also tripped to cut down the power supply by instantaneous overcurrent relay 50/50N. However, in such scenarios, the relay 7UV68 should not transfer. Therefore, the trip signal sends from overcurrent relay should also block the fast transfer 7UV68.

Overall, two binary signals are required for the relay: initial signal from the differential relay and block signal from the overcurrent relay. The settings of two relays should be tuned properly to ensure that the tripping and blocking signal would not occur simultaneously.

3-7-1 Simplification for Relay Modelling

This thesis focus on the performance of fast transfer relay and the function of overcurrent and differential relay is to send the auxiliary binary signal to the fast transfer relay. Therefore, some simplification should be made for the differential 87T and overcurrent 50/50N relay modelling.

General Simplification

1. Two relays have no signal resampling.
(Resampling has no impact on the relay tripping logic.)
2. The primary values are used.
(A lack of relevant measurement data, and for the normal operation the error caused by measurement instrument can be neglect.)

Differential Relay

1. The second harmonic block function is omitted.
(We do not simulate the reclosing of unloaded transformers for 7UV68 testing and no inrush current will flow through the differential relay. Therefore the second harmonic block is not needed.)

3-7-2 Differential Relay Modelling

The basic principle of the differential relay is quite intuitive. Based on Kirchhoff's current law, when a fault occurs in the protection zone, the differential current is $I_{dif} = \frac{I_1}{N_1} + \frac{I_2}{N_2} = C$ while when a fault occurs in out zone $I_{dif} = \frac{I_1}{N_1} + \frac{I_2}{N_2} = 0$. Therefore the in-zone fault and out-zone fault can be easily distinguished with very high sensitivity. However, in practice, the differential relay should have a constraint to prevent to mal-opreation when there is a small disturbance in the power system. Based on that a bias character of the differential relay is designed. The minimum bias is set to be larger than the sum of the disturbance current and possible CT errors.

Since the tertiary winding of the transformer is unloaded, the three winding transformer can be regarded as a two winding transformer for differential protection.

In order to get the differential current and constraint current, the fundamental frequency phasor of the primary and secondary current Ip and Is should be extracted respectively. Those current phasors are extracted by a widely used recursive DFT (Discrete Fourier Transform) algorithm.

First, let us consider a sinusoidal input signal with a constant frequency:

$$x(t) = \sqrt{2} X sin(\omega_0 t + \Phi) \tag{3-10}$$

This sinusoidal signal can be represented as a phasor:

$$\mathbf{X} = X\,(cos(\Phi) + jsin(\Phi)) \tag{3-11}$$

Assume that x(t) is sampled by N times per cycle and we have a discrete signal, the sampling should satisfy with Nyquist Criterion to prevent a loss of information:

$$x_k = \sqrt{2} sin(\frac{2\pi}{N} k + \Phi) \tag{3-12}$$

Based on the definition of discrete Fourier transform, x_k can be transformed to:

$$X_d = \frac{2}{N} \sum_{i=0}^{N-1} x_k cos(\frac{2\pi}{N} k) - j \sum_{i=0}^{N-1} x_k \frac{2}{N} x_k sin(\frac{2\pi}{N} k) = X_c - jX_s \tag{3-13}$$

For the real-time phasor measurement, the relay works with moving window, and for a particular window number 'w' we have:

$$
\begin{aligned}
X_c^w &= \frac{2}{N}\sum_{k=w}^{w+N-1} x_k cos\frac{2\pi}{N}k \\
&= \frac{2}{N}\sum_{k=w}^{w+N-1} \sqrt{2}Xsin(\frac{2\pi}{N}k+\Phi)cos\frac{2\pi}{N}k \\
&= \sqrt{2}\sum_{k=w}^{w+N-1}(sin(\Phi)+sin(\frac{4\pi k}{N}+\Phi)) = \sqrt{2}Xsin\Phi
\end{aligned}
\tag{3-14}
$$

Based on the same approach, the sine component X_s^w can be represented as: $X_s^w = \sqrt{2}X\cos\Phi$. Hence, the DFT transformation of the signal x_k can be represented as: $X_d = \sqrt{2}(Xcos\Phi + Xsin\Phi)$ and it can be proved that the DFT algorithm can extract the phasor representation of a sinusoidal signal.

Therefore, a full cycle recursive DFT method is designed. For a digital sequence x(m) with N values, the DFT result of window 'w+1' (X_c^{w+1} and X_s^{w+1}) is based on the value of window 'w' (X_c^w and X_s^w).

The two 230kV/25kV transformers in the feeder buses are three winding transformers with unloaded tertiary winding. Therefore those transformers can be regarded as two winding transformers which have a YnYn0 connection group. Such connection groups supply convenience for relay modelling, as there is no phase shift between the primary and secondary side. In the EMTP model is unnecessary to design the phase correction function.

Based on such RDFT method, we can obtain the current phasor in the primary side and secondary side of the transformer during steady state and fault conditions. Consequently, we can define the differential current and the restraining current phasors as: $\mathbf{I}_{dif} = |\frac{\mathbf{I_p}}{N1} + \frac{\mathbf{I_s}}{N2}|$ and $\mathbf{I_{Res}} = 0.3*|\frac{\mathbf{I_p}}{N_1}| + |\frac{\mathbf{I_s}}{N_2}|$. When a fault occurs out of the protection zone, it is apparent that the differential current phasor $\mathbf{I_{dif}}$ is almost zero and the restraining current $\mathbf{I_{Res}}$ is larger than $\mathbf{I_{dif}}$. Therefore, the relay will not trip. When an in-zone fault occurs, the differential current will be larger than constraint current and the differential relay can send a trip signal to the relevant breakers.

3-7-3 Instantaneous Overcurrent Relay Modelling

The modelling of the overcurrent current relay is simple. The relay model calculates the RMS value of the feeder current per phase. However, the configuration of the overcurrent relay must

take fault current contribution from motors into consideration.

The industrial motors during fault act as generators which feed the fault. Figure 3-27 indicates a three-phase short circuit which occurs near the stator winding. During the shortcircuit period, the motors lose a sustained power supply. In chapter 2, we derived that the rotating magnetic field generated by field winding still exist and induce a voltage when motors lose power supply. Driving by such voltage, there should be a current flow from the motor to the fault point.

The settings of overcurrent relay need to be tuned properly to ensure that the lowest operating threshold of such relay should be larger than the maximum current contribution from motors to prevent a mal-operation when a fault occurs in feeder bus. Based on the EMTP simulation result, the highest fault current (RMS value) contributing from motors is 3.1KA. Considering some margin (1.2 times higher than maximuim motor current contribution), this thesis sets the threshold of the operating current of the overcurrent relay as 3.8KA.

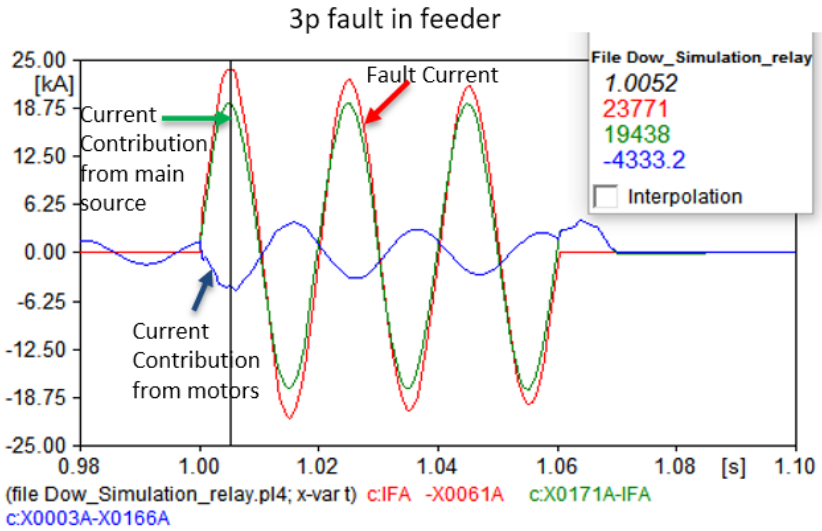

Figure 3-27: The Fault Current Contribution from All Motors

However, when a single phase fault occurs in the low voltage winding, the 600A ground resistor limits the fault current at 600A. Figure 3-28.a shows that the motor will not be affected during the fault period and operates as normal operation. Therefore, the RMS value of motor bus current is almost the same as normal operation.

Therefore, the overcurrent relay will not trip based on the 3.8KA threshold. In order to trip the single-phase fault, except for adding a directional component, a simple way is to detect the zero sequence current I_0, where $I_0 = I_A + I_B + I_C$. As figure 3-28.b shows, when a single phase fault occurs in the motor bus, the level of the zero sequence current is the same as fault current (600A). Based on that, the threshold of zero sequence current tripping is set as 500A. With a combination of instantons overcurrent relay and zero sequence current detection, the block signal can be sent to fast transfer relay reliably when a fault occurs in the motor bus.

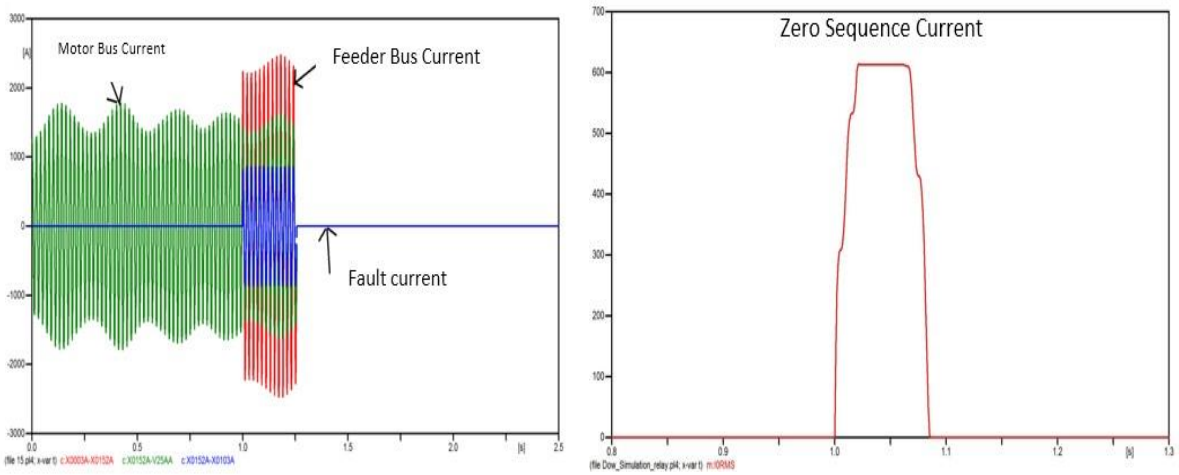

a.Fault Current in Time Domain b.Zero Sequence Current

Figure 3-28: Simulation of Single Phase Fault in 25kV Motor Bus

3-8 Motor Bus Residual Voltage Tracking

As mentioned in chapter 2, both the magnitude and frequency of the residual voltages decay after the feeder CB opens. Besides, the phase angle difference between the motor residual voltage and the reference voltage in auxiliary feeder varies. To configure a proper setting of fast transfer relay, it is necessary to track parameters of motor bus voltage after the feeder CB opens.

3-8-2 Voltage Frequency Tracking

The frequency tracking method which used in this thesis is quite intuitive. In this thesis, a method called full cycle zero crossing is used.

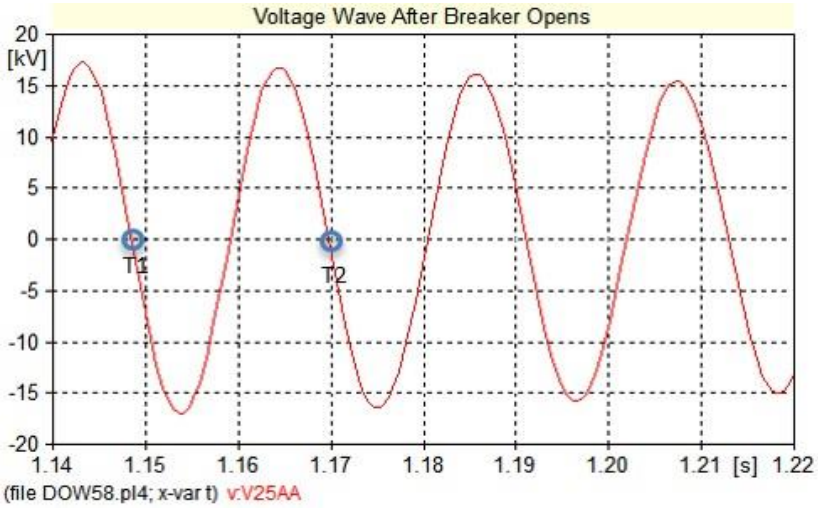

Figure 3-29: Illustration of Zero Crossing Method

As figure 3-29 shows, the frequency of one electrical cycle is measured by calculating the time difference between two zero-crossing point T_1 and T_2 .However, since the voltage signal is discrete, it is not possible to always have an exact '0' point. Therefore, for a sequence x(k) if x(N-1) is positive and x(N) is negative, the point x(N) can be regarded as a full cycle zero crossing point.

Figure 3-30 a shows the voltage signal after the breaker opens and 3-30 b illustrates the frequency of the voltage signal.

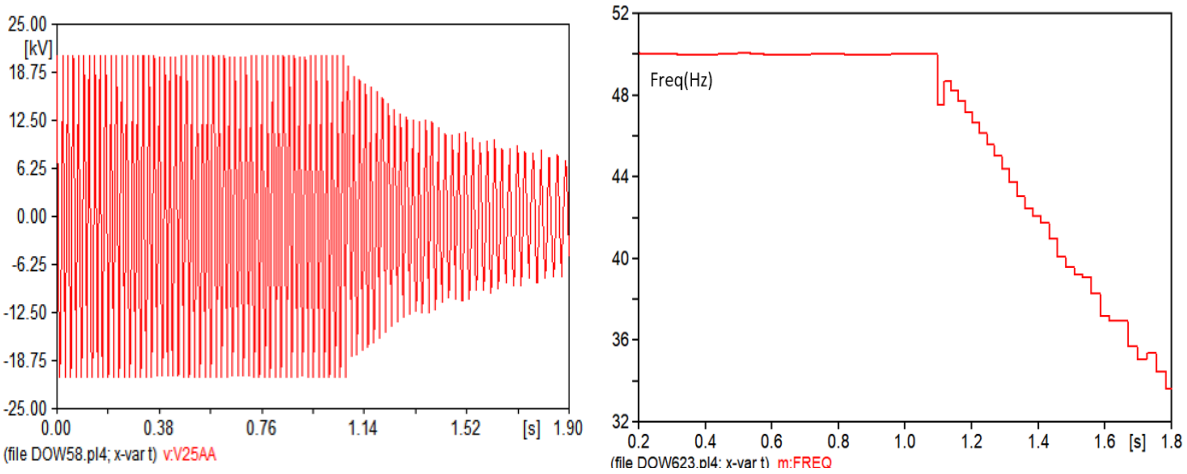

a.Voltage Signal b.Instantaneous Frequency

Figure 3-30: Frequency Measurement of Voltage Signal

Compared with other frequency measurement method, zero-crossing method is easier to implement for real-time measurement because of the extremely low computational complexity. Besides, since this method measures a global frequency of the period $T_m = T_2 - T_1$, the sharp changes and sparks would not contribute to instability of measurement. The main drawback of zero-crossing method is such method can only measure the average frequency of one electrical cycle which contributes to measurement inaccuracy. However, in this project, the frequency measurement does not require high accuracy, and zero crossing method is acceptable.

3-8-3 Voltage Amplitude and Phase angle Tracking

Typically, the amplitude of voltage signal can be measured by the RDFT (Recursive Discrete Fourier Transformation) method as we talked in 3-6-2. However, such method is only valid under fundamental frequency. As chapter 2 and chapter 3-7-1 shows, the frequency of voltage in motor bus decays and RDFT method is not possible. Fortunately, in this thesis, we only focus on the behavior of motor bus voltage after all motors lose power supply and in such period the residual voltages are symmetrical. Therefore, the Clarke transformation method which used for only symmetrical power system can be used.

Supposing we have symmetrical three-phase voltage signals $V_a = \sqrt{2}A\cos(\omega t)$ $V_b = \sqrt{2}A\cos(\omega t - \frac{2\pi}{3})$ and $V_c = \sqrt{2}A\cos(\omega t + \frac{2\pi}{3})$, such three signals can be represented by

a rotating space vector which can be composed by two perpendicular signals V_α and V_β. To maintain the same magnitude of voltage signals before and after the transformation, the transformation matrix is equation 3-15:

$$\begin{bmatrix} V_\alpha \\ V_\beta \\ V_0 \end{bmatrix} = \frac{2}{3}\begin{bmatrix} 1 & -\frac{1}{2} & -\frac{1}{2} \\ 0 & \frac{1}{\sqrt{3}} & -1 \\ \frac{1}{2} & \frac{1}{2} & \frac{1}{2} \end{bmatrix}\begin{bmatrix} V_a \\ V_b \\ V_c \end{bmatrix} \tag{3-15}$$

Based on equation 3-15 and the representation of signals V_a V_b and V_c, we can obtain:

$$\begin{aligned} V_\alpha &= A\cos(\omega t) \\ V_\beta &= A\sin(\omega t) \end{aligned} \tag{3-16}$$

Based on 3-16, the real-time amplitude of the three phase voltages can be easily acquired as:

$$A = \sqrt{V_\alpha^2 + V_\beta^2} \tag{3-17}$$

Besides, it can be derived that:

$$\theta = actan\frac{V_\beta}{V_\alpha} \tag{3-18}$$

where $\theta = \omega t$ is the real-time phase of the signal V_a. If the real-time phase angle of the motor bus residual voltage and the reference source voltage is θ_{res} and θ_{ref}, then the phase angle difference between such two signals is $d\theta = \theta_{ref} - \theta_{res}$.

Figure 3-31 indicates the voltage amplitude A and delta phase angle $d\theta$ between the motor bus and reference feeder bus when the breaker of faulty bus opens inadvertently.

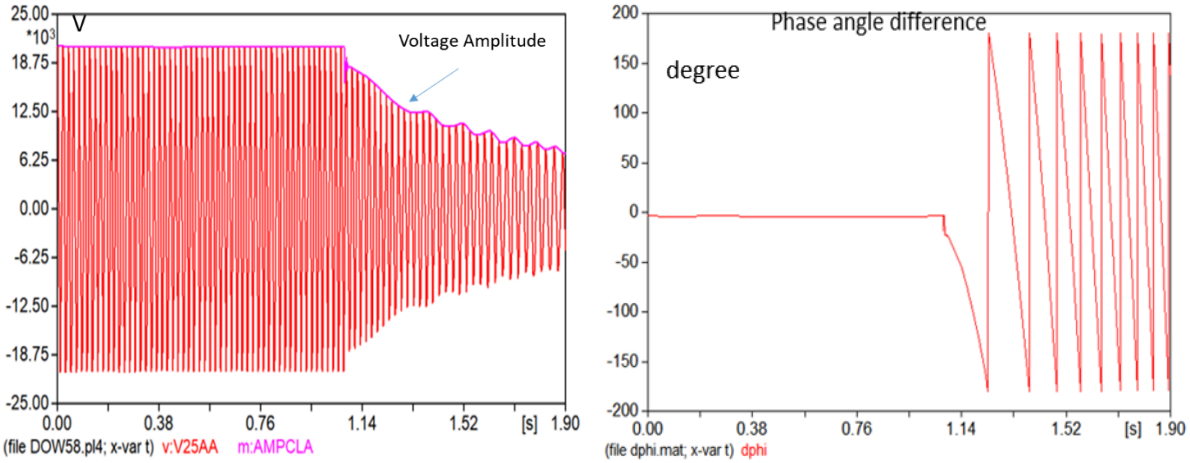

a.Voltage Amplitude A b.Phase Angle Difference $d\theta$

Figure 3-31: Voltage Amplitude and Phase Angle Difference in Open Circuit Condition

As we can see in figure 3-31， the Clarke transform method has a very fast response for system transients. Such a method will give a clear indication of how the amplitude and phase angle difference changes.

However, the fault cannot always be symmetrical, which leads to unsymmetrical voltages in the three phases during the fault. As figure 3-32 shows, the double-phase-to-ground fault in high voltage winding of the transformer leads to the unsymmetrical motor bus voltages. Therefore, in such an unsymmetrical fault period, both the magnitude (blue line in 3-32a) and phase difference measurement (3-32b) is unstable. When CB tripped by the differential relay, the three phase voltages become symmetrical again and consequently, the measurement starts to be accurate again. Since the goal of this thesis is to analyze the residual voltage after CB opens in fault bus, the unsymmetrical period (fault period) can be ignored.

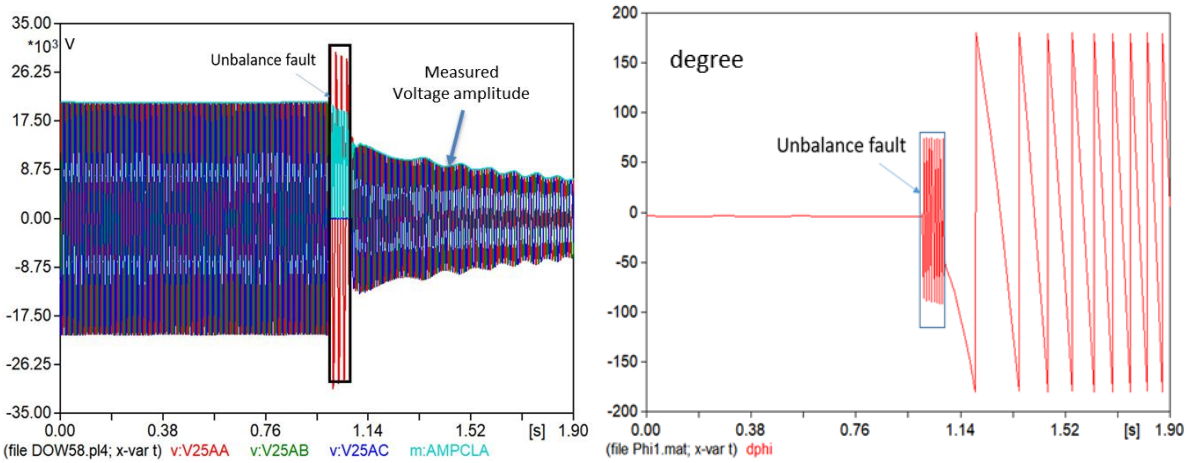

a.Voltage Amplitude b.Phase Angle Difference

Figure 3-32: Voltage Amplitude and Phase Angle Difference under unsymmetrical condition

Chapter 4

Testing Setup Design

4-1 Introduction

In chapter 3, the simulations are accomplished by ATP-EMTP, and both the analog and binary signals can be obtained from the simulation. In this chapter, the setup is proposed for the fast transfer relay testing. The overall hardware connection of the testing setup is shown in figure 4-1:

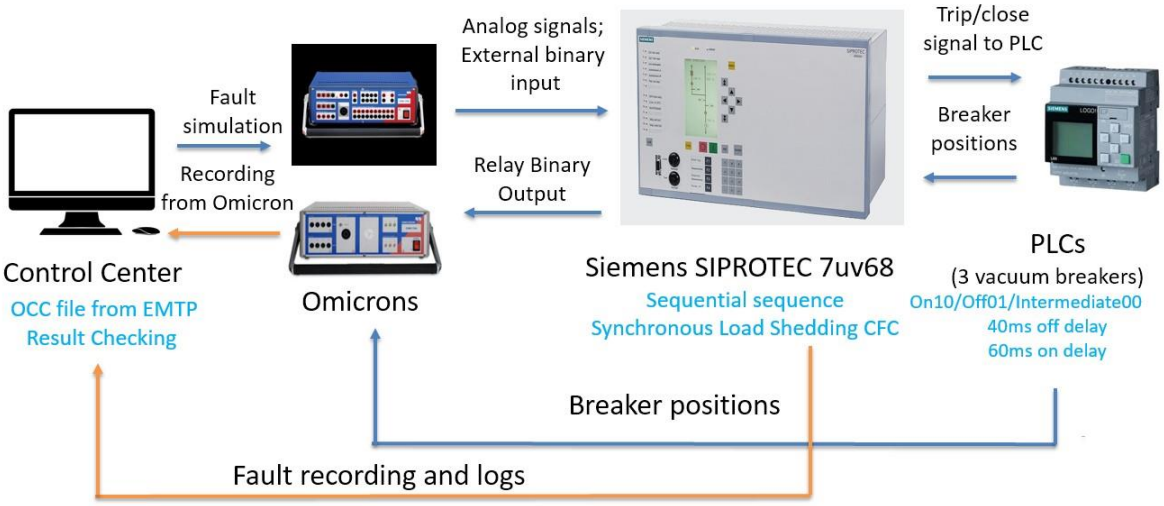

Figure 4-1: The Overall Testing Setup

As figure 4.1 indicates, the whole testing setup is composed of 2 Omicron amplifiers (CMC356 and CMS156), a computer controlled OCC control center, and a Siemens PLC. The OCC control center sends the fault signal recordings simulated by EMTP to Omicrons. After testing, the control center receives and visualizes all testing results and recording. The amplifiers are used to send the real test signals (analog and binary) to the relay and receive the breakers' reaction and relay binary output during testing. The PLC which shows a significant role in the testing is programmed as three 25kV vacuum breakers for main-tie configuration. The PLC sends the breaker states to the relay by 2-bit digital numbers, and

the position should change when the relevant command is sent by the relay. The following parts elaborate the details of designing test setups.

4-2 Simulation Results Recording

To prepare the testing, first step is to convert the EMTP simulation result into OCC files which can be used as the input of Omicron. Figure 4-2 is the schematic drawing of relay input and output connection. Based on that we can see there should be ten analog signals input for the relay operation. The line to line voltage V_{ab} (green line) and phase current I_b (blue line) of both feeder buses and three-phase motor bus voltages V_a V_b and V_c (yellow line) in both side of the motor bus should be recorded. Besides, three binaries signals (red line) inputs should also be saved to Omicron Control center to send the initiating and blocking commands to the relay 7UV68 in the testing

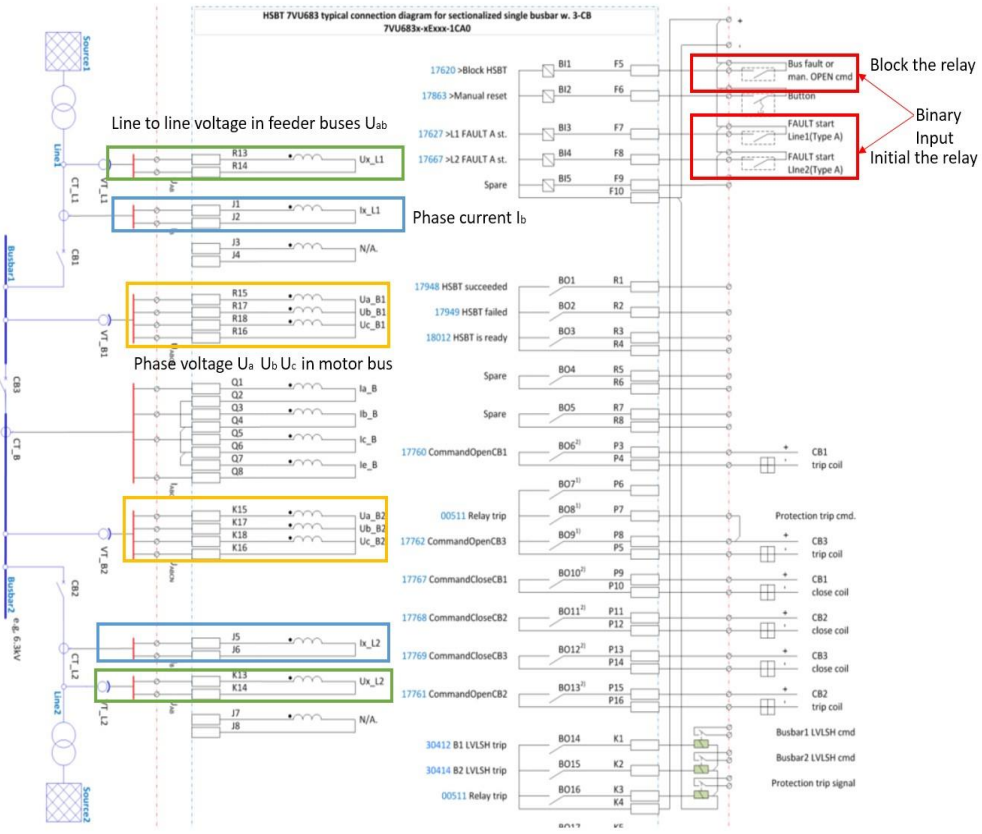

Figure 4-2: Analog and Binary Signals Sending to the Relay 7UV68

As discussed in chapter 3, the vacuum breakers are controlled both by fast transfer relay 7UV68 and auxiliary relays (instantaneous overcurrent relay 50N and differential relay 87T). Therefore, one additional binary output of Omicrons is required to simulate the trip signal which trips the vacuum breaker in 25kV feeders by auxiliary relays.

Therefore, four binary signals and ten analog signals should be recorded by ATP-EMTP and then converted to OCC (Omicron Control Center) files. The OCC files are created by the following steps: First is to save the interested signals to PL4 files for different fault scenarios, followed by converting PL4 files to COMTRADE files.

Next, a single advanced transplay test module can be made. Such a module can obtain the test signals from both COMTRADE and DAT format. Then signal repetitions are needed to enlarge the period of steady state signal since the operation of the relay 7UV68 requires at least 10s steady state signal input. (Considering the calculation complexity the steady state in the EMTP simulation is 1s).

Finally, all advanced transplay test modules for different test cases are integrated into the OCC test library as figure 4-3 indicates. When performing a test, each embedded function in OCC will be executed sequentially. However, in the testing for 7UV68, the breaker position should be reset before a new test module. In this thesis, all testing modules are executed manually instead of the automatic execution.

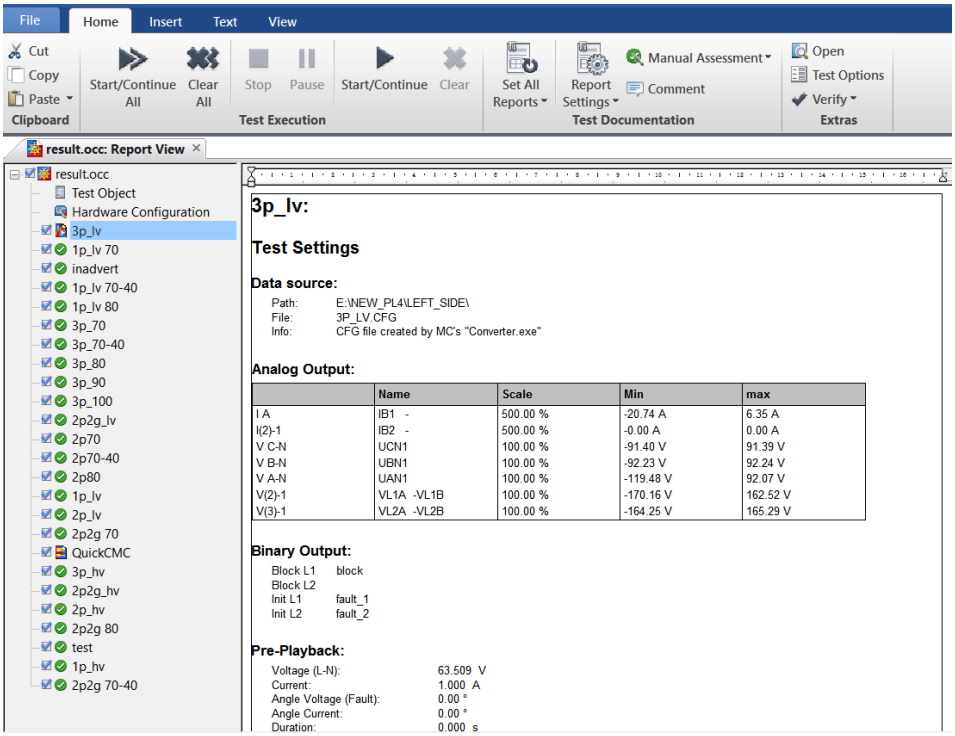

Figure 4-3: The OCC Test Library for Different Fault Scenarios

4-3 Test Signals Generation

Both the analog and binary signals sending to the fast transfer relay are generated by 2 Omicrons CMC356-ETH2 and CSM156. Those two Omicrons are connected by Ethernet, and can be controlled together by the OCC computer control center via WIFI or Ethernet. The basic technical data of 2 amplifiers are shown as follow:

Parameter	Output value
3*1 phase current (A)	3* 0-32
1*1phase voltage (V)	1* 0-500
3*1 phase voltage (V)	3* 0-300
DC Voltage(V)	0-300
DC Current(A)	0-80
Current resolution (mA)	1
Voltage resolution (mV)	5

a. Basic Data of CMC 356

Parameter	Output value
3*1 phase current	3* 0-32A
4*1 phase voltage	3* 0-300V
Current resolution	1mA
Voltage resolution	5mV

b. Basic Data of CMS 156

Figure 4-4: Basic Technical Data of Two Amplifiers

The connections of all analog signals are intuitive. The analog output of the Omicrons is just directly connected to the related relay terminals. However, the binary outputs of Omicrons (binary inputs of the fast transfer relay) as we can see in figure 4-2 connect a DC voltage output and act as a switch. Once the binary signal of Omicron output is '1' (high), the switch which connects the relay with the DC voltage supply closes. Subsequently the related terminals of the relay (block or initial) would see a 110v DC voltage, and the relevant commands will be executed by the fast transfer relay.

Except for sending the binary signals to the relay, amplifier CMC 356 also receives the binary signals which send from the relay 7uv68 and PLC (breaker close and open time, load shedding time, command sequence). The input binary signals '1' and '0' (high and low) to the Omicron correspond to the DC voltage potential difference of between the '+' and '-'. The threshold for '1' are set as 77V which means if the DC voltage potential of the two ports is larger than 77V then the binary input to the Omicron is regarded as '1'.

4-4 Breaker Time Delay Imitation

As we talked in chapter two, 25kV breakers in DOW power plant are controlled by both the differential relay 87T and the fast transfer 7UV68. When the trip command is sent by either differential or fast transfer relay, a DC voltage would be applied to the breakers. Then, the opening coil of the breaker would induce a magnetic force which unlatches the open spring. After that, the moving contact of the breakers separates very fast from the stationary contact and eventually the breaker trips. On the contrary, when the closing command is sent to the breakers, closing coils are energized, which leads to unlatch the close spring. Then the breaker close and the charging motors charge the spring to prepare for next closure.

However, in our testing setup design, it is unnecessary to connect the relay with 3 real breakers which increase the overall cost of the testing. Besides, the closing and tripping of the 25kV breakers contribute to enormous noises. Therefore, a PLC is used to imitate the breaker time constants. Before the time delay imitation, the basic theory of breaker should be clear.

The breakers, as the name indicates are used to break current under abnormal conditions such as short circuit. In normal conditions, the breakers which act as good conductors are in the closed position, and the current flows from the contacts. When a release latch is energized, the breaker cannot close or trip immediately because of the latch release delay and the moving time of the contacts. Therefore, it should have 3 states for a breaker: close state open state and a dynamic process between close and open called intermediate state. Besides, three constants are defined for vacuum breakers the total breaking time, open time and close time.

As figure 4-5 shows, when a breaker receives a trip command from the relay, it needs time for coils unlatch the springs to separate contacts of three phases. The time duration from receiving a trip command to contact separation is called close time. After the contact separation, there is arc ignition and the current still goes through the breaker until the arc extinguishes; this period is called arc time. The sum of both close time and arc time is called breaking time (tripping time). $T_{breaking} = T_{close} + T_{arc}$

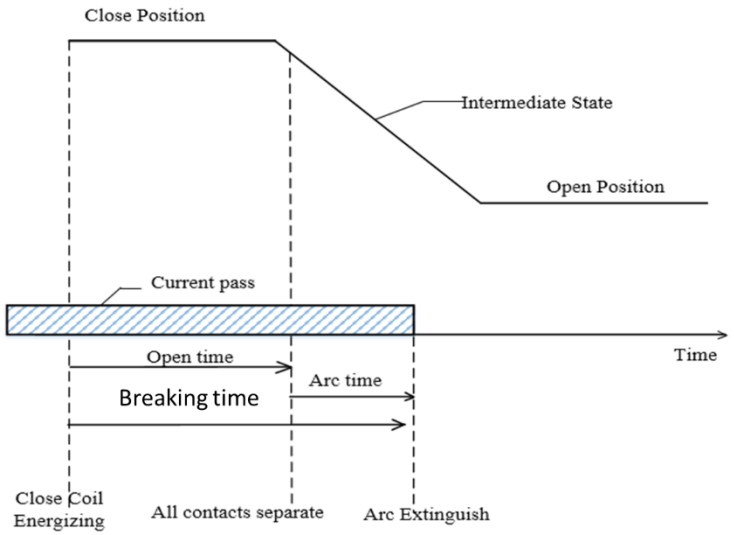

Figure 4-5: Time Constant of Breakers for the Breaker Opening

In contrast, when a breaker opens (figure 4-6), the close time for such breaker can be defined as the time period after coil receives closing command until all contacts in three phases are contacted with each other. However, the electric field of two contacts increases when the air gap decreases. Therefore, the vacuum gap will breakdown before contacts close and the current will flow through the breaker before contacts close.

The three breakers in DOW power plant have an average opening time about 30ms and close time 50ms. Considering the breaker usually takes about one electrical cycle to extinguish the arc (arc time 20ms), the total breaking time is about 50ms.

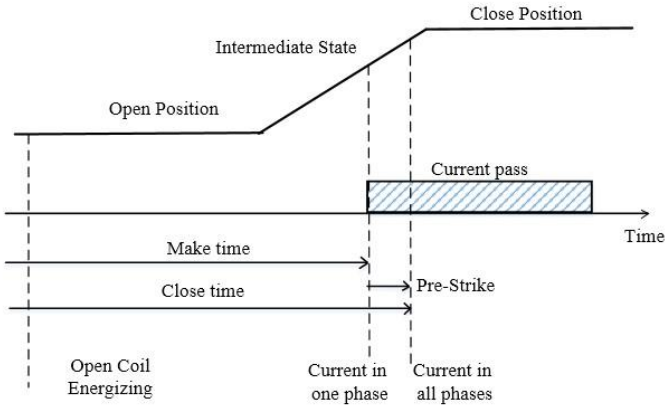

Figure 4-6: Time Constant of Breakers for the Breaker Opening

For simulating both the breaking and the opening time of the vacuum breaker, a Siemens LOGO PLC is used. The PLC is a universal logic module integrating analog and digital control functions as well as interface of Ethernet communication. The basic module of LOGO PLC with display and configuration panel contains 8 digital inputs and 4 digital outputs. If analog control functions and more digital portal are required, the PLC basics should be extended by expansion modules. LOGO basics support a maximum of 24 digital inputs, 8 analog inputs, 20 digital outputs, and 8 analog outputs. The expansion modules connect to the basic module by physical connection.

Table 4-1: Basic Technical Parameters of Basic Module and Expansion Module of PLC

Module Type	Power Supply	Input	Output
LOGO! 230RCE	115 VAC/VDC to 240 VAC/VDC	8 digital	4 relays(10A)
LOGO! DM16 230R	115 VAC/VDC to 240 VAC/VDC	8 digital	8 relays(5A)

Figure 4-7 shows the connections of the PLC. The input of the PLC connects to both the trip/close command terminals of the 7UV68 (red array) and one Omicron binary output (purple array) which imitates the trip signal from differential relay 87T.

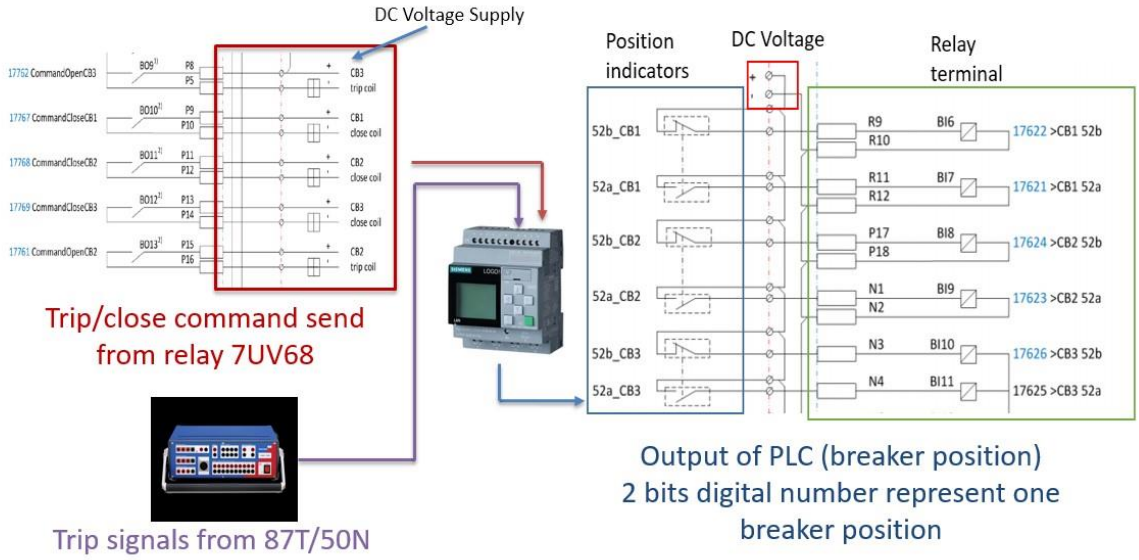

Figure 4-7: Connections of LOGO PLC

The outputs (digital outputs) of the PLC are simple switches between DC voltages and "position state" indication ports of the relay. By controlling the output of PLC, the relay will see different breaker states and based on that we can use PLC to imitate the breaker delay.

As figure 4-7 shows, in fast transfer relay, two ports represent one particular state of a breaker. Taking breaker CB1 as an example, a high voltage potential (110V) in terminal CB1_52b means the breaker is closed while high voltage potential in CB1_52a indicates that the breaker is open. If there is no voltage potential in both ports "CB1_52a" and "CB1_52b", the relay will know that the breaker is in the intermediate state. Both 'high' in those two ports are not available for the relay. If we regard high voltage potential as a digital number '1' and zero voltage potential as '0', then a 2 bits digital number can represent a particular position of the breaker and the truth table of breaker state as shown as below:

Table 4-2: Truth Table of Breaker State

Digital Output	Breaker State
10	Close State
01	Open State
00	Intermediate State
11	Undefined State(Error)

As there are 3 breakers in the testing, 6 digital inputs and outputs are required.

The controlling and programming of the PLC can be either realized by the control panel in LOGO basic or by a computer which connects the LOGO PLC by Ethernet. In practice, it is more convenient for users to control and program the PLC by a computer compared with using the control panel. The control software used in this thesis is LOGO Soft Comfort 8.1.

Internal logic in PLC is programmed by Ladder graph, a graphical way to indicate the relationships between input and output. Except for the basic functions which are given by the software, LOGO SOFT also allows users to create new logic and control functions.

The ladder graph which is designed for the breaker simulation is shown in figure 4-8:

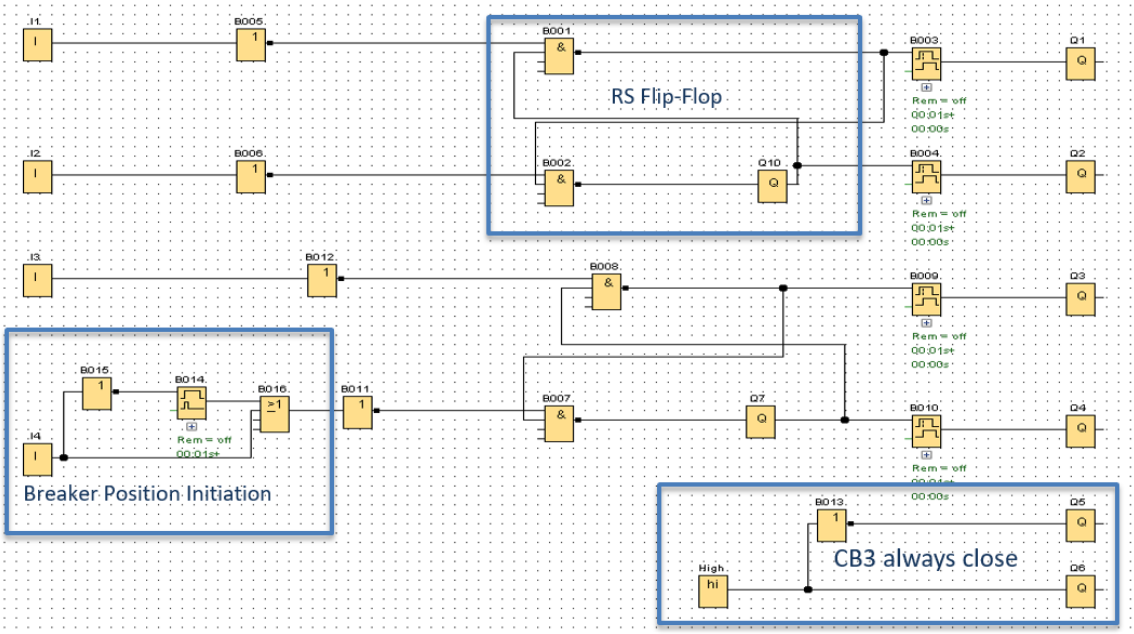

Figure 4-8: Ladder Diagram of PLC

In this thesis, we only focus on the main-tie configuration, so CB3 is always closed. Therefore, in the ladder diagram output Q5 and Q6 are '0' and '1' respectively.

Usually, the lasting time of the trip and close signals are very short (about 200ms), and the command only acts as a trigger which unlatches the closing and tripping spring of breakers respectively.

In PLC programming, the trigger functions are accomplished by $\overline{SR}$ flip-flops as figure 4-8 indicates. $\overline{SR}$ flip-flops have two inputs $\overline{R}$ $\overline{S}$ and two output Q , $\overline{Q}$. $\overline{SR}$ flip-flops is a rising edge sensitivity latch, which means that the output of SR flip-flop only changes when a single rising edge occurs. It is not available that the two inputs are in the high state. The table below is a truth table of an SR flip-flop (the outputs state at this moment right now have Q=Q, $\overline{Q} = \overline{Q}$).

Table 4-3: Truth table of SR Flip-flop

$\overline{R}$	$\overline{S}$	Q_{next}	$\overline{Q}_{next}$	Action
1	1	Q	$\overline{Q}$	Hold on
1	0	1	0	Reset
0	1	0	1	Set
0	0	X	X	Not allowed

As mentioned before, the tripping delay and the opening delay are both about approximately 50ms. Those delays are simulated in the LOGO by delay functions. When simulating the vacuum breaker delay, the internal delay of PLC should be taken into consideration. The internal delay of PLC is about 40ms. Therefore, a 10ms rising edge sensitivity delay is added before the PLC output.

In motor bus transfer, motors are required to transfer from one feeder bus to another. Before the feeder fault occurs, either CB1 or CB2 should be in closed state. The close state of breakers are fulfilled by a 'wiping relay function'. Although the binary input is '0' at the beginning, a combination of wiping relay block and 'or' block (as figure 4-8 indicates) can send a 10ms pulse with high voltage potential '1'. Such pulse leads to a high voltage potential output '1' in Q4 and low voltage output '0' in Q3. Consequently, relay will see a closed state of CB2.

Before transferring the logic data to PLC, the output can be simulated in LOGO Soft. Figure 4-9 shows the simulation result of PLC ladder graph for the initial state. The blue line indicates the low voltage potential '0' while red line represents the digital output '1'. Based on table 4-2, it is clear that CB1 is open while CB2 and CB3 are closed.

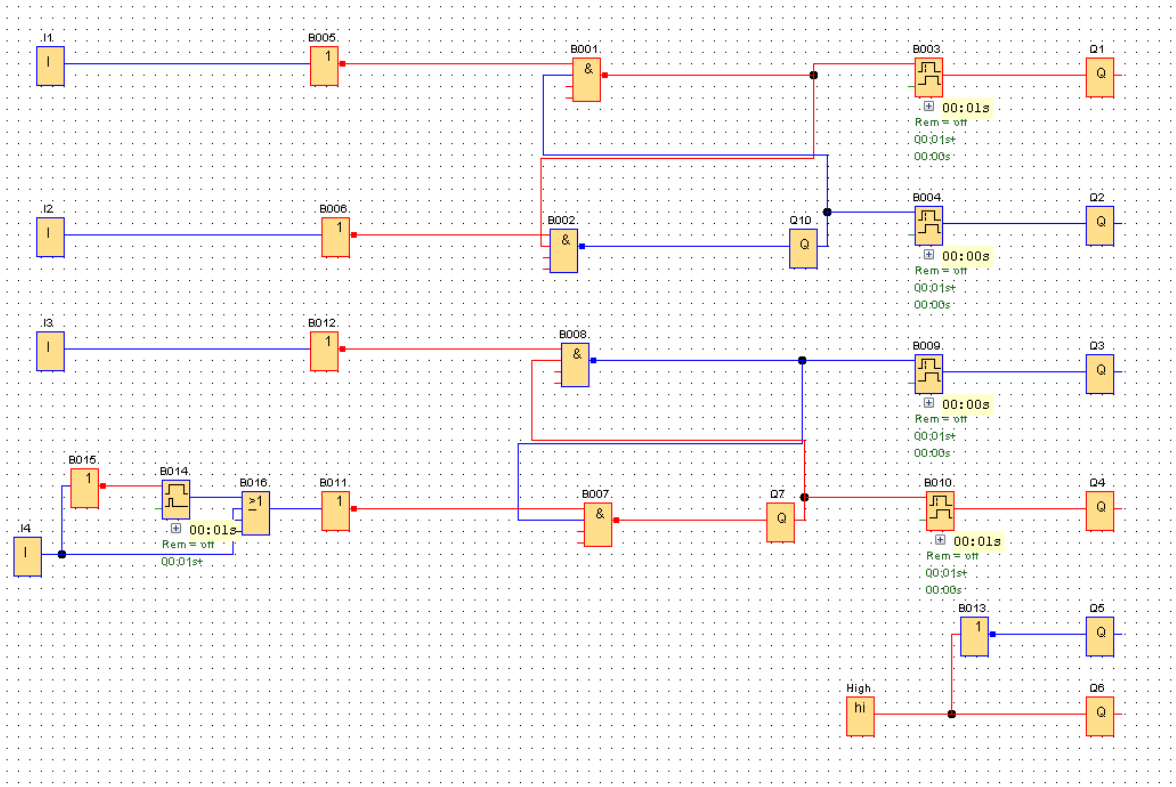

Figure 4-9: Simulation of PLC Ladder Graph

Chapter 5

Relay Testing

5-1 Introduction

All of the previous chapters are preparations of the relay testing. In chapter 3, the DOW power plant is modelled and testing hardware is designed in chapter 4. Before testing, the requirement should be specified. Based on different requirements the relay 7UV68 has a different setting. In this thesis, the desired relay setting should be configured based on having a short transfer time and small inrush current and torque when auxiliary feeder closes. The relay is tested under the desired setting. The whole testing process has two main parts. First, the testing should be done based on the fault locations to ensure the relay can operate in abnormal conditions and contingencies which the DOW power system may encounter. Next, to understand the impact of fault time and communication delay on the transfer behaviors, a sensitivity testing should be done. Based on the sensitivity testing the DSOs and DOW power plant will have a clear understanding of the worst scenarios and some relevant approaches can be implemented to prevent such scenarios.

5-2 Test Requirement and Test Cases Design

5-2-1 Test Requirement

From the perspective of system engineering, the testing should be done based on the relevant specification and requirements. Next, the test cases which acts as an input of the testing should be designed based on the requirements.

Figure 5-1 is a sketch of the power plant in Tarragona. As figure 5-1 indicates, the fault can occur in 230kV transmission grid, feeder buses, as well as the motor bus. For these three types of fault locations, different requirements should be developed.

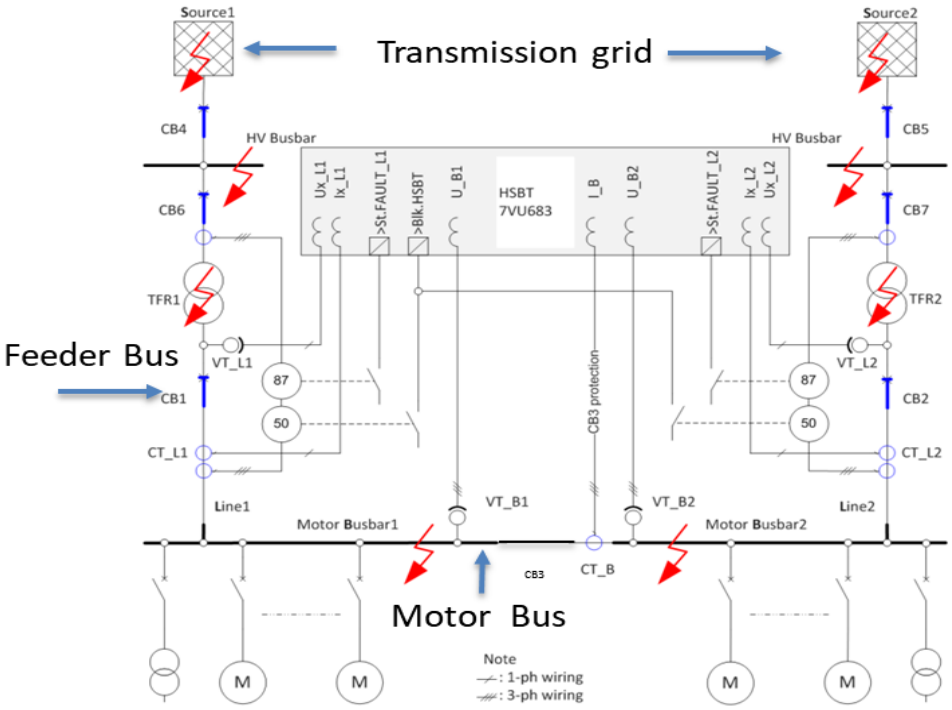

Figure 5-1: The sketch of Tarragona power plant

Basic requirement

1. The relay 7UV68 should ensure a safe ($\frac{U_{diff}}{freq} < 1.33\,\text{PU/Hz}$) and fast transfer for all abnormal and fault conditions in its protection zone.

2. Taking requirement one as a premise, the transfer time and transient torque caused by breaker shifting should be as small as possible.

3. Before shifting the fault feeder to auxiliary bus, all synchronous motors should be disconnected from the 25kV motor bus. During the fault and voltage dip period, the load angle δ of the synchronous increases and it is impossible to track the real-time load angle by 7VU68. Besides, from the simulation and the DOW's fault record, some synchronous motors lose their stability after about 100ms. Considering the breaker time and fault time, for most fault cases, the synchronous motors cannot maintain the stability before closing the auxiliary breaker. In order to prevent the instability caused by reconnecting the synchronous motors, the relay 7UV68 should trip such motors before bus shifting. After a successful transfer, the synchronous motors can be manually restarted.

The specific requirements of different fault locations are listed as follow:

Feeder Bus Fault

The relay should have a breaker inadvertent open detection function.

The elementary function of the fast transfer relay is to transfer from the fault feeder to the auxiliary feeder. Typically, the trip signal from the differential relay would initiate the relay. However, if the communication channel is congested or mal-operation of workers, the breaker in the feeder bus will open without any auxiliary relay indication. Therefore, the relay should detect the breaker opening and initiate a transfer.

Motor Bus Fault

The relay should be blocked reliably by a blocking signal.

As elaborated in chapter 3, the feeder breaker can also be tripped by motor bus over-current relay when a fault occurs in the motor bus. In such scenarios, the relay should be blocked as there is no fault in the feeder bus.

Fault in 230kV Transmission Grid

The relay should initiate a self-transfer which avoids a fault when a voltage dip is caused by the transmission grid fault.

The fault may also occur in 230kV transmission lines which are connected to TP or TR. Such a grid is owned by a relevant TSO Company. The protection in transmission grid such as line differential and distance protection will trip the relevant breaker and lead to a voltage dip in the 25kV motor bus. In order to ensure the system stability, the fault in transmission grid should be tripped less than a given time (critical clear time). Different TSOs has a different grid code for the critical fault clear time. Based on the grid code from Tennet [19], the critical fault clear time for EHV (extra high voltage) transmission grid is defined as 150ms.

Both the transmission grid fault and the feeder bus fault results in a voltage dip in the 25kV motor bus. However for a transmission grid fault, no fault indication is sent to the fast transfer relay. Therefore, in order to initiate a transfer to the auxiliary feeder when a fault occurs in transmission grid, a self-start function should be designed to initiate the transfer although no indication is sent to the fast transfer relay. However, we do not want to initiate the transfer during the fault period, which leads to a severe stability problem, so the transfer should be blocked during the fault period. A very simple way to prevent a transfer during a fault is to create a blank time which is longer than the critical fault clear time for 230kV transmission grid. The self-start transfer will be initiated after such a blank time. Based on the grid code, the self-start function should not initiate in 150ms after a voltage dip in the 25kV bus to wait for the extinguishing of fault current.

5-2-2 Test Cases Design

The test cases are designed by requirements. After each test, the fault records from Sigra and Omicrons are saved. The period after fault feeder trips until reference auxiliary feeder close is called transfer time in the following chapters. Such transfer time is recorded from the fault recording. All the testing cases are listed as follow:

Feeder Bus Fault

Faults are designed near the primary and secondary winding of both transformer TP and TR.

Since the fault location is near the transformer winding, the transformer differential relay will regard such fault as an in-zone fault. Therefore, the pre-designed differential relay model will trip the relevant breakers and send the initial signal to the testing object (7UV68).The test list for transfer from BUS1 to BUS 2 for feeder fault cases listed as table 5-1(BUS2 to BUS1 is the same):

Table 5-1: Test List for Feeder Fault

Transfer Direction	Fault Location	Fault Type
BUS1 to BUS1	25kV	Three-Phase
		Double-Phase-to-Ground
		Phase-to-Phase
		Single- Phase
		Inadvertently Open
	230kV	Three-Phase
		Double-Phase-to-Ground
		Phase-to-Phase
		Single- Phase
		Inadvertently Open

Motor Bus Fault

Since we only test the relay under the main-tie configuration, the motor bus voltage in motor bus 1 and 2 are the same. Therefore, only 4 testing cases are needed (single-phase, phase-to=phase, double-phase-to-ground, three-phase).

Transmission Grid Fault

The transmission grid fault can be either a short circuit fault or open circuit fault. In the transmission grid fault, the differential relay cannot send the initial signal. Five testing cases are designed with four types of short circuit cases and one open circuit fault case.

5-3 Relay Configuration and Testing for Feeder Bus and Motor Bus Fault

5-3-1 Motor Bus Residual Voltage Behavior after Fault

To configure a proper relay setting, first, the motor bus residual voltage behaviors after breaker opens should be analyzed. For most cases, the breaker is tripped by differential or overcurrent relay when a fault occurs. Different fault types should have different impacts on the motor residual voltage after the fault is cleared (breaker opens). (Fault time is designed as 70ms and communication delay are set as 20ms for all testing cases for the relay configuration). Besides, the breaker can be opened inadvertently by mal-operation or defection of breakers. Table 5-2 illustrates the phase angle difference $d\theta$ between the motor bus voltage and reference feeders, amplitude, and frequency of the motor bus voltage after the fault feeder trips for each fault scenarios.

Table 5-2: Voltage Amplitude and Delta Phase Angle after Fault

Fault Location	Fault Type	Phase Angle Difference(degree)	Voltage Amplitude Compared with nominal Value (%)	Frequency (Hz)
25kV side	Single-phase	27.76	91.31	48.91
	Three-phase	79.21	47.63	47.05
	Phase-to-phase	52.6	62.29	47.85
	Double-phase-to-ground	52.728	61.54	47.84
230kV side	Single-phase	41.21	72.63	48.31
	Three-phase	75.74	47.23	47.31
	Phase-to-phase	48.12	63.91	47.89
	Double-phase-to-ground	56.12	57.83	47.74
Breaker inadvertent open		27.28	91.72	48.94

At first, we can see that the inadvertent opening of the feeder breaker contributes to a small voltage and frequency decay, although there is no short circuit fault before the breaker opens. Moreover, there is a 27.28° phase angle shift between the motor bus voltage and the feeder bus voltage. The reason for the amplitude and angle change can be described as follows. Induction motors account for the majority of loads in DOW power plant. Such induction motors operate asynchronously at the instant when the feeder breaker opens. The amplitude, real-time phase and frequency of the induced voltage in the motor bus is directly relevant to the motor rotation speed. Therefore, the asynchronous rotating speed ω_r (lower than synchronous electrical speed) leads to a changing of both voltage magnitude, frequency and phase angle although there is no fault before the breaker open. Figure 5-2 indicates the voltage amplitude A and voltage phase difference $d\theta$ between the motor bus and auxiliary feeder source.

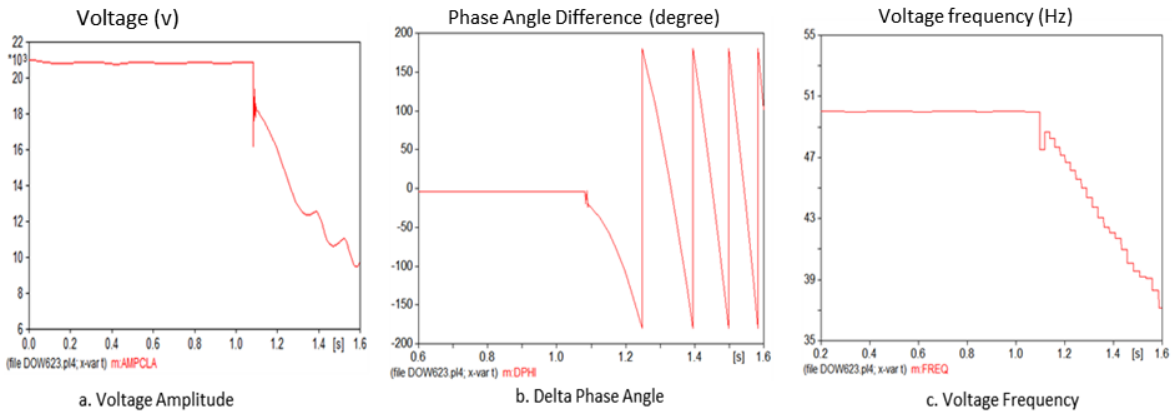

Figure 5-2: The Voltage Magnitude, Frequency and Delta Phase Angle for Breaker Inadvertent Opening

Besides, what should attract our attention is the single-phase fault. The amplitude of motor bus residual voltage A_u and phase angle difference $d\theta$ for single-phase fault in the

25kV feeder bus is almost the same as the inadvertent opening of the breaker. This means that the single-phase fault in 25kV feeder bus has almost no impact on the behavior of motor bus residual voltage. With the help of 600A ground resistors in the 25kV winding, the single-phase fault current is limited at 600A, and the current flows from the feeder to the motor bus is almost the same as normal operation. Seen from figure 5-3, the stator current and motor rotating speed during the single-phase fault is the same as normal operation. That is the main advantage of the 600A ground resistor in the 25kV winding.

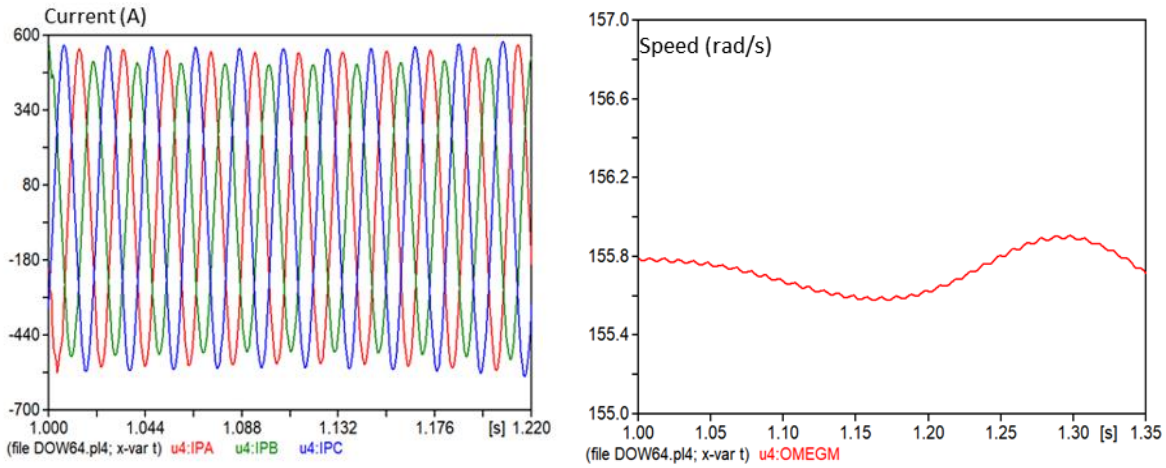

a.The stator current b.The rotor speed

Figure 5-3: The Stator Current and Speed Behavior of Induction Motor during Single Phase Fault

For a single phase fault in the 230kV side, as there is no grounding resistor, one of the stator winding loses power supply and motors supply current to the fault point which leads to a weakening of trapped magnetic energy in the fault period. Therefore, the voltage amplitude A_u and frequency f would be lower than single-phase fault in 25kV side after breaker opens.

Furthermore, in table 5-2, the three-phase fault leads to the highest voltage dip and phase difference. For the three phase faulty period, except for no electrical power input, all three phase supplies current to the fault location, which weakens the trapped magnetic energy dramatically and therefore, leads to a maximum voltage decay and phase difference.

5-3-2 Relay Setting Configuration

Before the testing, the fast transfer relay should be configured properly. As shown in chapter 2, the safety of the transfer is ensured by the boundary threshold of each transfer modes, so it is essential to set a proper threshold. Both the Siemens [16] and Beckwith company [20] give a different suggested threshold setting for fast transfer mode for typical industrial companies. However, such pre-configured thresholds may not be optimal for every power plant and should be adjusted based on the different requirements. Before tuning the relay setting for a different transfer mode, the synchronous motor load shedding should be added.

During both short circuit and open circuit period, the load angles of synchronous motors keep increasing.

As the load angle of synchronous motors is unknown, the re-energizing of synchronous motors may lead to instability of the system. Therefore, a conservative way is to trip all synchronous motors before auxiliary feeder closes.

The relay 7UV68 does not supply the synchronous load shedding function. Therefore, it is necessary to add such function by CFC logic. The CFC is an integrated logic programming tools in Digsi. Relay 7UV68 prepares the spare terminals for additional CFC functions. It is desired that the load shedding signal is sent at the moment when the relay sends the close signal to the auxiliary breaker. Based on such logic, the load shedding function is designed as follow:

As figure 5-4 shows, the input signals are the close commands for both CB1 and CB2. As such two signals connect to a 'or' logic, a close signal of both CB1 and CB2 lead to a load shedding and the synchronous motors can be tripped when shifting breakers.

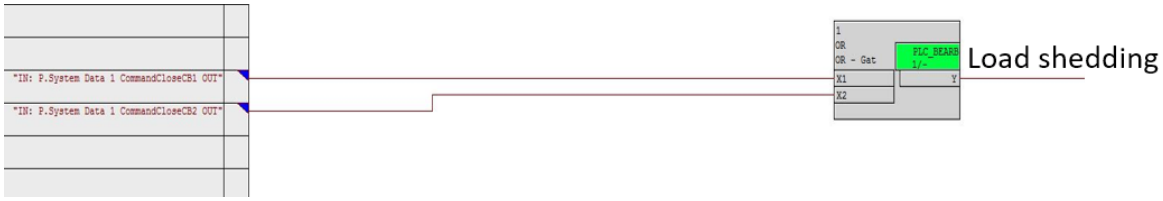

Figure 5-4: The CFC logic of Load Shedding Function

As table 5-2 shows, at the instant the breaker in fault feeder opens, except for the case of single-phase fault in the 25kV side, most fault cases leads to a severe voltage dip and a large delta phase angle. Therefore, for those fault case with large voltage dip and delta phase angle, it is not possible for the relay to transfer in fast mode (real-time fast mode) since the voltage angle cannot fulfill the relevant thresholds. The optimal way is to transfer such faults in the in-phase mode which can decrease the high inrush torque caused by a large voltage difference U_{diff} between reference feeder source and motor bus.

However, the single phase fault in the 25kV side would not contribute to large voltage dip and phase angle difference. Based on the simulation result (table 5-2), at the instant when CB1 is tripped the delta phase angle is 24.98° and the voltage amplitude is about 90% of the nominal voltage. Therefore, it is possible for the single phase fault in 25kV bus to initiate either a fast transfer or real-time fast transfer mode based on different setting configurations.

The selection of the fast transfer mode or the real-time fast mode is based on the testing result of transfer time and motor inrush torque. By such results, a proper transfer mode has been chosen.

If the boundary threshold of the delta phase angle $d\theta$ is set as 30°, then the relay will transfer in fast mode with a 98 ms transfer time. The fault recording and operation sequence of the relay are shown in 5-5 and 5-6 respectively:

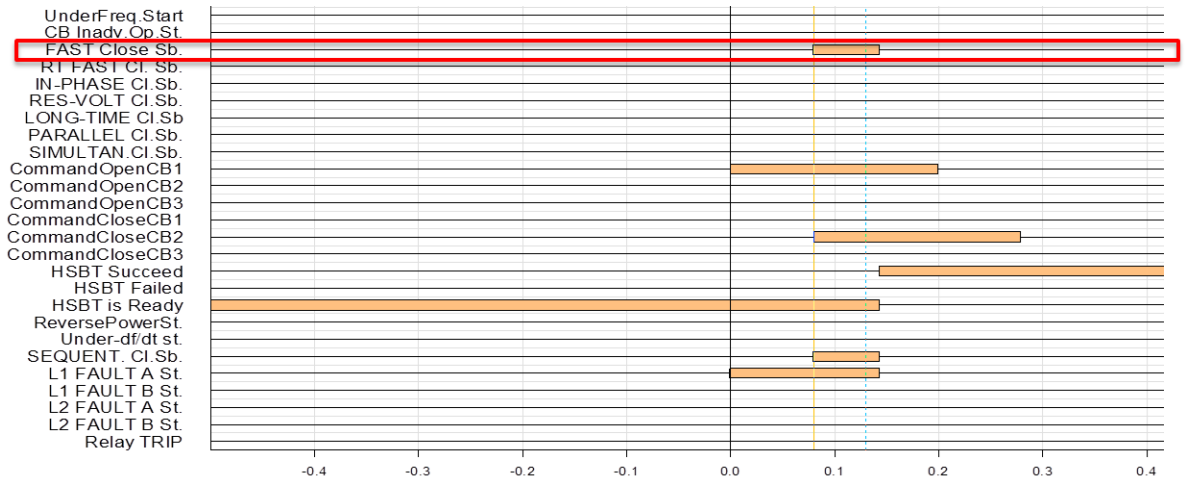

Figure 5-5: Relay Operation Sequence for 25kV single phase Fault

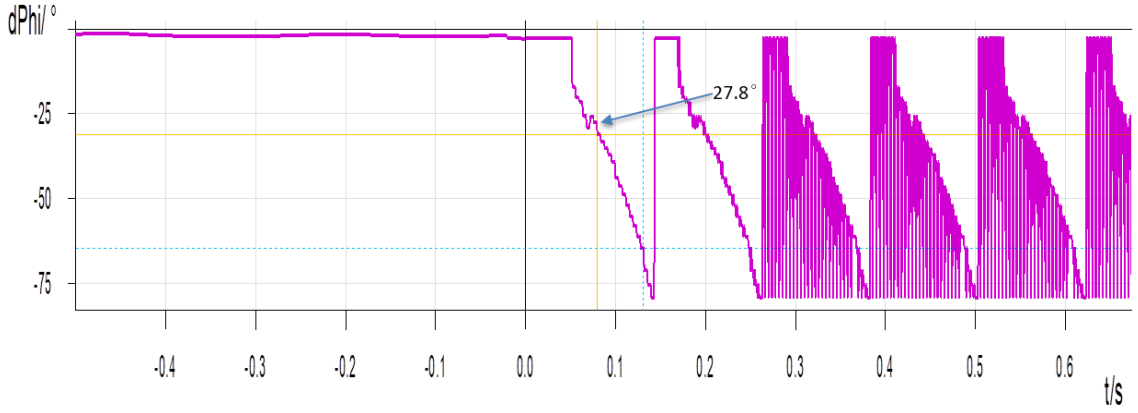

Figure 5-6: Delta Phase Angle Recording for 25kV single phase Fault

Following the same procure with different setting (delta phase angle $d\theta$ is set as 20 °), the single-phase fault in the 25kV side would initiate a real-time fast transfer mode with a 243ms transfer time. From the perspective of motor transfer time, fast transfer mode has a shorter transfer time compared with the real-time fast mode, which means the fast transfer motor has less interruption of the industrial process. However, the transfer time is only one dimension to evaluate the transfer performance. Except for the transfer time, another essential criterion to evaluate the transfer is the inrush torque when the auxiliary feeder closes. Therefore, the torque behavior should be analyzed for those two transfer modes.

By applying such transfer time in EMTP simulation, the inrush torque behavior of motors (taking induction motor M1b as an example) when auxiliary feeder closes for two transfer modes are shown in figure 5-7.

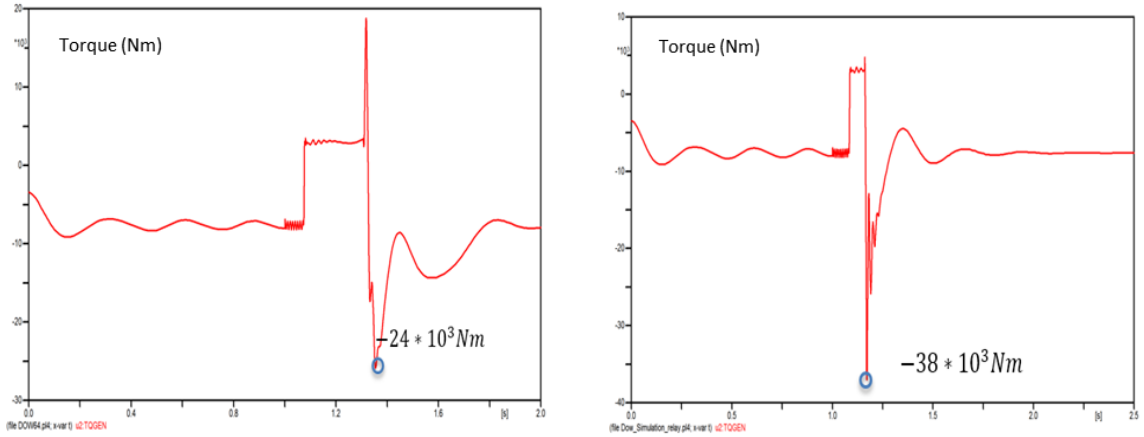

a.Real-time Fast Mode b.Fast Mode

Figure 5-7: Comparison of Inrush Torque by Two Transfer Modes

As illustrated in figure 5-7, the maximum inrush torque for fast mode transfer is almost twice as the real-time fast mode, although the transfer time for fast mode is quite short. The delta phase angle behavior during bus transfer is shown in figure 5-8. It can be shown that the phase angle difference in fast mode transfer is quite high (almost 90°) compared with the real-time fast transfer mode (31°). Such large voltage angle difference contributes to high inrush current and therefore, leads to a large inrush torque.

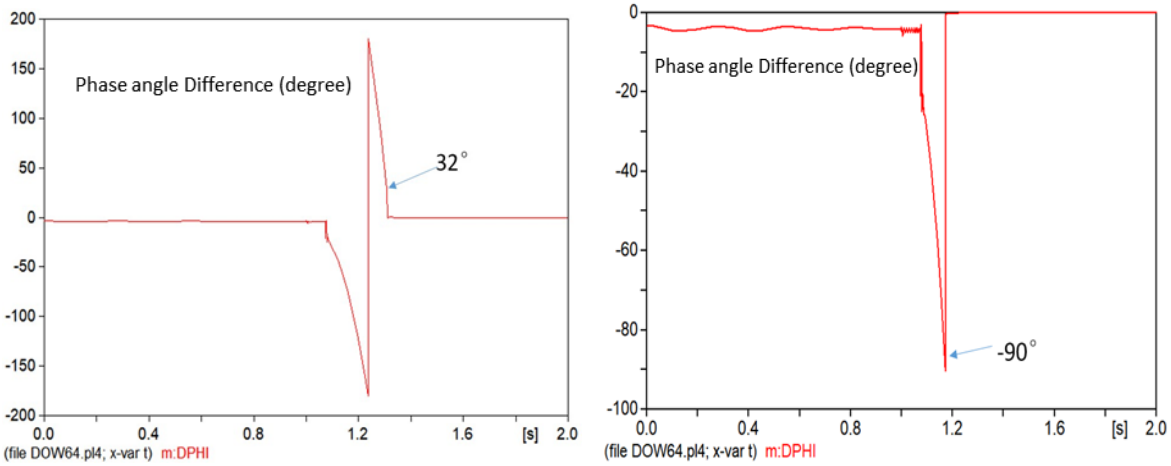

a.Real-time Fast Mode b.Fast Mode

Figure 5-8: Comparison of delta phase angle by Two Transfer Modes

Figure 5-9 shows the maximum torque behavior of all induction motors, and it can be concluded that although the magnitude of the inrush torque of each induction motors is different, the maximum inrush torques for all motors in fast mode are higher than real-time fast mode for single phase fault in 25kV side .

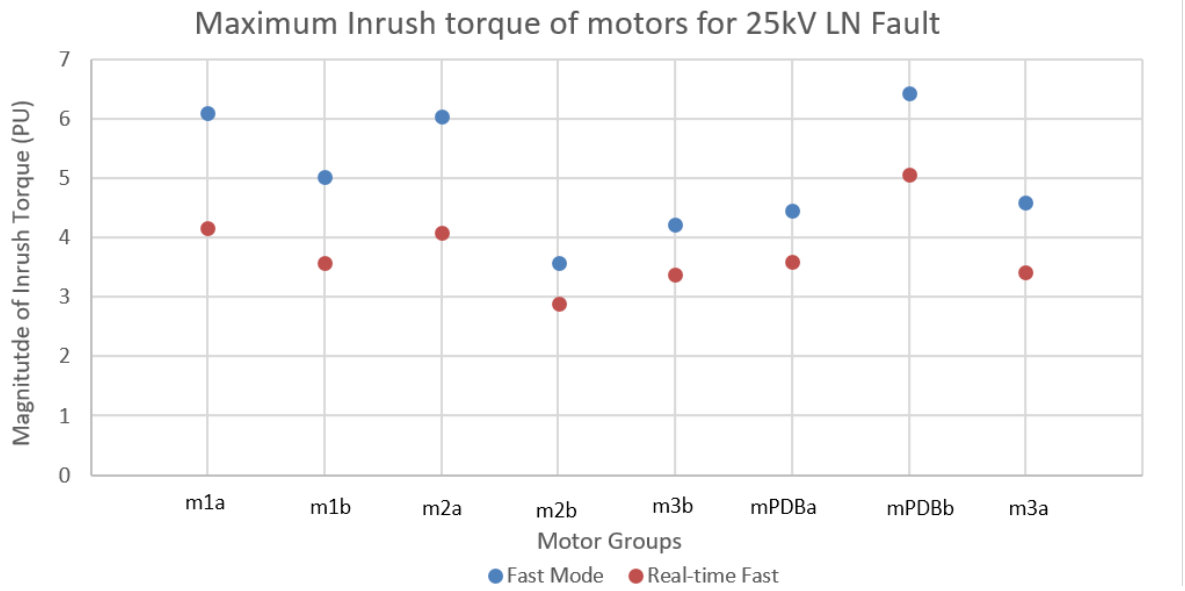

Figure 5-9: Maximum Inrush torque of motors for 25kV LN Fault

The reason why fast transfer mode leads to a high inrush torque compared with real-time fast mode are elaborated as follows. As we can see in chapter 4-3, after the breaker receives a close command, due to the delay of the magnetic coil and mechanical drag, the breaker cannot close immediately. Such delay is called breaker closing time. During such closing time, the motor bus is still disconnected from the power source. Therefore, the speed of all motors keeps decreasing and leads to a large voltage amplitude and phase angle difference.

However, the fast transfer mode requires a relay reaction with a high speed. To achieve such high-speed transfer, the computational complexity must be decreased, and there is no prediction of the voltage amplitude and phase angle difference U_{diff} and $d\theta$. For large power system with high overall inertia, the breaker closing time will not have too many impacts, since the mechanical speed ω_r of all the motors cannot drop too fast. However, in DOW Tarragona, except for low inertia, the static loads exacerbate the decreasing of motor speed. Thus, the difference of phase angle and voltage changes dramatically during the breaker closing time and even leads to a 90◦ phase angle difference. In summary, for the power system with low inertia, the fast transfer mode is not a good choice from the perspective of enhancing the lifetime of motors.

Compared with the fast transfer mode, the real-time fast mode as the name indicates， can estimate the real-time amplitude and phase angle difference caused by the breaker closing time. The relay in real-time fast mode sends a closing signal to the breaker based on the estimation of voltage parameters in the next 50ms instead of the instant right now.

Overall, since the 240ms transfer time is acceptable for DOW Tarragona, it is better for all motors in 25kV single-phase fault to transfer in real-time fast mode to decrease the inrush.

5-3-3 Relay Testing Based for Feeder or Motor Bus Fault

As the fault time and signal transmission delay would impact the transfer time and mode, which will be illustrated in chapter 5-5 and 5-6, the testing based on fault locations and fault types should have a constant fault time and a signal communication delay. In this case, we suppose that both the auxiliary relays (transformer differential relay 87T) and communication links operate in normal condition. Based on that, a typical fault time 50ms and communication delay 20ms is used in the following testing.

The testing is to ensure that the relay can operate when contingencies occur in feeder bus and are blocked when faults occur in the motor bus. The figure 5-10 gives an overview of the transfer modes and transfer time (time period after fault feeder trips until auxiliary feeder close) in different locations with different fault types. The fault locations for feeder fault testing are designed near the 230kV and 25kV winding which is in the protection zone of the transformer differential relay 87T. The fast transfer relays are required to have a bi-directional transfer, so the testing results include the transfer time and modes from bus1 to bus2 or the opposition.

For the motor bus fault, the relay should be blocked by the block signal sent from overcurrent relay, and no transfer would be imitated when faults occur in the motor bus, which ensures the selectivity of the relay. As illustrated in figure 5-10 and figure, no motor faults initiated a motor transfer.

For all feeder fault cases, there is no big difference on transfer time whether the transfer is initiated from feeder1 to feeder2 or the other way around. The time differences between two transfer directions are less than 10ms. Such time differences are caused by the inaccuracy of the PLC. The PLC has a ±5ms inherent operation error. Such error can be eliminated by repeating one testing case for several times and choose the numerical average of the transfer time, but it is unnecessary to do such averaging since the real vacuum breakers also have an inaccuracy in both closing and opening time.

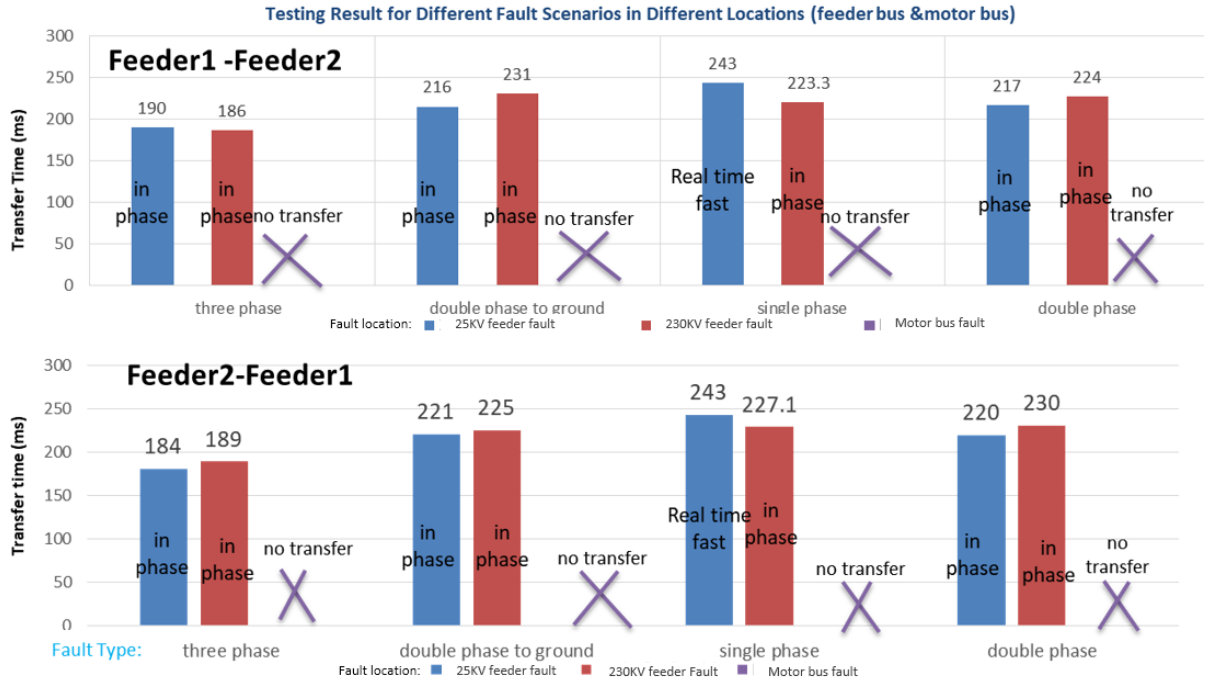

Figure 5-10: Motor Bus Transfer Time Based on Fault Type and Location

Except for the single-phase fault, whether a fault occurs in the high voltage or in the low voltage side of the transformers, there is a slight impact on the motor bus transfer behavior. Such small transfer time differences are caused by the internal impedance of the transformer TP and TR. Due to the internal transformer impedance, the current contribution from motors are different when a fault occursin 230kV or 25kV feeder. Consequently, the voltage behaviors of the motor bus are different after breaker trips, which leads to a small difference in transfer time.

For a single-phase fault, as table 5-2 indicates, with the help of 600A ground resistor, the single phase fault in the 25kv side has almost no impact on the motor residual voltage in whole short-circuit period. Based on the configuration, the single phase fault in 25kV side leads to a real-time fast transfer. The fault in the high voltage side leads to a high voltage dip and phase angle difference after breaker trips, so the relay will go to in-phase mode transfer mode with a different transfer time.

As we get the transfer time from the relay testing, the maximum inrush torque of all motors based on different faults can be obtained. As figure 5-10 shows, the transfer time from bus 1 to bus 2 or the opposite is almost the same. Therefore, we only analyze the torque behavior when the transfer happens from feeder 1 to feeder 2. Figure 5-11 and 5-12 shows the maximum inrush torque of all motors when the breaker closes in the auxiliary bus.

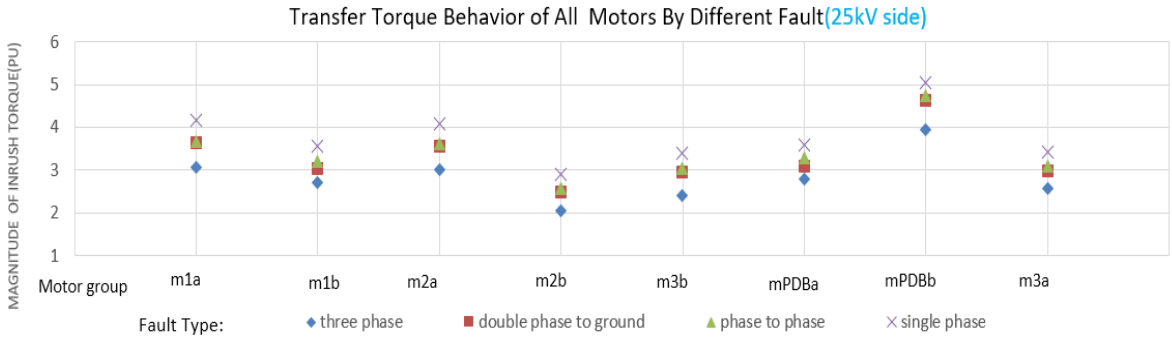

Figure 5-11: Maximum Inrush Torque for 25kV side fault

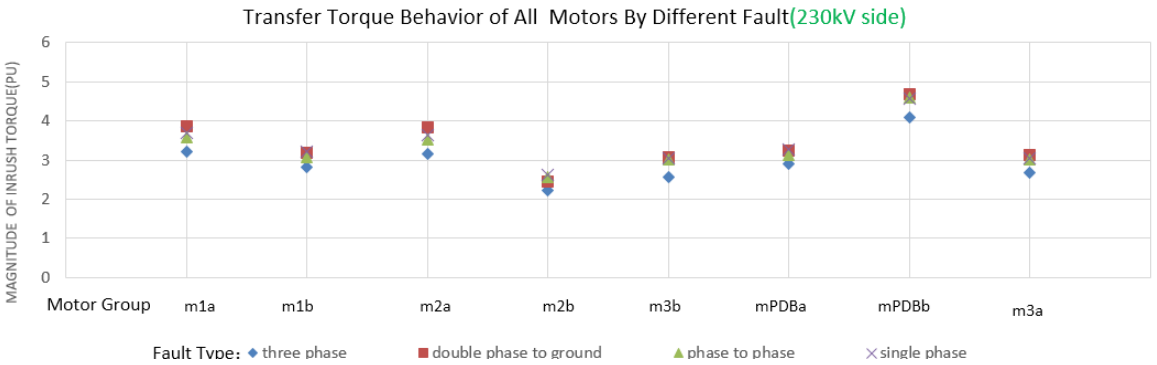

Figure 5-12: Maximum Inrush Torque for 230kV side fault

For the same fault scenario, the magnitudes of inrush torques of all motors are different. The induction motor group 'mPDBb' has encountered the highest inrush torque among all motors while motor 'm2b' faces the lowest inrush torque. The reason why different motor groups have different inrush torques is explained as follows. First, the parameters of each

25kV/6kV are different, which contributes a different equivalent impedance between the feeder bus and all motors and leads a different inrush current and torque. Besides, the air-gap torque of the induction motors for dynamic studies is deduced by [15]

$$T_e = \frac{3}{2} p \frac{M^2}{L_r} (-i_{S\alpha} i_{R\beta} + i_{S\beta} i_{R\alpha}) \tag{5-1}$$

Where p is the number of poles; M is the mutual inductance between the rotor and stator; L_r is the self-inductance of rotor winding; $i_{S\alpha}$, $i_{S\beta}$ and $i_{R\alpha}$, $i_{R\beta}$ is the stator current and rotor current in $\alpha\beta$ frame respectively.

Based on equation 5-1, it is clear that the self and mutual inductances of the induction motor also affects the inrush torque behavior. As the inductance of all motors is different, the magnitude of inrush torque must be different.

For different fault conditions, the relative relationship of inrush torque between all motor keeps the same. Therefore, it is reasonable to analyze the impacts of fault types on motors' inrush torque by examining one motor instead of all motors.

Based on that, we just take motor groups 'm1a' as an example. In most fault cases (except for single phase fault), there are no large differences of the inrush torque either the fault occurs in 25kV winding or in 230kV winding, as the transfer time and transfer mode is almost the same for such two fault locations. The motor inrush torque decreases when a single phase fault occurs in 230kV side compared with the fault in the 25kV side. As figure 5-10 shows, the single phase fault in the 25kV winding initiates a real-time fast transfer, while the same fault in the 230kV side leads to an in-phase transfer mode. Based on the simulation results of inrush torque, we can deduce that although the real-time fast transfer mode leads to a lower inrush torque than fast mode, the real-time fast transfer mode still results in a bit higher inrush torque compared with the in-phase transfer mode. The in-phase mode transfer can limit the delta phase angle $d\theta$ less than 10° compared with the 30° delta phase angle in real-time fast mode.

5-4 Relay Configuration and Testing for Transmission Grid Fault

For transmission grid fault, there is no initial signal sending to the fast transfer relay, although the motor bus would encounter a voltage dip. Based on the requirements in chapter 5-2, the relay needs to initiate a self-start when a fault occurs in the transmission grid and be blocked during the fault period.

The difficulty of configuring the transmission grid fault is that the DOW power plant does not know the exact fault point. We do not want to initiate a self-start transfer during the fault period. DOW does not know where the exact fault point is in the transmission grid, but the motor acts as a generator and supplies a current to the fault point. As the relay also measures the feeder current, the feeder current detection function can be added to detect the current contribution from motors and block the transfer when current flows through one of the feeder buses when a fault occurs in tranmission grid. Besides, the transmission grid may also encounter open circuit fault. Then the DOW power plant would see a voltage dip. With the help of self-start function, the relay can also initiate a transfer when transmission

grid faces an open circuit fault. In order to prevent the motor bus transfer caused by a small voltage oscillation, it is desired to set a relatively low threshold of self-start (0.8 PU of nominal motor bus voltage, 2Hz frequency decay and the change rate of frequency: -0.5Hz/s in the motor bus voltage). Based on the combination of those three self-start thresholds and fault current detection functions (line dead current), we can ensure that the fast transfer relay cannot transfer during the fault period. Figure 5-13 shows the settings changed from the default setting.

HBST settings which should be changed from the Siemens Suggest Setting			
setting number	setting name	default value	new value
8821	Normal start	off	on
8834	change rate of frequency	off	sequential
8827	Under voltage	off	sequential
8824	Under frequency	off	sequential
8837	Fault Detection	off	on
8838	Motor Start Detection	off	on

Self Start (Transfer after fault clear)

Figure 5-13: The Changed Setting from Suggested Values for self-Start

Based on such configuration, the relay can have a blank time (time period after a fault occurs until relay sends the pick-up signal) shown in table 5-3 for self-start in transmission grid fault. After such a blank time, the fast transfer relay will initiate a transfer which avoids the transfer during the fault period. The transfer time and the mode of transmission grid fault are listed as follow:

Table 5-3 Blank Time for Transmission Grid Fault

Fault Type		Self-start Blank Time (ms)
Short Circuit Fault	Single-Phase Fault	196
	Double-Phase Fault	184
	Phase-to-Phase Fault	181
	Three-Phase Fault	171
Open Circuit Fault		174

After the blank time in table 5-3, the fast transfer relay will initiate a transfer which avoids the transfer during fault period. The transfer time and modes of transmission grid fault are listed as table 5-4:

Table 5-4 Transfer Time and Transfer Mode for Transmission Grid Fault

Fault Type	Transfer Time (ms)	Transfer Mode
Single-Phase Fault	214	In-Phase
Double-Phase Fault	187	In-Phase
Phase-to-Phase Fault	408	Residual-Voltage
Three-Phase Fault	310	Residual-Voltage
Open-Circuit Fault	186	In-Phase

As table 5-3 shows, all transmission grid faults will initiate a self-start transfer with a blank time longer than 170ms, and the motor bus voltage keeps decaying during the blank time. Therefore, a large voltage decay will occur in the motor bus when the feeder bus breakers are tripped by the fast transfer relay. Due to the high voltage dip, not all cases can fulfil the threshold of in-phase mode transfer. The double-phase to ground and three phase fault leads to a residual voltage transfer with a higher longer transfer time.

Phase-to-phase fault takes the longest time to accomplish a motor bus transfer. As there is a blank time before the fast transfer relay starts, the voltage keeps decaying. Therefore, the transfer initiated by a phase to phase fault in the transmission grid cannot fulfill the threshold of the in-phase mode and takes a long time to wait for a residual voltage transfer. However, a three phase fault also does not fulfill the threshold of an in-phase mode transfer, but the trapped magnetic energy decays fast in the faulty period which leads to the lowest residual voltage among all faults. Therefore, the three phase fault takes less time to reach the threshold of residual voltage mode.

5-5 Sensitivity Testing on Differential Relay Trip Delay

When a fault occurs in the protection zone of the differential relay, the transformer differential relay can detect the in-zone fault and send a tripping signal to trip the relevant breakers. However, in practice, the time delay of the differential relay cannot always be constant. The longer relay trip delay leads to a longer fault time and a different fault time impacts motor bus transfer behaviors. Therefore, to examine the impact of relay trip time on fast transfer relay, a sensitivity study is designed. The relay delay is programmed from 10ms to 50ms in EMTP model.

DOW and DSOs are more interested in the transfer behavior when a fault occurs in the 25kV feeder. Therefore, the fault locations during sensitivity studies are only selected in the 25kV winding of transformers in feeder bus.

The previous study shows that there is no big difference on transfer time when motors transfer from feeder1 to feeder2 or the opposition. Thus, the sensitivity testing is only designed in 25kV feeder bus with only one transfer direction (feeder1 to feeder2). Figure 5-14 shows the transfer time and transfer mode for all kinds of faults when fault clear time changes when relay trip delay for 87T in sensitivity testing ranges from 10ms to 50ms.

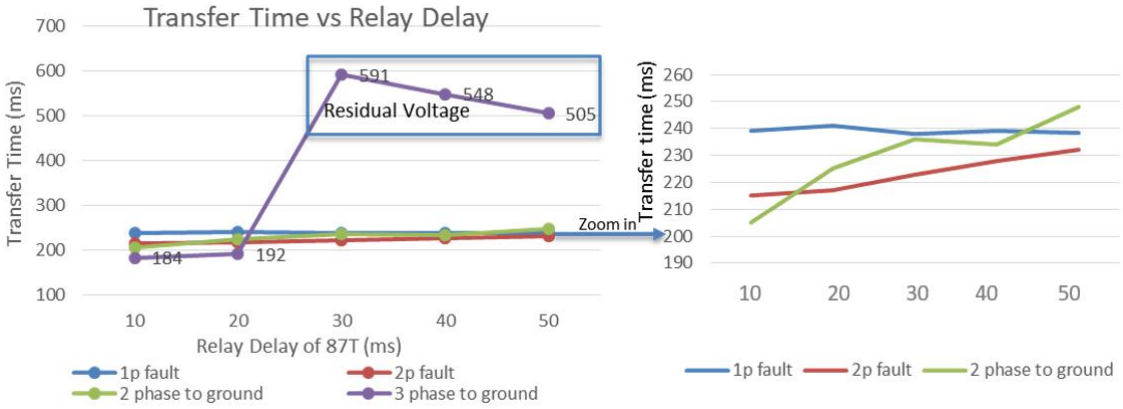

Figure 5-14: Sensitivity Study of Relay Trip Time

When a relay trip delay changes from 10ms to 50ms, the transfer time initiated by a three-phase fault changes dramatically from a minimum transfer time 184ms (in-phase mode) to a maximum transfer time 591ms (residual transfer mode). When the relay trip delay is relatively small (less than 30ms), the fast transfer relay is transferred in the in-phase mode for most fault cases (except for single phase fault). Besides, the transfer time for all fault scenarios increases except for single phase fault with the increase of 87T trip delay.

For single phase faults, the trip delay of 87T has no impact on the transfer time. The ground resistor in the low voltage side limits the fault current, and all motors in DOW power plant operates normally. Therefore, no matter how long the single-phase fault lasts, the motors cannot be affected during the fault period. Consequently, the motor bus residual voltage cannot be affected although single-phase fault time changes. That is the reason why the relay trip delay has no impacts on the motor bus transfer time.

For a phase-to-phase fault and a double-phase-to-ground fault, the dynamic behavior of the motor bus voltage can be impacted by different fault time. A long fault time leads to a low voltage amplitude and frequency.

During the period of three-phase fault, all three phases of the motors are lost power supply and motors contributes to a relatively high fault current level to the fault point. Based on the law of conservative of energy, the trapped magnetic energy depletes very fast and leads to a relatively low voltage amplitude which is lower than the threshold of in-phase mode after breaker opens.

As the voltage amplitude threshold A_U for a residual voltage mode transfer is set at a relatively low value, the relay needs time to wait for a residual mode transfer, which means the amplitude of the motor bus should be lower than 0.25PU (suggested threshold are given by Siemens [16] and Beckwith [20]). That is the reason why the 50ms trip delay leads to a shorter transfer time than 40ms for three-phase faults. The 50ms 87T trip delay results in a higher voltage dip than 40ms delay and therefore, takes less time to reach the 0.25PU threshold to have a residual-voltage transfer.

Then, the inrush torque can be obtained based on the same method in chapter 5-4-1. As the

relative relationships of the inrush torque for different motors keep the same, the motor group 'm1a' is chosen for the inrush torque study.

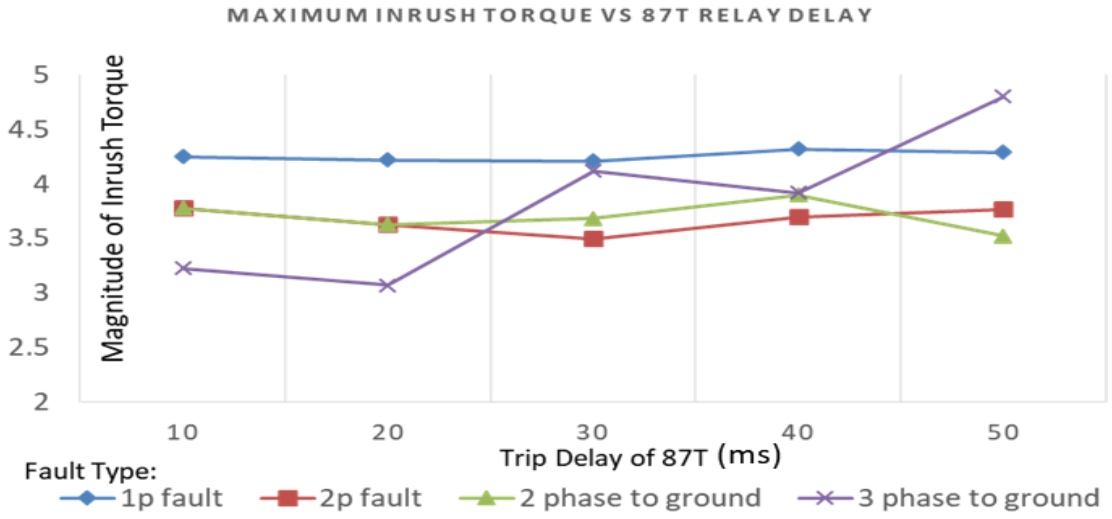

Figure 5-15: Sensitivity Study (Inrush Torque) of Relay Trip Time

As figure 5-15 indicates, except for a three-phase fault, the relay trip delay (less than 50ms) has almost no impact on the inrush torque behavior because such fault cases initiate the same transfer modes (in-phase transfer mode).

However, we can see a sharp increase in the inrush torque when the 87T trip delay is larger than 30ms for a three-phase fault. In figure 5-15, it can be seen that the motor bus is transferred in the residual voltage mode if the trip delay is larger than 30ms. Compared with the in-phase transfer mode, there is a high inrush torque in the residual voltage mode due to a long transfer time. A long transfer time leads to a low voltage amplitude of the motor bus voltage and contributes to a high voltage difference between the feeder bus and the motor bus compared with the in-phase transfer mode. Therefore, such high voltage difference leads to a large inrush torque. In practice, the operators should take measures to avoid a residual voltage mode transfer.

5-6 Sensitivity Testing on Communication Delay

The trip signal of 87T acts as an initial signal to pick up the fast transfer relay. However, the differential relay is always installed very far away from the fast transfer relay and therefore, the trip signal must be sent via the communication channel (optical fiber). Consequently, it needs time for fast transfer relay 7UV68 to receive such an initial signal. Typically, the communication delay takes 20ms, but in practice, it is inevitable for a communication network to encounter congestions which increase the communication delay. For some particular cases, such as broken communication links or routers, the fast transfer will not receive the initial signal although the relative breaker is tripped by the 87T. The relay is still required to transfer in such cases. The transfer is ensured by the breaker inadvertent opening detection if no trip command is received by the fast transfer. Once the relay detects the opening of the healthy breaker, the transfer will be initiated after a 50ms time delay.

The sensitivity testing for communication delay is also only designed for fault in the 25kV

bus, and only one direction transfer is considered (feeder1 to feeder2). In the sensitivity testing, the communication time is ranged from 10ms to 70ms. Besides, a special scenario where the fast transfer relay cannot receive is also added into the sensitivity testing.

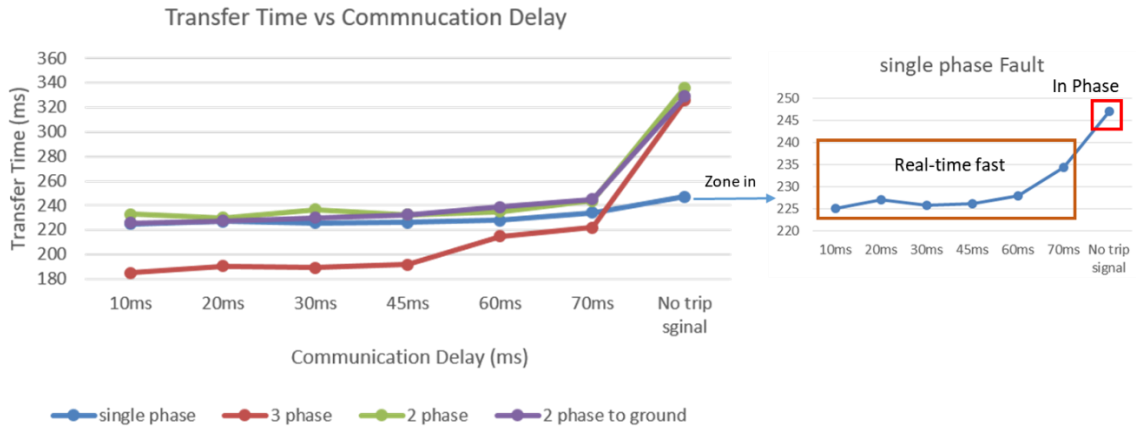

Figure 5-16: Sensitivity Study of Communication Delay

As figure 5-16 shows, the transfer time and the transfer mode will not be affected when the communication delay is less than the breaker breaking time (50ms) because the relay has already received the initiation signal before fault feeder opens.

However, if the communication time is longer than breaking time (60ms and 70ms cases), there would be a blank time period that the breaker opens, but no tripping signal is received by the relay. The longer the communication delay is, the longer the blank time will be. During such blank time, the motor bus residual voltage U_{res} keeps decaying and leads to a longer transfer time for long communication delay, especially for three-phase fault. For fault cases where the communication delay is less than 70ms, the real-time fast mode transfer is initiated by a single phase fault, and other fault leads to in-phase mode transfer.

Besides, this thesis also considers the most severe cases where no initial signals are received by the fast transfer relay, the bus transfer needs a long time because the relay regards the faults without tripping signal as an inadvertent breaker opening. It needs time for the breaker-opening-detection function to initiate the transfer. Such time delay results in an in-phase mode transfer for a single phase fault and the transfer mode for other fault scenarios do not change (still in in-phase modes).

Based on the transfer time of the sensitivity study, the inrush torque behaviors of motors can be analyzed. Figure 5-17 shows the inrush torque of motor group 'm1a'when communication delay ranges from 10ms to infinite (no tripping signal).

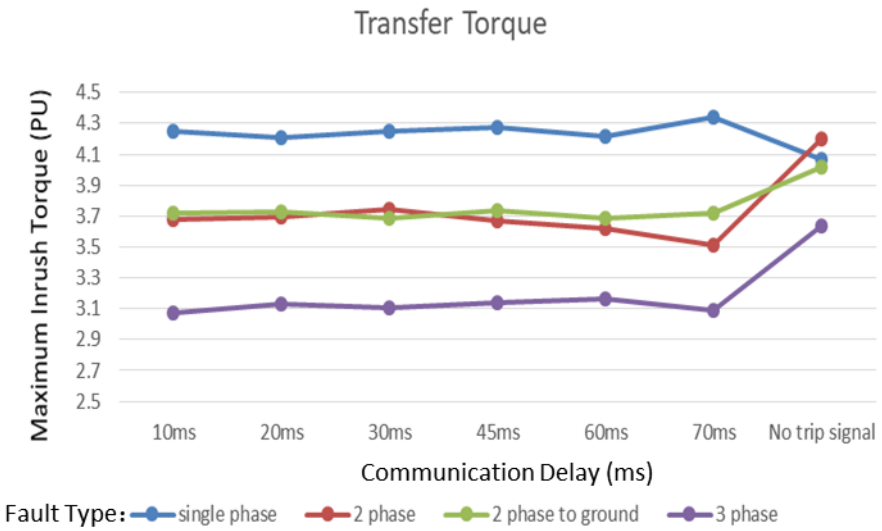

Figure 5-17: Sensitivity Study (Inrush Torque) of Communication Delay

As figure 5-17 shows, there are no big differences for the inrush torques when the communication delay varies from 10ms to 70ms. The small torque variation is caused by the slight differences in transfer time. However, if the fast transfer relay cannot receive the trip signal, except for a single phase fault, other fault types lead to a higher inrush torque. For such fault scenarios, the transfer modes do not change, but the transfer takes a long time (more than 300ms). As we can see in chapter 5-5, a long transfer time will lead to a high inrush torque. That's the reason why we can see an increase in the inrush torque when no trip is sent to the relay.

Nevertheless, for the single-phase fault cases without tripping signal, the transient torque decreases a bit compared with the normal communication delay. Such decrease is caused by the changing of the transfer mode (from real-time fast mode to in-phase mode). In chapter 5-3, we can see that the in-phase transfer mode has less inrush torque compared with the real-time fast mode.

Chapter 6

Conclusion and Future Work

6-1 Conclusion

Although some testing has been already designed to examine the transfer behavior of fast transfer relay by engineers from industries, that testing is general testing, and no testing is designed based on the actual power system model. Besides, no testing results have been proposed about the motor inrush torque behavior. This thesis deals with testing of the fast transfer relay 7UV68 based on the EMTP modelling of DOW Tarragona. Except for fast transfer relay testing, such a power plant model can also be used for stability analysis and configuration of other types of relays. Based on the EMTP simulation and the relay testing result, overall conclusions are given as follows:

1. The power loss in the motor bus with running motors leads to a residual voltage U_{res} with a decaying magnitude and frequency in the motor bus. The reclosing of the auxiliary feeder bus leads to a high inrush current and a torque due to the voltage parameter difference between the reference feeder and the motor bus.
2. Sequential transfer scheme has the longest transfer time, but such scheme absolutely avoids the motor bus transfer and the parallel operation of the two sources during the fault period and increase the stability of the system.
3. Transfer in fast (real-time fast) mode will only happen with a single-phase to ground faults in the 25kV feeder in DOW Tarragona plant. Other fault scenarios in such plant will lead to transfers in in-phase or residual voltage transfer modes.
4. From the perspective of decreasing inrush torque, a fast transfer mode is not suitable for a power system with low inertia, because such mode cannot make an estimation on the voltage change caused by the breaker close delay.
5. The trip delay of the differential relay (87T) affects the behavior of the motor bus transfer. A three phase fault with a long 87T trip delay is the most severe case for a relay to transfer, as such faults contribute to the longest transfer time and the highest inrush torque.

6. A Short communication delay between the fast transfer relay and the transformer differential relay (87T) has no impact on the transfer behavior of the motor bus whilst a long communication delay (longer than breaker breaking time) will lead to a long transfer time.

6-2 Future Work

1. Testing of the relay can be designed by a hardware-in-the-loop testing system with RTDS (real-time digital power system simulator). With the help of real-time simulation, it is much easier to have a comprehensive understanding of the dynamic behavior of the motors and the impact of different faults on the performance of the fast transfer relay. There will be two stages of designing the hardware-in-the-loop testing. The first step is the same as this thesis, which is the power system modelling. The second step is to design the testing hardware. The analog signals to the fast relay will be generated from the RSCAD simulation via Gigabit Transceiver Analogue Output (GTAO) cards and amplifiers to the relay. The binary inputs and outputs should connect to Gigabit Transceiver Front Panel Interface (GTFPI) cards.

2. The vacuum breakers of the 25kV bus may experience overvoltages after they are switched off. The transient recovery voltage behavior can be analyzed by designing suitable vacuum breakers and arc models in EMTP.

Appendix A

Testing Setup and Installation

1 Figure of Testing Setup

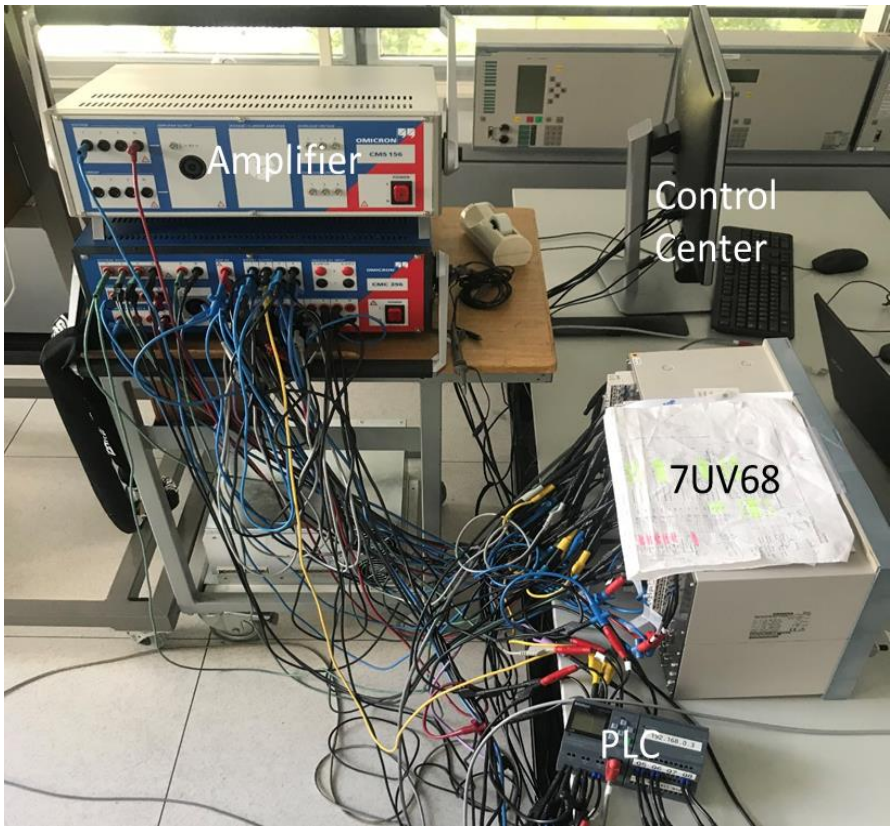

Figure Appendix A.1 Testing Setup and Connection

Appendix B

System Data of DOW Tarragona

1. Cable Data

Table Appendix B.1 Cable Data

Cable type	Nominal/Maximum Voltage(kV)	AC Resistance 90℃ (Ω/km)	Reactance 50Hz (Ω/km)
Feeding cable bus3:3**240 sqmm XLPE CU 500m(BusA and B)	18/30	0.0976	0.117
Feeding cable bus2:3*240 sqmm XLPE AL 990m BusA 360m BusB	18/30	01.61	0.117
Feeding cable PDB:3*240 sqmm XLPE CU 360m (BusA and B)	18/30	0.0976	0.117
Feeding cable TR-MC:3*240 sqmm XLPE CU 60m	18/30	0.0976	0.117
Feeding cable principle:3*240 sqmm XLPE CU 30m (BusA and B)	18/30	0.0976	0.117
Cable TP to TR:3*3*1 630 sqmm XLPE AL 600 (BusA and B)	19/33(36)	0.063	0.102
Cable 230kV gird:3*1*630 sqmm XLPE CU 800m (BusA and B)	3.8/6.6(7.2)	0.063	0.11

Appendix B

2. Load Data

Table Appendix B.2 Load Data

Plant	Total static load bus A		Total static load bus B		Induction motors A	Synchroneous motors A	Induction motors B	Synchroneous motors B	Capacitor A	Capacitor B
	P [MW]	Q [Mvar]	P [MW]	Q [Mvar]	P [MW]	P [MW]	P [MW]	P [MW]	[Mvar]	[Mvar]
25kV bus 2								2.35		
25kV bus 1	3.2	0.3			0.88					
PDB-III 6kV	2.6	0.8	1.6	0.5	0.59	1.6	0.5	7.46	0	14
Train II 6kV	0.3	0.2	0.3	0.2	3.5		4.2		1.15	2.3
Train III 6kV	1	0.5	1	0.5	4			4.2	0.6	0.6
Poly/primacor /train I	2	1	2	1	2		2	0.37		
Totals	9.1	2.8	4.9	2.2	10.97	1.6	6.7	14.38	1.75	16.9

The yellow cells are synchroneous motors.

Appendix C

Model for Auxiliary Relay and Additional Measurement

1 Differential Relay Model

```
MODEL Simple Differential Relay Model

DATA
  FREQ {dflt:50} -- Frequency of the first harmonic
  SampleFreq {dflt:400}
  Scale {dflt:1}
  Algorithm  {dflt:1}  --DFT recursive
INPUT
  xt[1..3]
  xm[1..3] -- The input signal which is to be analyzed
OUTPUT
  --re[1..3]  -- Magnitude values of the fundamental frequency component.
Phase ABC
  --im[1..3]
  irest[1..3]
  isum[1..3] -- Magnitude values of the fundamental frequency component.
Phase ABC
  trip2
VAR
re[1..3], im[1..3],OMEGA,NSAMPL,alpha,D,i,delta_T[0..7],

x7,x72,xre,xim,x[1..3],ab[1..3],ab2[1..3],re2[1..3],im2[1..3],D2,xm7,n,trip
1
 irest[1..3],isum[1..3],
 trip[1..3],flag,trip2,isum1[1..3]

TIMESTEP min:recip(SampleFreq)
DELAY CELLS (X[1..3]): recip(FREQ*timestep)+2
DELAY CELLS (XM[1..3]): recip(FREQ*timestep)+2 -- Need at least one first
harmonic periode of sampling
HISTORY X[1..3] {DFLT:0}
        xm[1..3]{DFLT:0} -- Fills the signal with zeroes when time <= 0
         trip1{dflt:0}
INIT
  FOR i:= 0 TO 7 DO
    delta_T[i] := i/(FREQ*8)
  ENDFOR
```

Appendix C

```
alpha:=1/sqrt(2)
  OMEGA:=2*PI*FREQ
  NSAMPL:=recip(FREQ*timestep)
  if abs(NSAMPL-trunc(NSAMPL))>1e-9 then
    write('%%%WARNING in ABC2PHR2: SAMPLEFREQ/FREQ is not an integer
number')
  endif
  re[1..3] :=0
  im[1..3] :=0
  re2[1..3] :=0
  im2[1..3] :=0
  trip[1..3]:=0
  trip1:=0
  flag:=0
ENDINIT
EXEC
  for i:=1 to 3 do
  x[i]:=8.702*xt[i]
    if Algorithm =1 then
    --DFT recursive moving window
      x7:=delay(X[i],1/FREQ,2)
      x72:=delay(XM[i],1/FREQ,2)
      D:=2/NSAMPL*(X[i]-x7)*cos(OMEGA*T) --recursive DFT

      re[i]:=re[i]+D*Scale
      D:=2/NSAMPL*(X[i]-x7)*sin(OMEGA*T)
      im[i]:=im[i]-D*Scale
      xm7:=delay(XM[i],1/FREQ,2)
      D2:=2/NSAMPL*(XM[i]-x72)*cos(OMEGA*T)
      re2[i]:=re2[i]+D2*Scale
      D2:=2/NSAMPL*(XM[i]-x72)*sin(OMEGA*T)
      im2[i]:=im2[i]-D2*Scale
    endif
   ab[i]:=sqrt(re[i]**2+im[i]**2)
   ab2[i]:=sqrt(re2[i]**2+im2[i]**2)
  endfor
 if flag=0 then
 for n:=1 to 3 do
isum1[n]:=sqrt((re[n]+re2[n])**2+(im[n]+im2[n])**2)
if isum1[n]<20 then
isum[n]:=0
endif

irest[n]:=1/2*(sqrt(re[n]*re[n]+im[n]*im[n])+sqrt(re2[n]*re2[n]+im2[n]*im2[
n]))
```

Appendix C

```
 isum[n]:=sqrt((re[n]-re2[n])**2+(im[n]-im2[n])**2)
 if t>1.06 then
 isum[n]:=0
 endif
 if isum[n]>0.3*irest[n] then
 trip[n]:=1
 flag:=1
 endif
 endfor
 else
 trip[1..3]:=1
 endif
 trip1:=or(trip[1],trip[2],trip[3])
 trip2:=delay(trip1,0.02,1)
ENDEXEC
ENDMODEL
```

Appendix C

2 Overcurrent Relay Model

```
MODEL   currentrelay1
DATA
  freq          -- base frequency
  xrms_ini {dflt:-1} -- initial rms value
  scale {dflt:1} --multiply output by this number
  SampleFreq
INPUT
  x[1..3]     -- monitored signal
  --block
OUTPUT
  trip[1..3]
  trip1 -- rms value of monitored signal
  i0rms
VAR
  xrms[1..3]
  x2[1..3]       -- internal, x*x
  ix2[1..3]
  ix20
  period         -- 1/freq
  n
  trip[1..3]
  trip2
  flag
  trip1
  i0
  i0rms

 x20
 trip0

History
 trip2 {dflt:0}
 ix2[1..3]{dflt:0}
init
 trip[1..3]:=0
 trip2:=0
 flag:=0
 trip0:=0
endinit
TIMESTEP min:recip(SampleFreq) --this restricts local timestep to avoid
overflow
DELAY CELLS(ix2[1..3],ix20,trip2,trip1,trip0): 2*recip(freq*timestep)
INIT
```

Appendix C

```
  period:= recip(freq)
  histdef(ix2[1..3]) := 0
  histdef(ix20) := 0
  histdef(trip2):=0
  integral(x2[1..3]) := 0
  integral(x20):=0
  flag:=0
  IF xrms_ini <0 THEN xrms[1..3]:=0 ELSE xrms[1..3]:=xrms_ini ENDIF
ENDINIT
EXEC
   i0:=x[1]+x[2]+x[3] -zero sequence current
   x20:=i0*i0
   ix20:=integral(x20)
   i0rms:= sqrt((ix20 - delay(ix20, period))*freq)*scale-RMS value
   if flag=0 then
   FOR n:=1 TO 3 DO
    x2[n]  := x[n]*x[n]
    ix2[n] := integral(x2[n])
    IF t>period THEN
      xrms[n] := sqrt((ix2[n] - delay(ix2[n], period))*freq)*scale
    else
    xrms[n]:=0
    ENDIF
   if (xrms[n]>6000) then
   trip[n]:=1
   flag:=1
   else
   trip[n]:=0
   endif

  ENDFOR
  else
  trip[1..3]:=1
  endif
  if (i0rms>500) then -threshold of zero current sequence measurement
  trip0:=1
  flag:=1
  else
  trip0:=0
  endif
  trip2:=or(trip[1],trip[2],trip[3],trip0)
  trip1:=delay(trip2,0.015)
ENDEXEC
ENDMODEL
```

Appendix C

3 Frequency Measurement

```
MODEL fremea
  DATA   f0       -- initial frequency
         band     -- max acceptable change
  INPUT  x        -- monitored signal
  VAR    f        -- measured frequency
         txing    -- time of last detected zero-crossing
         xprev    -- previous value of signal
         dtmin    -- minimum sampling half-period
         dtmax    -- maximum sampling half-period
         a        -- temp variable
  OUTPUT f
  INIT
    f     := f0
    txing := -2
    xprev := x
    dtmax := 1/(1-band/100)/f0
    dtmin := 1/(1+band/100)/f0
  ENDINIT
  EXEC
    IF txing = -2 THEN txing := -1
    ELSIF txing = -1 AND xprev*x <=0 AND xprev<x THEN txing:=t
    ELSIF xprev*x <=0 AND xprev<x AND t-txing >= dtmin AND t-txing <= dtmax
THEN - Finding Zero Crossing Point
      a := backtime(x,0,1)
      f := 1/(a-txing)
      txing := a
    ENDIF
    xprev := x
  ENDEXEC
ENDMODEL
```

Appendix C

4 Amplitude and Phase measurement

```
MODEL phasormeasure

INPUT  u[1..3]   -- phase voltages

OUTPUT vamp,  ure, uim ,angle,freq

---DATA
  --sample {DFLT:0.0}          -- phase betw. d-axis and alpha-axis}
VAR
  ualpha,ubeta,angle,vamp,ure,uim,vampt,freq
history
 angle{dflt:0.00}
EXEC
  -- From three-phase to alfa-beta-zero
  ualpha := 2/3*(u[1] - 0.5*(u[2]+u[3]))
  ubeta := 1/(SQRT(3))*(u[2] - u[3]) - Clarke Transformation

  vampt := SQRT(ualpha*ualpha+ubeta*ubeta)
  vamp := vampt
  angle := atan(ualpha/ubeta)/(2*3.141596)*360
  ure := ualpha
  uim := ubeta
  if uim >=0 then angle:= acos(ure/vampt)
  else
  angle:= -acos(ure/vampt)
  endif
ENDEXEC

ENDMODEL
```

Appendix D

The relay setting of 7UV68

1 Power System Setting for Fast Transfer Relay

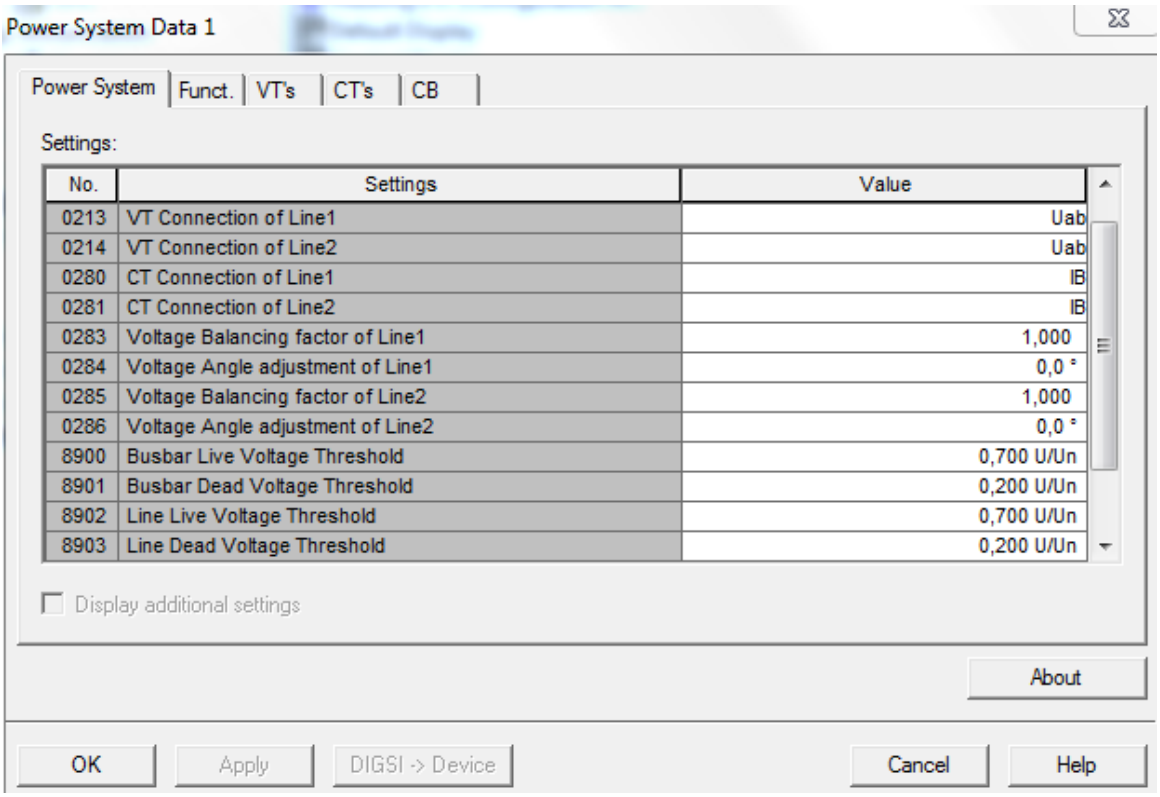

Figure Appendix D.1 Basic Power System Data

Appendix D

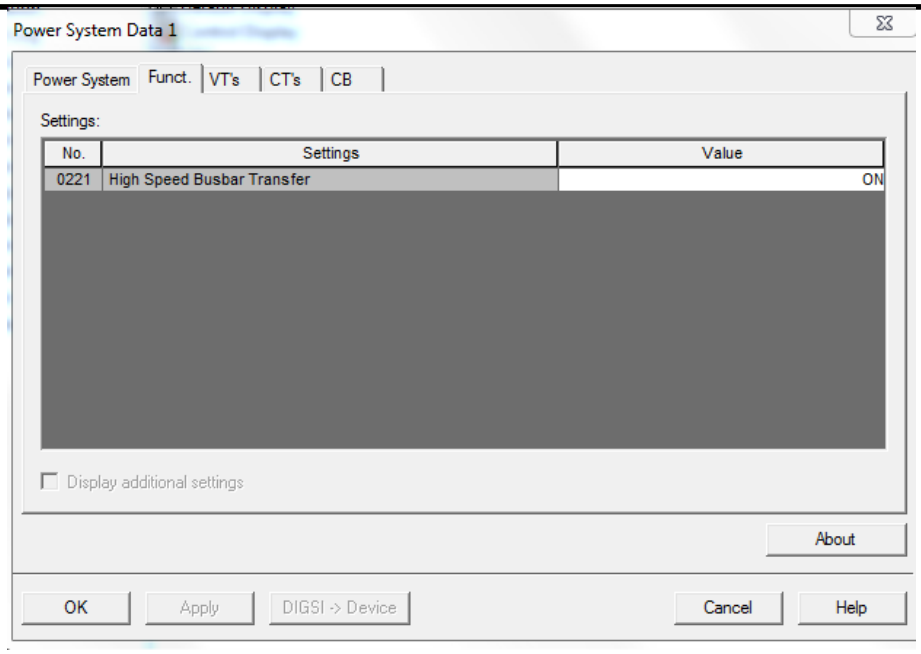

Figure Appendix D.2 Relay Startup

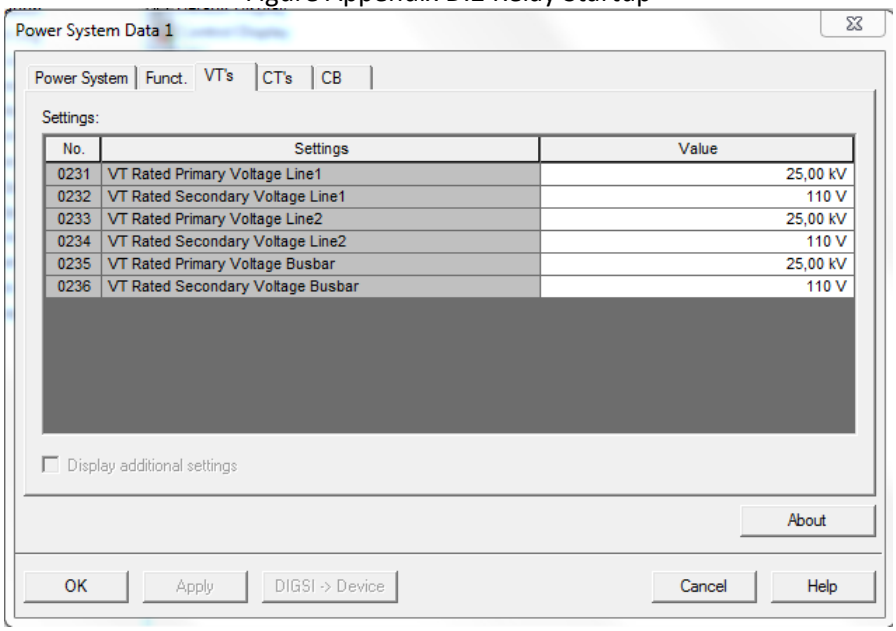

Figure Appendix D.3 VT Setting

Appendix D

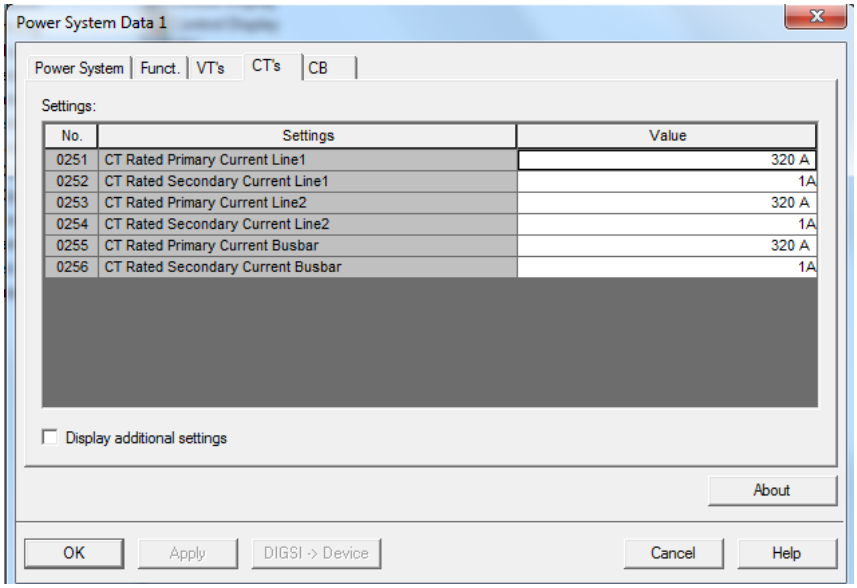

Figure Appendix D.4 CT Setting

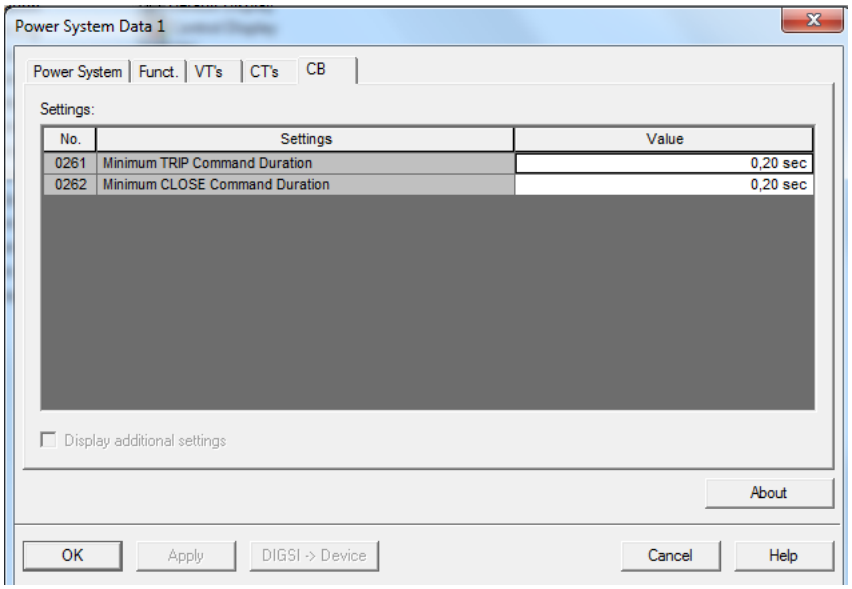

Figure Appendix D.5 Minimum CB Duration Setting

Appendix D

2 HSBT (high speed bus transfer) Function Setting

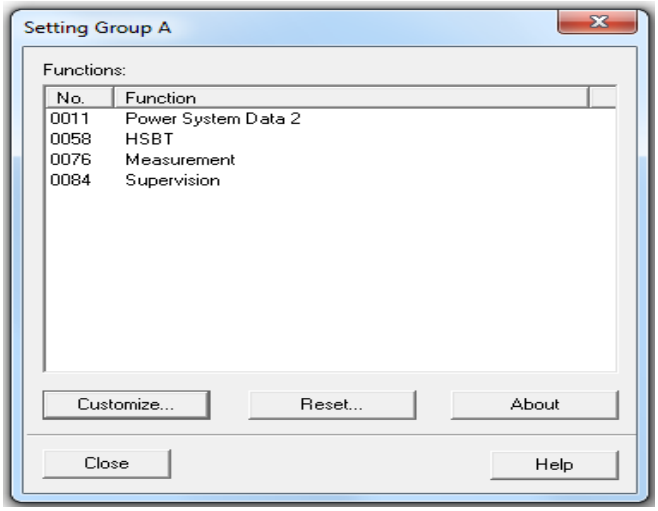

Figure Appendix D.6 Overall Setting Group

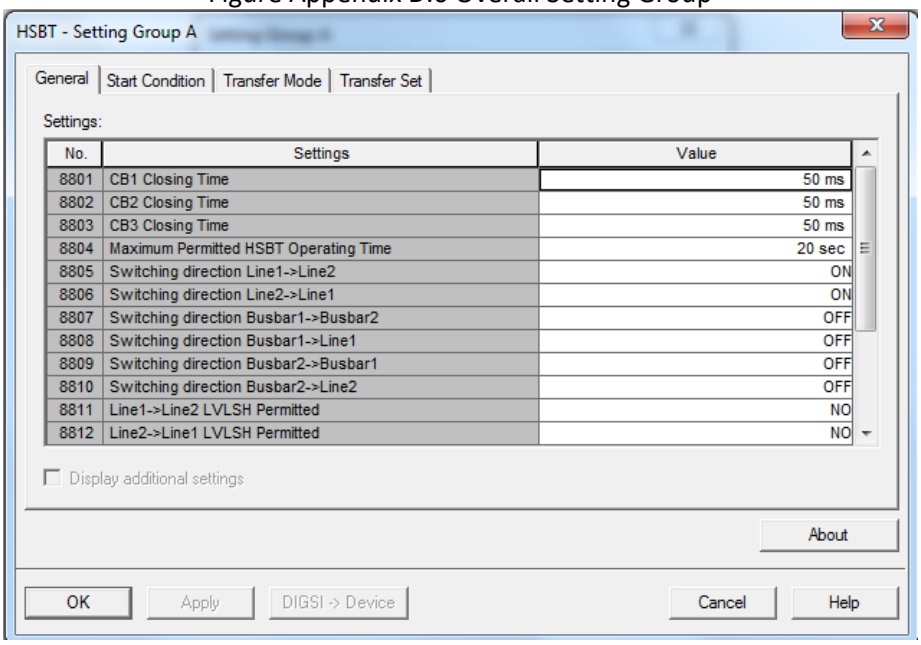

Figure Appendix D.7 Setting of Transfer Initialization Function (A)

Appendix D

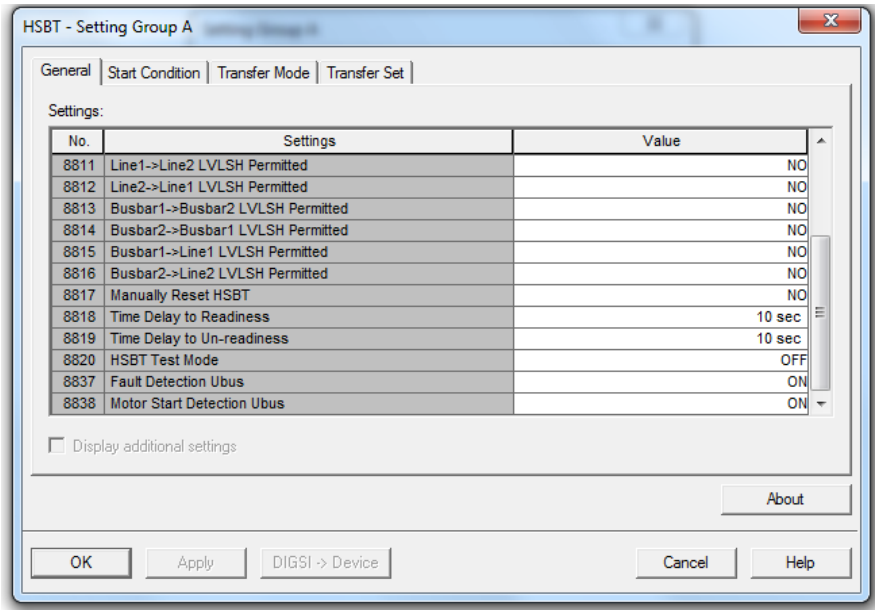

Figure Appendix D.8 Setting of Transfer Initialization Function (B)

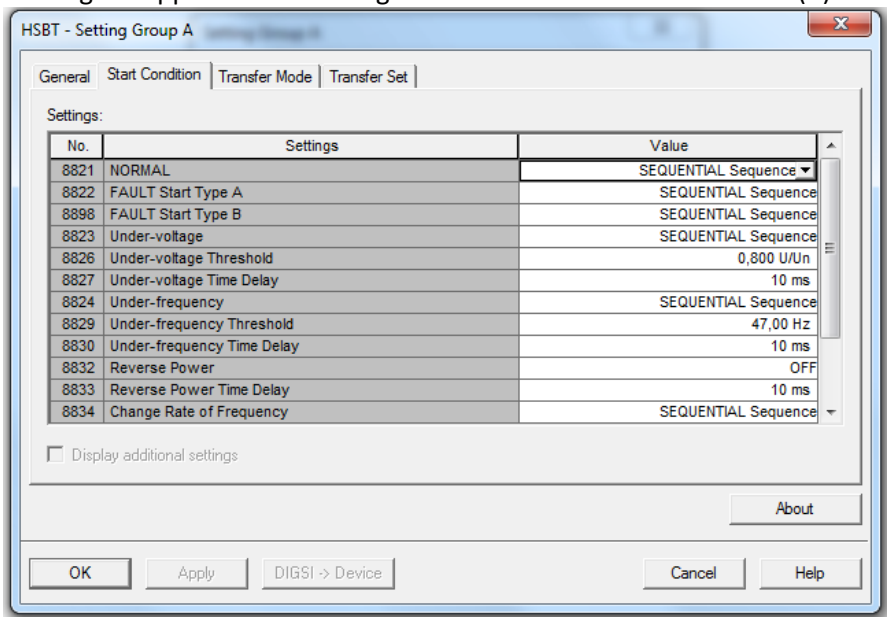

Figure Appendix D.9 Transfer Sequence and Self-start Function Design (A)

Appendix D

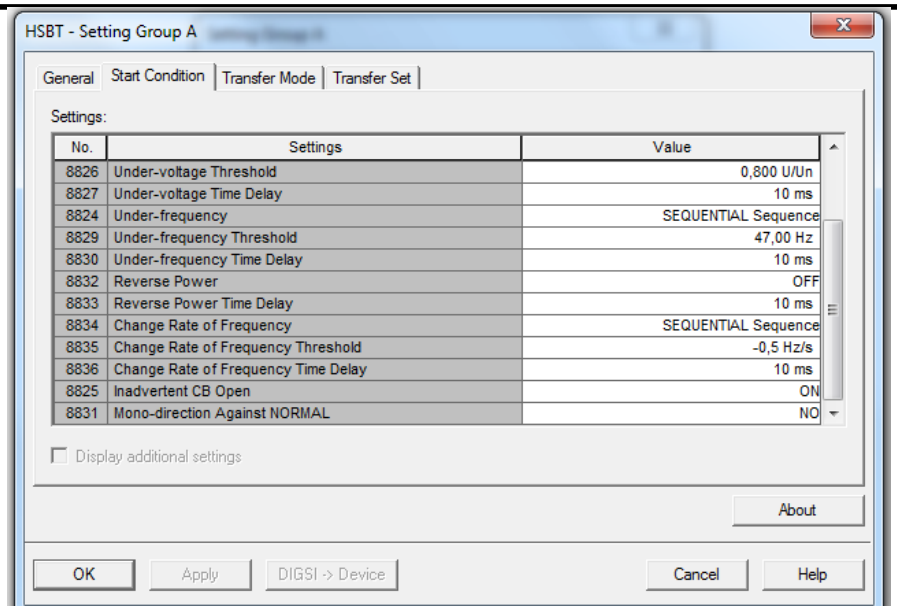

Figure Appendix D.10 Transfer Sequence and Self-start Function Design (B)

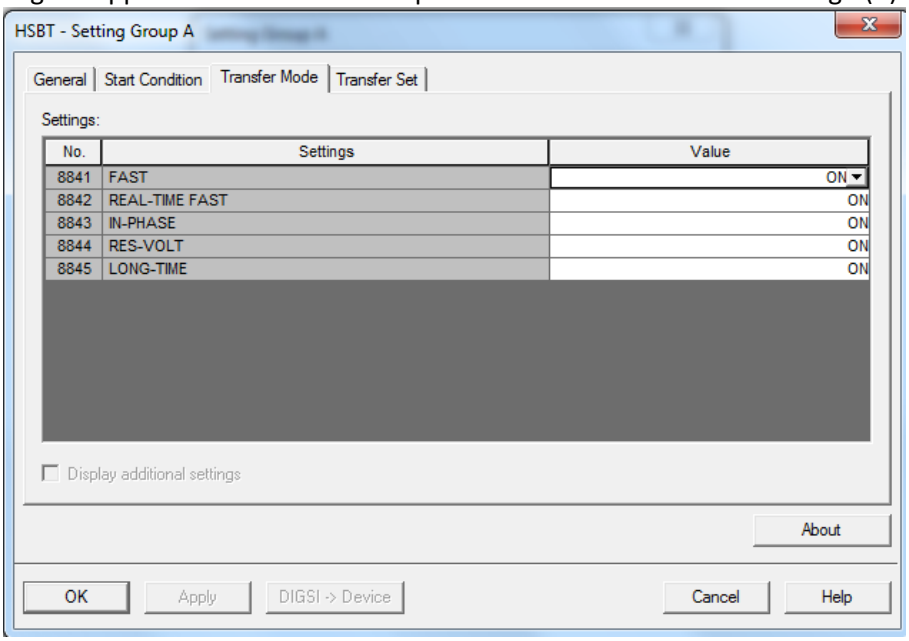

Figure Appendix D.11 Transfer Mode Selection

Appendix D

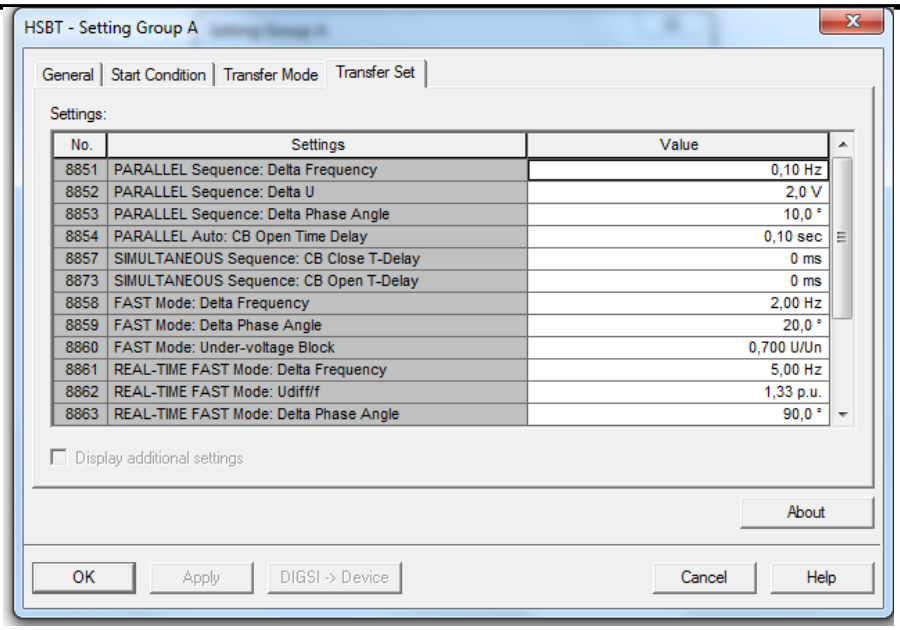

Figure Appendix D.12 Transfer threshold of Different Transfer Mode (A)

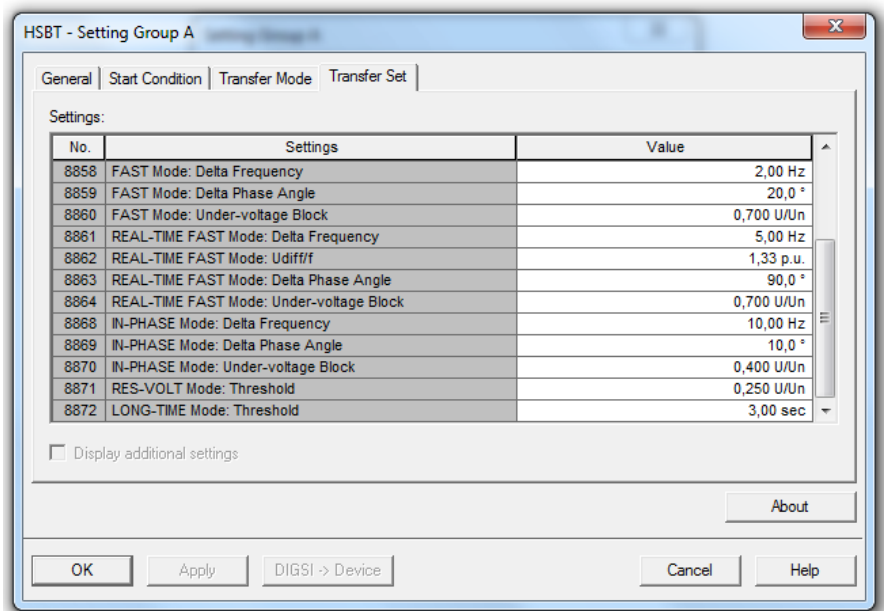

Figure Appendix D.13 Transfer threshold of Different Transfer Mode (B)

Appendix D

3 Supervisory Function Setting

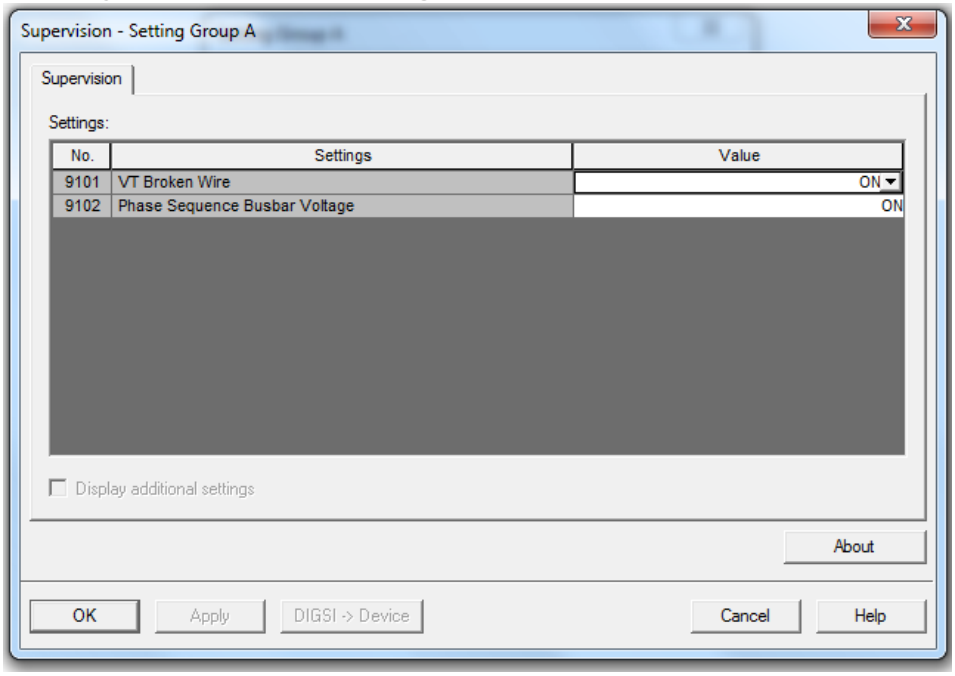

Figure Appendix D.13 Additional Supervisory Function

Appendix E

EMTP Modelling For Starting a Synchronous Motor

This part is not relevant to this thesis. Such model is used as a reference for DOW to simulate the motor start for Tarragona and other power plant.

Except for the startup of synchronous motor by varying frequency, which uses power electronic converters, a simpler way can be used for starting such motors.

The synchronous machines can be directly connected to AC voltage power source. As figure 3-17 shows the synchronous motors have excitation winding and damper windings which damps the oscillations. Such short-circuited windings act as the rotor winding of the induction motors and with the help of such windings, the synchronous motor can start as an induction motor. As the speed increases to the asynchronous speed, the excitation of the motor is added. With the help of the excitation field, the synchronous motors can run in a synchronous speed.

To simulate the startup, all parameters of the EMTP model S.M.59 should be tuned precisely. The initial machine speed should be set as a very low value (1%- 2% the nominal speed). Besides, the initial voltage, the frequency and the capacity in the relevant synchronous motor model should be 2% of the nominal value. When the motor speed reach 98%, the excitation field can be added.

The synchronous motor used in this thesis is a 28 poles motor with a 6kV nominal voltage and a 9.6 MW nominal power. The nominal speed of the motor can be calculated as:

$$n = \frac{60 f}{p} = 214.28 \qquad (1)$$

The mechanical load used in this chapter is the reciprocated industrial load (seen from chapter 3-4), such load is added when synchronous motor reach to the nominal speed (after 5s). The input data of the startup simulation are shown in figure Appendix E.1

Appendix E

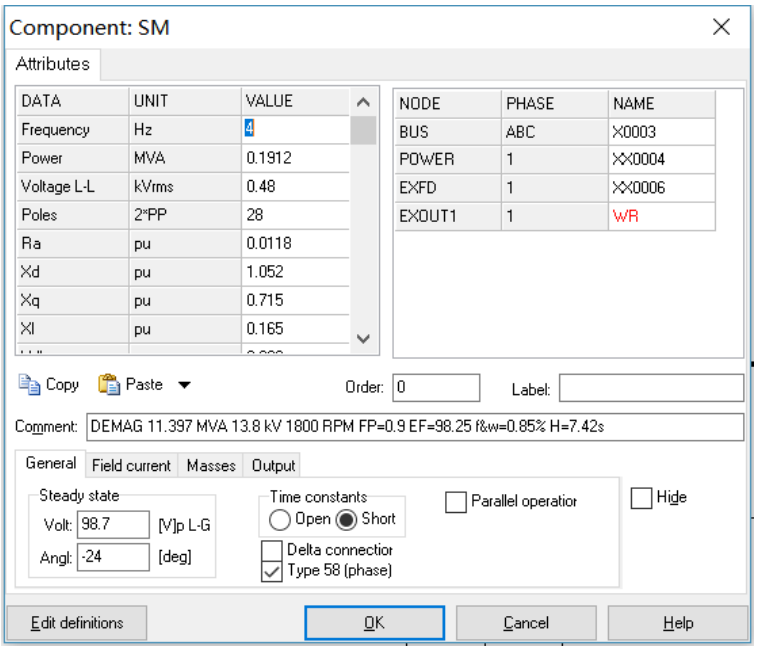

Appendix E.1 input data of the startup simulation

As we can see from figure appendix E.2, the motor can reach to the synchronous speed at about 2s and at such period the excitation is added.

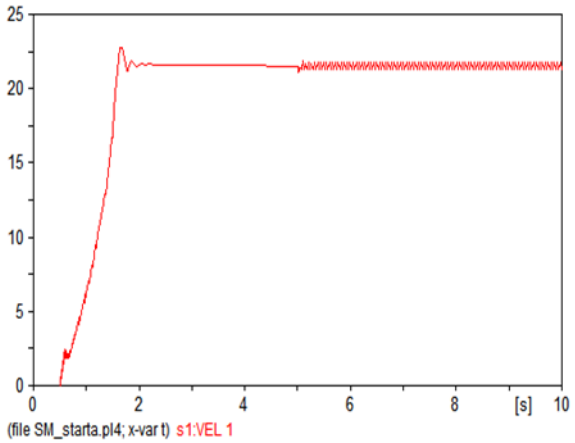

Appendix E.2 The startup of Synchronous Motor

Appendix F

Basic Testing for Simultaneous Transfer Sequence

Such transfer sequence is not used in the relay testing in this thesis. As discussed in chapter 2, in simultaneous transfer scheme, a trip command is sent to the breaker in the faulty feeder at the same time when the close command is sent to the switch of the auxiliary bus.

As the figure indicates, the feeder breaker is already tripped by the differential relay when a short circuit occurs. Based on the internal logic of the simultaneous scheme, the relay sent both the trip command to fault breaker (although such breaker has already received the trip signal) and the close command to the healthy feeder. If the fault clearing time is longer than the breaker closing time, the breaker in the auxiliary bus will close although the fault does not clear. The auxiliary feeder continues to feed the fault, which makes more difficult for the fault to be cleared and this leads to instability of the whole power system. That is the reason why simultaneous schemes are not used in this thesis.

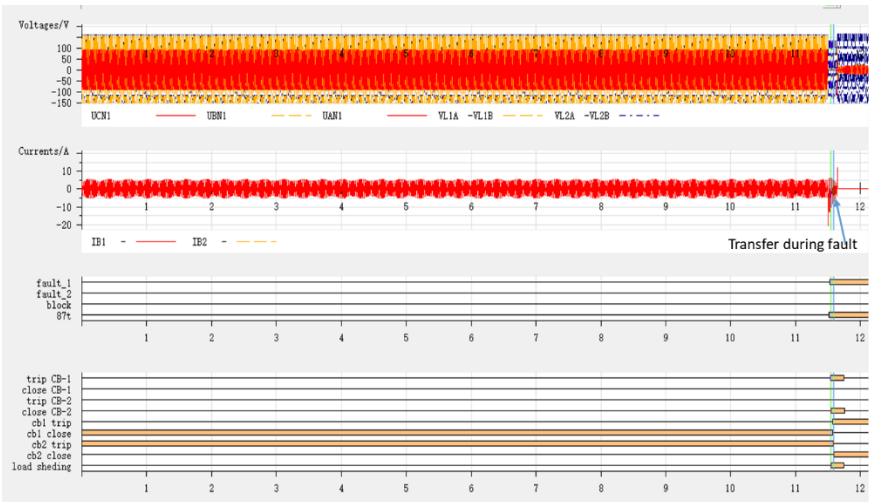

Figure Appendix F.1 Simultaneous Transfer for 150ms Three-phase Fault

Appendix F

However, the simultaneous transfer sequence has some drawbacks, as some basic testing for such transfer scheme as a reference for DOW has been done. The test is only performed for the feeder bus with 50ms breaker closing and opening time, 20ms communication delay, and 20ms 87T trip delay.
The testing result are shown as table Appendix F.1:

Table Appendix F.1

Fault Location	Fault Type	Transer Time (ms)
25kV Side	Single-Phase Fault	41.2
	Double-Phase Fault	42.3
	Phase to Phase Fault	45.7
	Three Phase Fault	40.3
220kV Side	Single-Phase Fault	43.7
	Double-Phase Fault	42.1
	Phase to Phase Fault	36.7
	Three Phase Fault	40.1

From the testing result, it is clear that the fault time has only impact on the transfer time when the simultaneous transfer scheme is chosen. Since the close command is sent to the auxiliary breakers at the same time when the trip command is sent to breaker in the faulty feeder.

Bibliography

[1] F. I. Khan and S. Abbasi, "Techniques and methodologies for risk analysis in chemical process industries," *Journal of Loss Prevention in the Process Industries*, vol. 11, no. 4, pp. 261 – 277, 1998.

[2] D. G. Lewis and W. D. Marsh, "Transfer of steam-electric generating-station auxiliary busses [includes discussion]," *Transactions of the American Institute of Electrical Engineers. Part III: Power Apparatus and Systems*, vol. 74, Jan 1955.

[3] W. C. Huening, "Calculating short-circuit currents with contributions from induction motors," *IEEE Transactions on Industry Applications*, vol. IA-18, pp. 85–92, March 1982.

[4] K. E. Yeager, "Bus transfer of multiple induction motor loads in a 400 megawatt fossil power plant," *IEEE Transactions on Energy Conversion*, vol. 3, pp. 451–457, Sep 1988.

[5] T. R. Beckwith and W. G. Hartmann, "Motor bus transfer: considerations amp; methods," in *IEEE Systems Technical Conference on Industrial and Commercial Power 2005.*, pp. 62–76, May 2005.

[6] M. V. V. S. Yalla, "Design of a high-speed motor bus transfer system," in *Conference Record 2009 IEEE Industrial Commercial Power Systems Technical Conference*, pp. 1–12, May 2009.

[7] L. Asnin, V. Backmutsky, M. Gankin, J. Blashka, and M. Sedlachek, "Dsp methods for dynamic estimation of frequency and magnitude parameters in power system transients," in *2001 IEEE Porto Power Tech Proceedings (Cat. No.01EX502)*, vol. 4, pp. 6 pp. vol.4–, 2001.

[8] M. M. Begovic, P. M. Djuric, S. Dunlap, and A. G. Phadke, "Frequency tracking in power networks in the presence of harmonics," IEEE Transactions on Power Delivery, vol. 8, pp. 480–486, Apr 1993.

[9] E. Aboutanios, "An adaptive clarke transform based estimator for the frequency of balanced and unbalanced three-phase power systems," in *2017 25th European Signal Processing Conference (EUSIPCO)*, pp. 1001–1005, Aug 2017.

[10] V. Eckhardt, P. Hippe, and G. Hosemann, "Dynamic measuring of frequency and frequency oscillations in multiphase power systems," *IEEE Transactions on Power Delivery*, vol. 4, pp. 95–102, Jan 1989.

[11] J.-Z. Yang and C.-W. Liu, "A precise calculation of power system frequency," *IEEE Transactions on Power Delivery*, vol. 16, pp. 361–366, Jul 2001.

[12] T. Lobos and J. Rezmer, "Real-time determination of power system frequency," *IEEE Transactions on Instrumentation and Measurement*, vol. 46, pp. 877–881, Aug 1997.

[13] "C50.41-2000," *American National Standard for Polyphase Induction Motors for Power Generating Stations*, 2000.

[14] T. R. Beckwith and C. J. Mozina, "Motor bus transfer system performance testing and the search for a new transfer success criterion," *IEEE Transactions on Industry Applications*, vol. 53, pp. 653–659, Jan 2017.

[15] M. Hoeijmakers, *Modelling of ac machines.* Delft University of Technology, 2004.

[16] Siemens AG, *Multi-function High Speed Motor Bus Transfer 7VU683*, 2016.

[17] D. Homa and W. WrÃşblewski, "Modelling of flow with cavitation in centrifugal pump," *Journal of Physics: Conference Series*, vol. 530, no. 1, p. 012032, 2014.

[18] J. Wang, Z. Bao and D. Chen, "Frequency spectrum analysis of vibration signals and fault diagnosis of reciprocating compressor," *Applied Mechanics and Material*, Vols. 336-338, pp 982-987, 2008

[19] Tennet TSO GmbH, *Grid Code for high and extra high voltage*, 2015.

[20] Beckwith Electric Co., *Digital Motor Bus Transfer System*, 2004.